

DEFORMATION ENHANCED GRAIN GROWTH IN A  
SUPERPLASTIC Sn - 1% Bi ALLOY

by

MALCOLM ARTHUR CLARK

B.A.Sc., University of Toronto, 1966

A THESIS SUBMITTED IN PARTIAL FULFILMENT OF  
THE REQUIREMENTS FOR THE DEGREE OF  
MASTER OF APPLIED SCIENCE

in the Department

of

METALLURGY

We accept this thesis as conforming to the  
required standard

THE UNIVERSITY OF BRITISH COLUMBIA

February, 1971

In presenting this thesis in partial fulfilment of the requirements for an advanced degree at the University of British Columbia, I agree that the Library shall make it freely available for reference and study.

I further agree that permission for extensive copying of this thesis for scholarly purposes may be granted by the Head of my Department or by his representatives. It is understood that copying or publication of this thesis for financial gain shall not be allowed without my written permission.

Department of Metallurgy

The University of British Columbia  
Vancouver 8, Canada

Date April 23, 1971

ABSTRACT

A Sn - 1% Bi alloy has been studied to determine the effects of superplastic deformation on the grain growth kinetics. Using both constant crosshead speed and creep tests, the grain size was measured as a function of deformation time and strain over a wide range of strain rates.

It was found that during deformation, considerable increases in the grain growth rates occurred when compared to static annealing. The effect was most pronounced at intermediate strain rates ( $\approx 10^{-2}$ /minute) in the high strain rate sensitivity region. However, the grain growth rates on annealing after deformation were found to be less than static rates.

To aid in understanding the mechanism of the enhanced growth, alternating tension-compression tests were performed. The amount of grain elongation and the changes in preferred orientation with deformation were also measured.

Grain type and grain size distributions after deformation and after annealing were established and analyzed in terms of a grain coalescence mechanism. However, the most favourable mechanism appears to involve the production of excess vacancies in the grain boundary region leading to increased boundary mobility.

ACKNOWLEDGEMENT

The author wishes to express his gratitude for the advice and encouragement of his research supervisor, Dr. T.H. Alden. Thanks are also extended to faculty members, fellow graduate students, and technical staff for helpful discussions and assistance.

Financial assistance from the Defence Research Board (Grant No.9535-41) is gratefully acknowledged.

TABLE OF CONTENTS

	<u>Page</u>
INTRODUCTION .. .. .	1
1.1 Superplasticity .. .. .	1
1.2 Deformation Induced Grain Growth .. .. .	3
1.3 Purpose of the Present Investigation .. .. .	7
EXPERIMENTAL .. .. .	8
2.1 Specimen Preparation .. .. .	8
2.2 Tensile Testing .. .. .	9
2.3 Creep Testing .. .. .	10
2.4 X-Ray Analysis .. .. .	12
2.5 Metallography .. .. .	13
RESULTS .. .. .	15
3.1 Superplastic Properties .. .. .	15
3.1.1 Log $\sigma$ - Log $\dot{\epsilon}$ Curves .. .. .	15
3.1.2 Stress-Strain Relationship .. .. .	18
3.2 Grain Growth During Annealing .. .. .	23
3.3 Grain Growth During Deformation .. .. .	31
3.3.1 Effect of Deformation Time .. .. .	31
3.3.2 Effect of Strain .. .. .	34
3.3.3 Grain Elongation .. .. .	39
3.3.4 Alternating Tension-Compression .. .. .	49
3.3.5 Grain Type Distribution .. .. .	43
3.3.6 Grain Size Distribution .. .. .	44

	<u>Page</u>
3.4 X-Ray Analysis Results .. .. .	50
3.5 Grain Growth After Deformation .. .. .	57
3.5.1 Growth by Annealing .. .. .	57
3.5.2 Growth Enhanced by Deformation .. .. .	57
DISCUSSION .. .. .	66
4.1 Superplasticity .. .. .	66
4.2 Grain Growth .. .. .	67
4.3 Mechanisms of Deformation Enhanced Grain Growth ..	71
4.3.1 Grain Coalescence .. .. .	71
4.3.2 Increased Driving Force .. .. .	74
4.3.2.1 Recrystallization .. .. .	74
4.3.2.2 Grain Boundary Sliding .. .. .	75
4.3.2.3 Grain Elongation .. .. .	78
4.3.2.4 Grain Boundary Width .. .. .	78
4.3.3 Mobility Enhancement .. .. .	79
SUMMARY AND CONCLUSION .. .. .	92
APPENDIX A .. .. .	93
Effect of Coalescence Mechanism on Grain Type and Size	
Distribution .. .. .	93
BIBLIOGRAPHY .. .. .	104

LIST OF FIGURES

<u>Figure No.</u>		<u>Page</u>
1	Typical Stress-Strain Rate Relationship in Superplastic Materials .. .. .	1
2	Grain Size versus True Strain for Two Initial Grain Sizes (from data by Alden and Schadler <sup>(14)</sup> ) .. .. .	4
3	Grip Arrangement for Tension-Compression Testing on Instron .. .. .	11
4	Effects of Processing Conditions on Stress- Strain Rate Relationship .. .. .	16
5	Effects of Processing Conditions on Strain Rate Sensitivity Parameter "m" .. .. .	17
6	Comparison of Stress-Strain Rate Data Be- tween Single Strain Rate Change Test and Individual Instron Tests .. .. .	19
7	Comparison of Stress-Strain Rate Data Be- tween Single Strain Rate Change Test and Individual Creep Tests .. .. .	20
8	Comparison of Stress-Strain Rate Data Be- tween Present and Previous Investigations .. .. .	21
9	True Stress-True Strain Curves at Various Initial Strain Rates .. .. .	22
10	Creep Curves at Stresses of 500, 350 and 250 p.s.i. .. .. .	24
11	Creep Curves at Stresses of 150, 100 and 40 p.s.i. .. .. .	25

<u>Figure No.</u>		<u>Page</u>
12	Grain Size versus Time During Static Annealing of Low Ratio Room Temperature Extrusion Material .. .. .	27
13	Grain Size versus Time During Static Annealing of High Ratio Room Temperature Extrusion Material .. .. .	28
14	Grain Size versus Time During Static Annealing of Low-Ratio-0°C Temperature Extrusion Material .. .. .	29
15	Grain Size versus Time for Different Processing Conditions .. .. .	30
16	Grain Size versus Time During Instron Deformation .. .. .	32
17	Grain Size versus Time During Creep Deformation .. .. .	33
18	Relative Grain Size Change versus Strain During Instron Deformation .. .. .	35
19	Relative Grain Size Change versus Strain During Creep Deformation .. .. .	36
20	Relative Grain Size Change After 25% Strain versus Strain Rate .. .. .	38
21	Relative Grain Size Change After 25% Strain versus "m" .. .. .	40
22	Degree of Grain Elongation After 35% Strain at Various Strain Rates .. .. .	41
23	Stress-Strain Relationships During Tension- Compression Testing .. .. .	42

<u>Figure No.</u>	<u>Page</u>
24	Grain Type Distribution for Annealed and Deformed Structure .. .. . 45
25	Cumulative Frequency Diagram for Grain Type Distribution of Fig.24 .. .. . 46
26	Grain Size Distribution for Annealed and Deformed Structures .. .. . 47
27	Cumulative Frequency Diagram for Grain Size Distribution of Fig.26 .. .. . 49
28	Grain Size Distribution for Annealed and Deformed Structures of Equivalent Mean Grain Size .. .. . 51
29	Back Reflection Pattern for Extruded Rod .. 52
30	Location of Fiber Axis on Standard Stereo- graphic Projection of Tin .. .. . 54
31	(110) Pole Figure for Extruded Rod .. .. . 55
32	Degree of Texture Before and After Deformation 56
33	Grain Size versus Time During and After Deformation at $\dot{\epsilon} = 10^{-2}/\text{min.}$ .. .. . 58
34	Effect of Strain on Grain Size versus Time Curves After Deformation .. .. . 59
35	Comparison of Grain Size versus Time Curves for Static Annealing and Annealing After De- formation of 70% Strain .. .. . 60
36	Comparison of Grain Size versus Time Curves for Static Annealing and Annealing After De- formation of 7% Strain .. .. . 61

<u>Figure No.</u>	<u>Page</u>
37	Comparison of Stress-Strain Rate Data for Annealed and Deformed Material .. .. . 63
38	Effect of Pre-Deformation on Grain Size In- crease During Deformation .. .. . 64
39	The Grain Coalescence Mechanism .. .. . 72
40	Surface Grain Boundary Migration Associ- ated with Internal Boundary Sliding .. .. 76
41	Comparison of Theoretical and Experi- mental Grain Size versus Time During De- formation Curves .. .. . 84
42	Comparison of Theoretical and Experimental Relative Grain Size Change versus Strain Curves .. .. . 86
43	Comparison of Theory and Experiment for the Relative Grain Size Change After 25% Strain .. .. . 87
44	Comparison of Theory and Experiment for Post Deformation Annealing .. .. . 89
45	Illustration of Grain "Encounter" During Grain Growth .. .. . 90
46	Effect of a Grain Boundary Coalescence .. .. 94
47	Comparison of Calculated and Experimental Grain Type Distributions .. .. . 100
48	Comparison of Calculated and Experimental Grain Size Distributions .. .. . 103

LIST OF TABLES

<u>Table No.</u>		<u>Page</u>
1	Power Law Constants for Grain Size versus Time Curves .. .. .	26
2	Power Law Constants for Grain Size versus Time Curves During Deformation ..	34
3	Straight Line Constants for Relative Grain Size Change versus Strain Curves .. ..	37
4	Estimated Values for Terms of Equation (10) <sup>(45)</sup> .. .. .	70
5	Areas of Coalesced Grains .. .. .	101

## INTRODUCTION

### 1.1 - Superplasticity

Superplastic materials are characterized by large amounts of neck-free elongation in tension and by a high value of the strain rate sensitivity parameter, "m", defined as  $\frac{d \log \sigma}{d \log \dot{\epsilon}}$ . The  $\log \sigma$

-  $\log \dot{\epsilon}$  relationship in superplastic alloys is usually an "S" shaped curve which can be divided into three stages. (Fig.1).

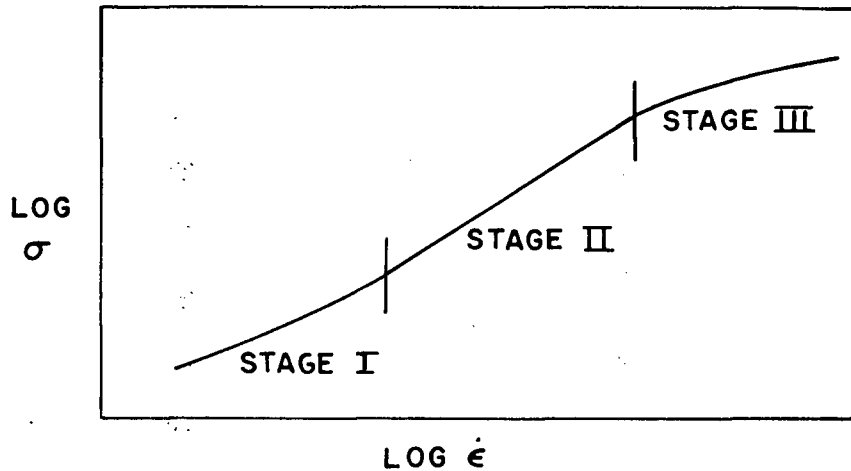


Fig.1. Typical Stress-Strain Rate Relationship  
in Superplastic Materials.

Although this type of curve is typical, not all alloys display a Stage I region within the range of experimentally obtainable strain rates<sup>(1)</sup>. The largest elongations occur in the region of highest strain rate sensitivity, Stage II. The amount of extension appears to increase with the value of "m"<sup>(2)</sup>. This relationship has been explained phenomenologically by Backofen et al<sup>(3)</sup>. The formation

of an incipient neck in a deforming sample causes a local increase in strain rate. When the strain rate sensitivity is high, this increased strain rate causes the necked region to harden so that deformation will tend to continue in the softer region away from the neck.

If certain conditions are fulfilled, superplasticity will occur in a wide range of alloys including two phase eutectic or eutectoid systems such as Pb-Sn<sup>(4)</sup> and Zn-Al<sup>(3)</sup> as well as phase pure systems; Sn-Bi<sup>(5)</sup>, Ni<sup>(6)</sup> and Pb-Th<sup>(7)</sup>. For most alloys these conditions are: 1) an homologous temperature greater than .5 T<sub>m</sub>, 2) a fine grain size and 3) phases of similar hardness. For the purpose of forming operations it is necessary that the superplastic properties be displayed at high strain rates. The major requirement for such behaviour is a fine grain size. An increase in grain size shifts the "S" curve horizontally to the left so that the high "m" region occurs at lower  $\dot{\epsilon}$ .

During a constant strain rate or constant crosshead speed (Instron) test above 0.5 T<sub>m</sub>, the grain size may increase in some materials. In this case the original value of "m" will gradually change as the stress-strain rate relationship shifts on the  $\dot{\epsilon}$  axis. A sample that was originally deforming in Stage II could, after grain growth occurs, be deforming in Stage III. The amount of elongation obtained would then be decreased. Experimental results indicate, in fact, that the highest elongations are obtained in alloys with substantial amounts of second phase which anchor the grain boundaries and retard grain coarsening.

The microstructure of superplastic alloys and the changes

which occur during deformation have been well studied. Deformation in Stage II is accompanied by larger amounts of grain boundary sliding and grain rotation than is observed in the Stage III region<sup>(27)</sup>. The grains retain their equiaxed shape even after large amounts of elongation. No dislocation substructure is formed by the deformation<sup>(1)</sup>. Grain boundary migration is observed on the specimen surface and is associated with grain sliding.

### 1.2 - Deformation Induced Grain Growth

A structural change, associated with superplasticity, which has not received detailed attention is an apparent enhancement of grain growth during the deformation. In the Pb-Sn eutectic<sup>(8)</sup>, the grain size after 600% elongation was considerably larger (4.4  $\mu$ ) compared to the grain size (3  $\mu$ ) of a sample held at the testing temperature for an equivalent length of time. The grain size increased linearly with % elongation, with larger changes occurring at lower strain rates. Morrison<sup>(9)</sup>, also studied the Pb-Sn eutectic and produced micrographs displaying an increasing grain size with strain. On creep testing of the Pb-Sn eutectic, Surges<sup>(10)</sup> found a steadily decreasing creep rate in Stage I deformation which was tentatively attributed to either diffusional creep or grain growth. Other studies<sup>(4,11-13)</sup> on Pb-Sn made no specific mention of grain growth effects however.

In the eutectoid Zn-Al system, Alden and Schadler<sup>(14)</sup> found that significant grain growth occurred after large strains. They deformed two samples of different initial grain size at the same strain rate in Stage II until a neck began to form, then

sectioned the samples at various places along the neck and measured the grain size. In this way specimens were obtained which had been deformed for the same length of time but to different strain levels. The relationship between grain size and strain appeared to be linear initially (Fig.2). In the time taken for deformation the grain size would not have changed significantly with annealing only. Alden and Schadler reported no grain elongation but noted increased boundary curvature with deformation which disappeared upon annealing.

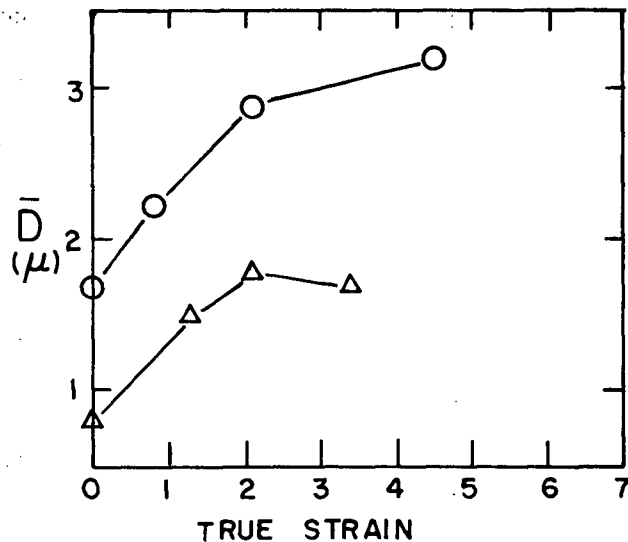


Fig.2. Grain Size versus True Strain for Two Initial Grain Sizes (from data by Alden and Schadler<sup>(14)</sup>).

Kossawsky and Bechtold<sup>(15)</sup> also studied the Zn-Al eutectoid system and their micrographs showed that growth of the zinc-rich phase was occurring. Less growth appeared to take place at the lower strain rates. Micrographs and X-ray patterns revealed grain growth in the Zn-Al eutectoid in a study by Chaudhari<sup>(16)</sup>. On the other hand, Packer and Sherby<sup>(17,18)</sup> reported little change in grain size up to 1280% elongation although rounding of the grain boundaries did occur.

Nutall and Nicholson<sup>(19)</sup> also reported little grain growth up to 500% elongation. In a study of the Zn-Al eutectic (95 wt.% Zn), Packer, Johnson and Sherby<sup>(20)</sup> found that the Al second phase lost its directional nature produced on rolling and coarsened with superplastic deformation.

With a dilute alloy of Zn-Al (.2 wt.% Al) Cook<sup>(21)</sup> found a log-log relationship between grain size and true strain up to elongations of 1000 %. In other words, growth is rapid during the initial stages of deformation but decreases as strain continues. These results have been confirmed by Turner<sup>(22)</sup> in the 1 wt.% Al alloy and by Naziri, Pearce and Williams<sup>(23)</sup> in the .4 wt.% Al alloy.

Naziri and Pearce<sup>(24)</sup> investigated commercial purity zinc which had been rolled to 90% reduction to produce a 1 to 2 micron grain size. The strain rate sensitivity was only .2 and the maximum elongation obtained was only 200% so that the material was not considered superplastic. However, after 100% elongation, the grains doubled in size, remained equiaxed and showed no evidence of slip, i.e. results similar to those in superplastic materials.

Superplasticity has been studied extensively in a 45% Ni, 38% Cr, 14% Fe two phase alloy by Brophy and co-workers<sup>(1,25,26)</sup>. In their first paper an increase in grain size with deformation was noted and then studied more completely in the two later papers<sup>(25,26)</sup>. They found that the matrix grain size was dependent on the average size and volume fraction of the second phase particles. The results were in agreement with the Zener-McLean equation which predicts a limiting grain size by considering the effect of second

phase particles on the grain boundary energy:

$$\text{Grain Size} = \frac{2}{3} \frac{d}{V_f}$$

where  $d$  is the average particle diameter and  $V_f$  is the volume fraction of second phase. With superplastic deformation the diameter of the second phase particles increased roughly proportional to the  $\frac{1}{2}$  power of the deformation time. The matrix grain size increased accordingly so that the Zener-McLean equation was still obeyed. Lower strain rates produced a larger change in grain size for the same amount of strain. No theory was proposed to explain the coarsening of the second phase.

Other superplastic alloy systems also display enhanced grain growth with deformation. Alden<sup>(27)</sup> noted that in a Sn - 5% Bi sample elongated 1000% the grain size had increased to 4 microns whereas it would have increased to only 1.6 microns on annealing without deformation. In an Al-Cu eutectic alloy Stowell et al<sup>(28)</sup> found coarsening of the intermetallic  $\text{CuAl}_2$  phase taking place with deformation. Their micrographs show evidence of sintering or coalescence of some of the  $\text{CuAl}_2$  particles. They proposed that the coalescence occurred as a consequence of grain boundary sliding which tended to sweep the particles together. Grain growth during deformation has also been reported in Mg-Al,<sup>(29,30)</sup> Ti<sup>(31)</sup>, Mg-6Zn-.5Zr<sup>(32)</sup>, and low alloy steels<sup>(33)</sup>.

Some contradictory results have been obtained by other workers however. Gifkins<sup>(7)</sup> observed no grain growth in Pb-Th alloys. The initial grain size was 100  $\mu$  however, which is much larger than most superplastic materials. The alloys did display large elongations and a high "m" value.

Despite being apparently inherent to superplastic creep, the enhancement of grain size effect has been studied in detail only

by Brophy et al<sup>(25,26)</sup>. Few attempts to explain the effect have been made in the literature. Cook<sup>(21)</sup> tentatively suggested that in dilute Zn alloys boundary sliding caused a difference of dislocation density on either side of the shearing boundary. The boundary would then tend to move to eliminate the areas of highest dislocation density.

### 1.3 - Purpose of Present Investigation

In view of the almost universal occurrence of enhanced grain growth in superplastic alloys and its importance in limiting the amount of elongation, it was decided to study the phenomenon in more detail and attempt to understand the mechanism promoting the growth.

For relative simplicity, a single phase alloy was chosen, namely Sn - 1% Bi which had been shown to be superplastic by Alden<sup>(5)</sup>. This alloy system offered several advantages:

- 1) The melting point is low so that annealing at room temperature corresponded to an homologous temperature of  $.6 T_m$ .
- 2) Casting and extrusion could be done easily at, or near, room temperature, and
- 3) Normal grain growth in dilute Sn - Bi alloys had been extensively studied and theoretically discussed by Holmes and Winegard<sup>(34)</sup>, and by Gordon<sup>(35)</sup>. The two phase Sn - 5% Bi<sup>(27)</sup> alloy is also superplastic and could provide a good comparison if time permitted.

## EXPERIMENTAL

### 2.1 - Specimen Preparation

The alloy was prepared from high purity tin (99.999%) and bismuth (99.999%). Melting was done in graphite crucibles, either in air with a molten salt cover to lessen oxidation or in vacuum. The melts were held at a temperature between 300 and 350°C with intermittent stirring for at least 10 minutes after alloying was completed. Casting was performed by bottom pouring into copper molds producing cylindrical billets approximately 5" long and 1" in diameter.

After casting all billets were homogenized in an air oven at  $130^{\circ}\text{C} \pm 7^{\circ}\text{C}$  for seven days. The ends of each billet were removed and the diameter machined down.

To produce a fine grain size superplastic material, the billets were back extruded into rod form using high extrusion ratios. Two finished sizes were produced; .150" diameter (extrusion ratio 40:1) and .083" diameter (extrusion ratio 130:1). The extrusion speed was approximately 12"/minute at 70,000 to 80,000 psi for the .150" diameter rod. Speed control with the .083" diameter rod was difficult to attain and wide fluctuations of rate were unavoidable. The mechanical properties were not affected by this variation. Two extrusion temperatures were used; room temperature (22°C) and 0°C. To obtain the 0°C extrusion temperature, the billet, die blocks, ram and container were assembled and placed in a freezer for 24 hours. The whole assembly was immediately transferred to the extrusion press and immersed in an ice-water mixture during the extrusion process. For all extrusions, a die lubricant was used, either a powdered

graphite-oil mixture or polyethylene glycol. Immediately after leaving the die, the rod was cut into short lengths and quenched into liquid nitrogen. All material was stored in liquid nitrogen in a Union Carbide LD-17 container which maintained a temperature of  $-184^{\circ}\text{C}$  above the liquid nitrogen level so that the rods were maintained below this temperature at all times.

For tensile or creep testing most specimens were used "as-extruded" with no reduction in the cross-sectional area. To obtain high elongations in Stage II deformation and for all testing in Stage III, a reduced cross-section specimen was produced. The gauge length was machined on a jewellers' lathe using a cold machining technique<sup>(21)</sup> in which cold nitrogen gas was blown on to the specimen continually. To ensure that no grain growth or excessive damage was introduced by this procedure, a specimen was machined and examined in the optical microscope. The overall grain size was the same as in samples annealed for the same length of time. The damaged surface layer appeared to extend to a depth of only  $10\ \mu$ .

## 2.2 - Tensile Testing

Tensile testing was done on Instron floor model machines using constant crosshead speeds. The specimen was gripped using threaded split grips. During tightening of the grips, overloading of the specimen was prevented by automatic load cycling of the crosshead. The gauge length was taken as the distance between the grips for a uniform cross-section specimen and as the length having constant diameter with the machined specimens.

The stress-strain rate relationships were determined on single samples by a variable crosshead speed technique. After a

steady load was obtained at each crosshead speed the speed was changed by a factor of 2 or 2.5. True stress and strain rate values were computed using values for instantaneous area and length. In most cases steady stress values were obtained after approximately 1% strain at each crosshead speed. Total strain during testing through the complete speed range normally amounted to less than 25%. Although some grain growth occurred during these tests its effect on the shape of the  $\sigma - \dot{\epsilon}$  curve was slight since the values obtained in individual tests at constant crosshead speed agreed with the strain rate change tests. (Results section, Figs. 6 and 7).

For grain size versus strain measurements, the true strain of the specimen after testing was determined by measuring the final diameter at the section where the grain size was measured.

Alternating tension-compression tests were also carried out on an Instron. A special grip arrangement was made (Fig.3) to hold the specimen to minimize slack in the linkages. Specimen extension was measured with an Instron strain gauge extensometer attached to the aluminum mounts. The gauge length of the specimen was kept below .3" to minimize bending in compression.

### 2.3 - Creep Testing

Creep testing was performed to obtain lower strain rates than the Instron tests. The specimens were mounted in threaded grips with the load hung directly on to the bottom grip. The stress was kept constant within  $\pm 5\%$  by removing periodically a small portion of the load. Creep strain was measured with a travelling microscope by following the movement of two marks scribed on the specimen. The error

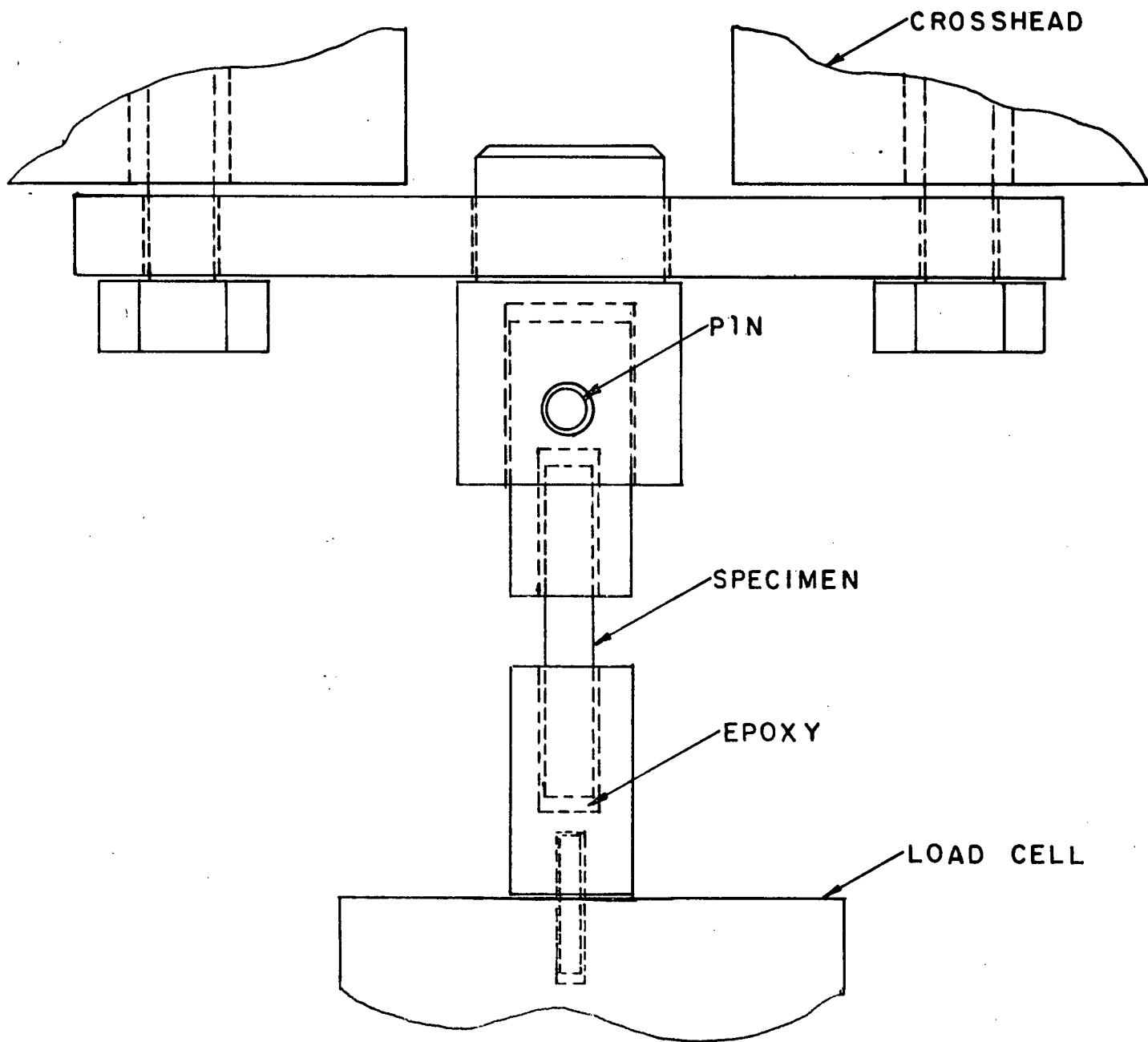


Fig.3. Grip Arrangement for Tension-Compression Testing on Instron.

in the true strain was estimated as  $\pm 1\%$ . For comparison with the tensile results, strain rate was measured from the slope of the strain versus time curve at 2% true strain. All creep and tensile testing was carried out at room temperature.

#### 2.4 - X-ray Analysis

To determine the preferred orientation of grains in the material, back reflection photographs were taken using monochromatic (Cu-K $\alpha$ ) radiation. Since the grain size was too large to produce complete Debye rings with a static exposure, the samples were rotated in the X-ray beam around the rod or tensile axis at a speed of 4 rpm. In this way many more grains were exposed to the X-ray beam and complete Debye rings were produced. The orientation of the fiber axis was determined from the photographs<sup>(36)</sup>.

To eliminate any surface effects, all specimens immediately before X-raying were electropolished with a stainless steel cathode and a voltage of 50-60 volts in a solution of the following composition<sup>(37)</sup>:

ethyl alcohol	- 144 ml.,
water	- 32 ml.,
n-butyl alcohol	- 16 ml.,
aluminum chloride	- 10 gm.,
zinc chloride	- 45 gm.,

In order to obtain an estimate of the degree of texture, a microdensitometer was used to scan the X-ray film and measure the relative intensity around the Debye arc.

## 2.5 - Metallography

Surfaces were prepared for etching and examination with a Porter Blum diamond knife ultramicrotome, following the procedure of Russell and Alden<sup>(38)</sup>. The method is fast, particularly for soft metals, and can produce an extremely smooth almost distortion free surface. However, only a small area,  $\frac{1}{2} \times 2$  mm., can be prepared. Thus, a wedge tip of this area had to be shaped on each sample with a fine jewellers' file. Kerosene was used as a lubricant to minimize knife wear. Initial cuts were about .5 microns thick and were progressively reduced in steps of 250A<sup>o</sup> until final slices of 500A<sup>o</sup> were taken. At each step, at least 7 slices were taken to remove the distorted layer from the previous cuts. All specimens were etched to reveal the grain boundaries in either a 2% HCl in ethyl alcohol solution or a solution containing 5 c.c HCl, 2 gm. ferric chloride, 30 c.c. water and 60 c.c. ethyl alcohol. Photomicrographs were taken in at least three separate areas of each surface.

Grain size was measured on the micrographs using the intercept method with a 10 cm. circumference circle<sup>(39)</sup>. The average lineal intercept,  $\bar{D}$ , was computed from the formula:  $\bar{D} = \frac{10 A}{N M}$

where A = number of applications of the circle

N = total number of boundary intersections

M = magnification of the photomicrograph

At least 320 intersections were counted for an error in  $\bar{D}$  of better than  $\pm 7\%$  at the 95% confidence level. In the remainder of the text the lineal intercept  $\bar{D}$  will be referred to as the grain size unless otherwise indicated. To determine the amount of grain elongation pro-

duced by deformation, some specimens were sectioned longitudinally and the average lineal intercept determined parallel and perpendicular to the tensile axis.

To determine the distribution of grain "types" the number of sides per grain were counted for each grain within a designated area. Grain size distributions were determined using the method of Johnson<sup>(40)</sup>. However, the Swedish grouping method<sup>(41)</sup> was adopted rather than the method of Johnson which is based on the ASTM grain size number. If  $\bar{A}$  is the mean planar grain area in square microns of a grain class P then :

$$\bar{A} = 2. P. \quad (1)$$

where P takes integer values  $\geq 0$ . The area limits of each class are given by  $2^{P+1/2}$ . Thus, grains having an area between 0 and  $1.4 \mu^2$  fall into class 0, between  $1.4$  and  $2.8 \mu^2$  into class 1, between  $2.8$  and  $5.8 \mu^2$  into class 2 etc. A series of squares having areas equivalent to the class limits times the photomicrograph magnification were scribed on to a sheet of clear plastic. The sheet was applied to each grain in turn to estimate its class. Approximately 1000 grains were counted for each sample.

## RESULTS

### 3.1 - Superplastic Properties

#### 3.1.1 - Log $\sigma$ - log $\dot{\epsilon}$ Curves

Incremental strain rate change tests were performed to study the effects of processing variables on the stress-strain rate relationships (Fig.4). All tests were performed after a 20 minute anneal at room temperature. Three variables are compared: 1) casting method, 2) extrusion ratio and 3) extrusion temperature. The reasons for studying these variables were to attempt to produce agreement with published results<sup>(5)</sup> and to shift the high "m" region toward higher strain rates.

All samples show at least a two stage curve with low and high "m" regions typical of superplastic materials. A slight indication of Stage I region is shown by the high extrusion ratio material (curve 4). The effect of both a lower extrusion temperature (curve 2) and higher extrusion ratio (curve 4) is to shift the high "m" region to higher strain rates with extrusion ratio having the more powerful effect. By comparing curves 2 and 3 it is seen that the melting and casting conditions have no effect on the stress-strain rate curve i.e. any oxidation or contamination produced by air casting had little effect on the deformation characteristics.

The "m" values (Fig.5) of the samples of Fig.4 were obtained graphically by measuring the slopes on the log  $\sigma$  - log  $\dot{\epsilon}$  plot. Values taken from the creep data (see Fig.7) have been added to curve 4. Higher extrusion ratio and lower extrusion temperature have produced higher peak "m" values than in the room temperature 40:1 ratio

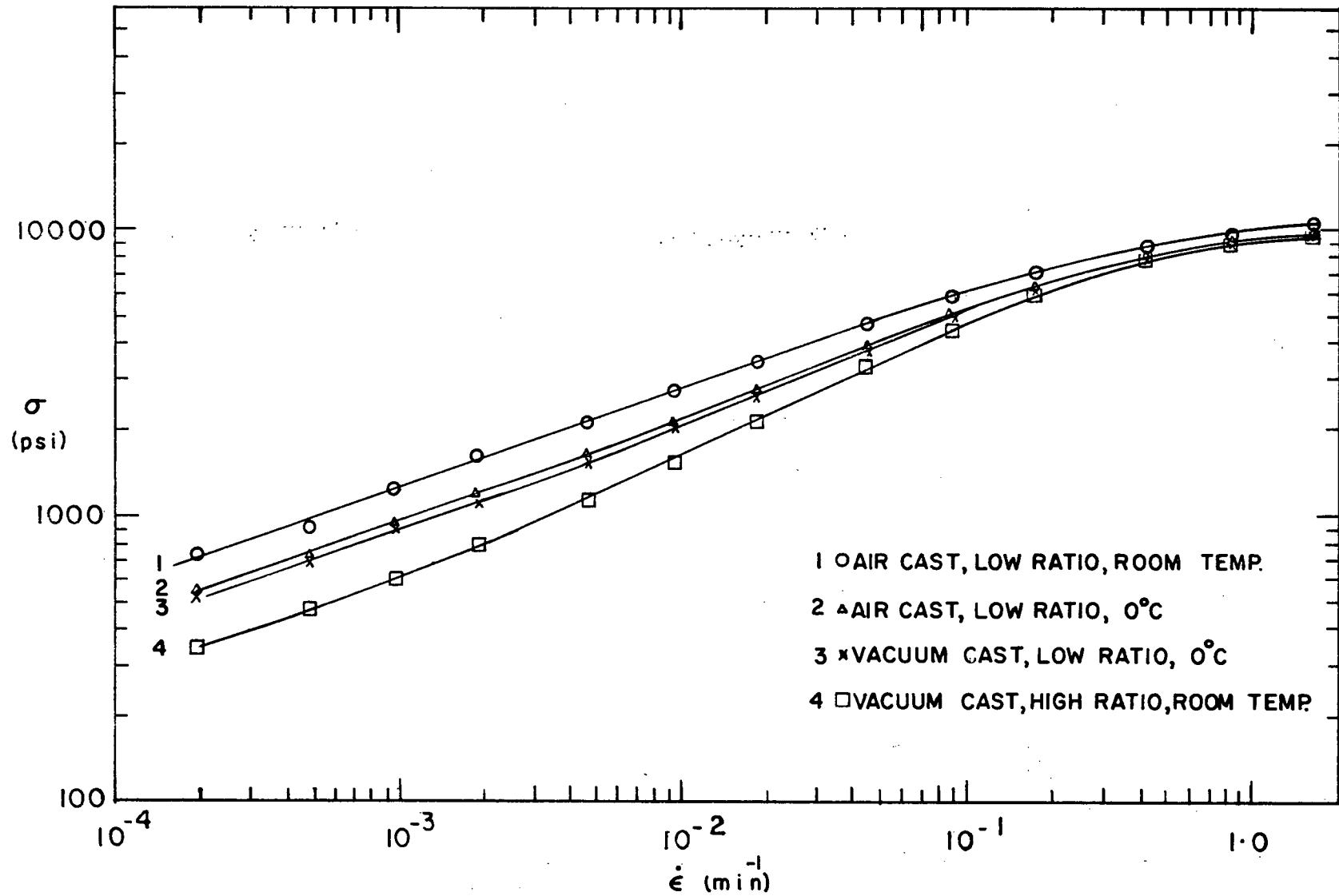


Fig.4. Effects of Processing Conditions on Stress-Strain Rate Relationship.

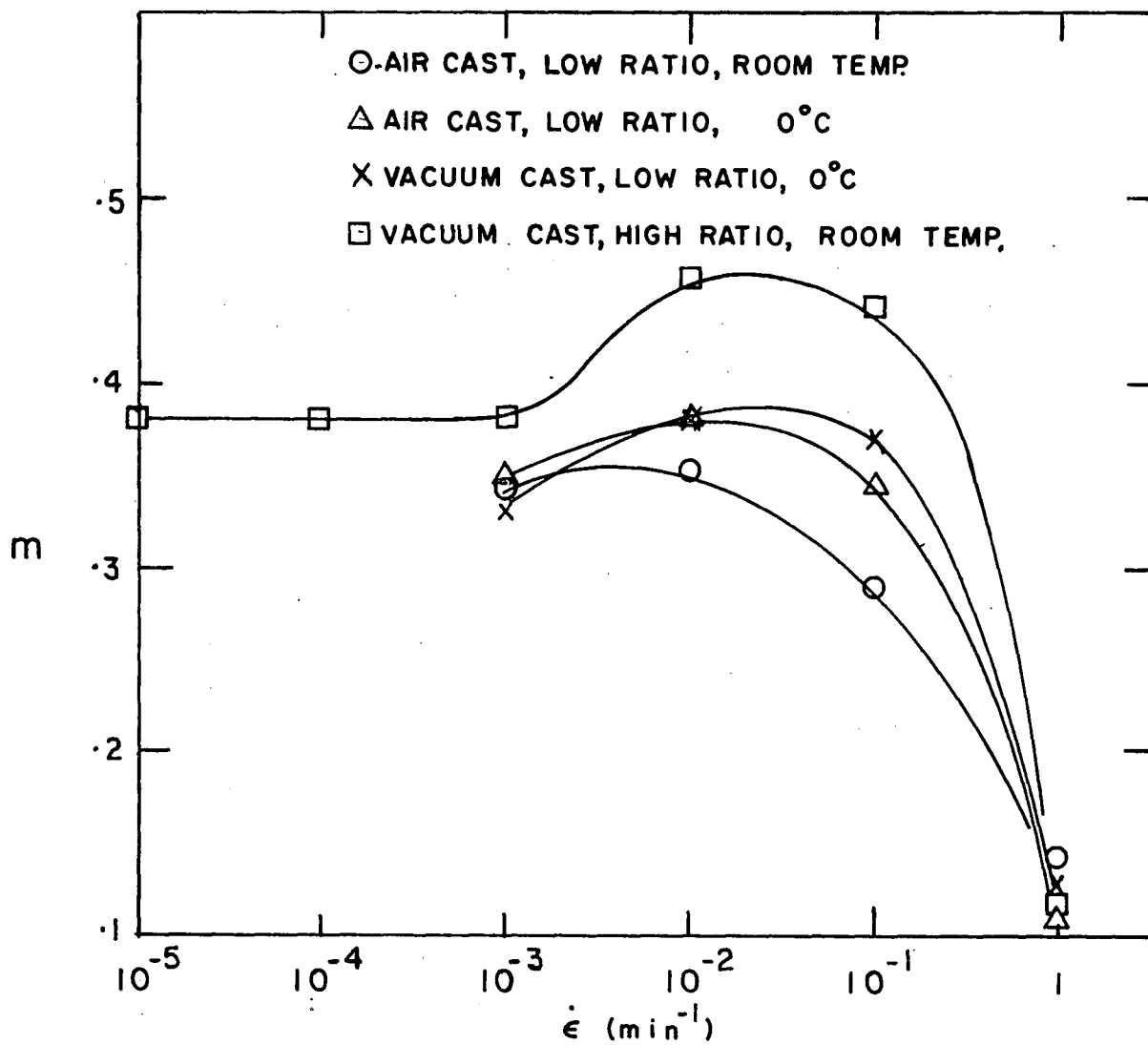


Fig.5. Effects of Processing Conditions on Strain Rate Sensitivity Parameter "m".

material. The extrusion ratio increase produced the more pronounced effect. The peak "m" values have been shifted to higher strain rates by both variables. The value of "m" in the Stage I region of curve 4 is approximately the same as the peak "m" of the other curves.

During the course of the incremental strain-rate change tests some grain growth occurred which could have affected the shape of the  $\sigma - \dot{\epsilon}$  curves. To establish a  $\log \sigma - \log \dot{\epsilon}$  curve free from growth effects, individual specimens with the same initial grain size were tested at each strain rate. Instantaneous stress-strain rate values were taken after approximately 2% strain for both the Instron and creep tests. The plotted points (Figs.6 and 7) are actually the average of at least four individual tests at each strain rate or stress level. Agreement between individual tests and the strain rate change tests is good indicating that grain growth had little effect in the strain rate change test.

One sample of air cast, 40:1 extrusion ratio, 0°C extrusion temperature material, annealed to a grain size of 5.8  $\mu$ , was used for an incremental strain rate change test. The resultant  $\log \sigma - \log \dot{\epsilon}$  curve (Fig.8) could then be compared with previously published results (5) on similarly processed Sn - 1% Bi of 5  $\mu$  grain size. The agreement is good considering the slight difference in grain size between the two samples.

### 3.1.2 - Stress-Strain Relationships

The true stress-true strain curves of the Sn - 1% Bi alloy appear to be typical of superplastic materials (Fig.9). At the highest strain rate (1.0"/min.), a "steady state" stress is not maintained, but

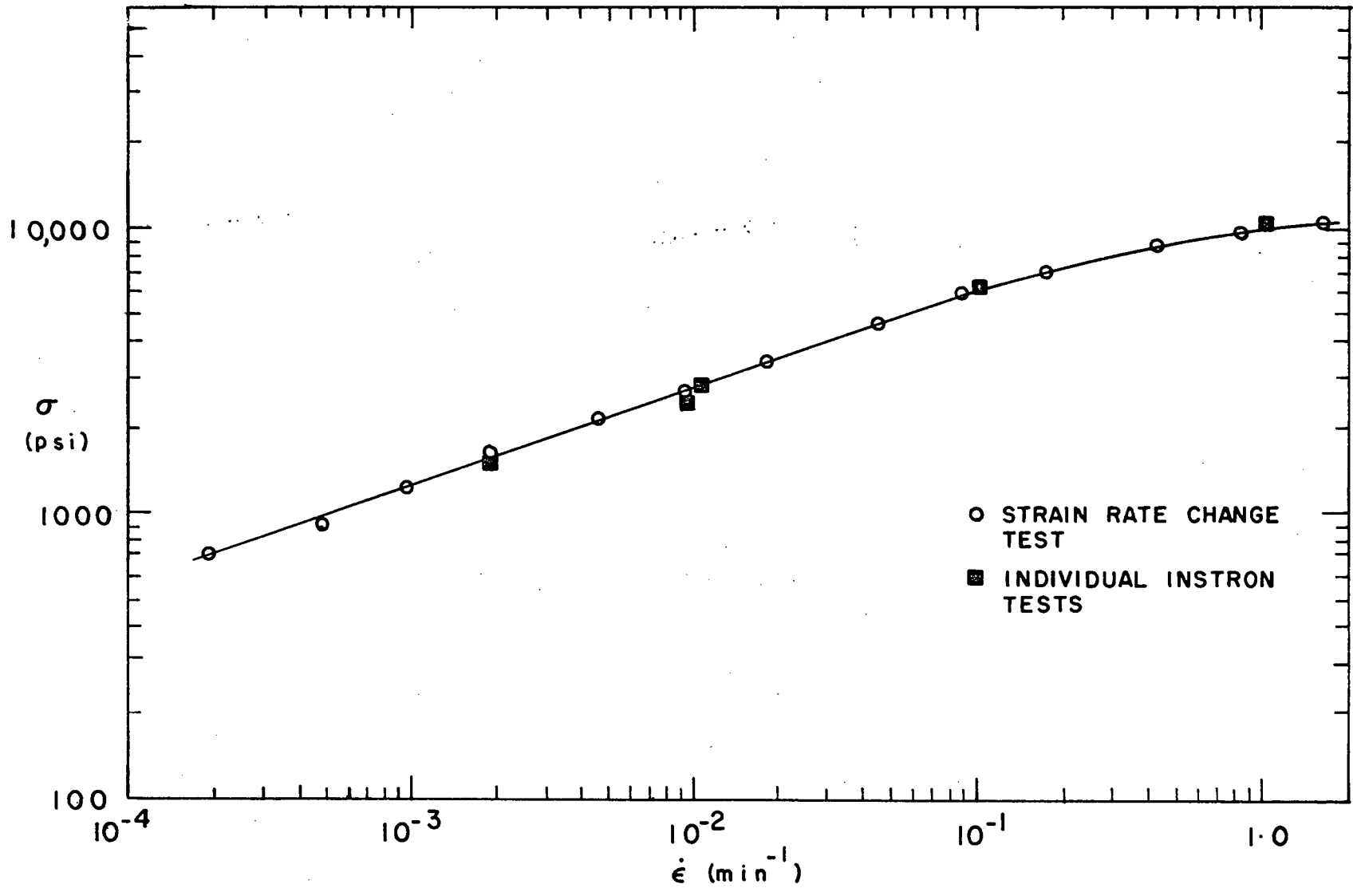


Fig.6. Comparison of Stress-Strain Rate Data Between Single Strain Rate Change Test and Individual Instron Tests.

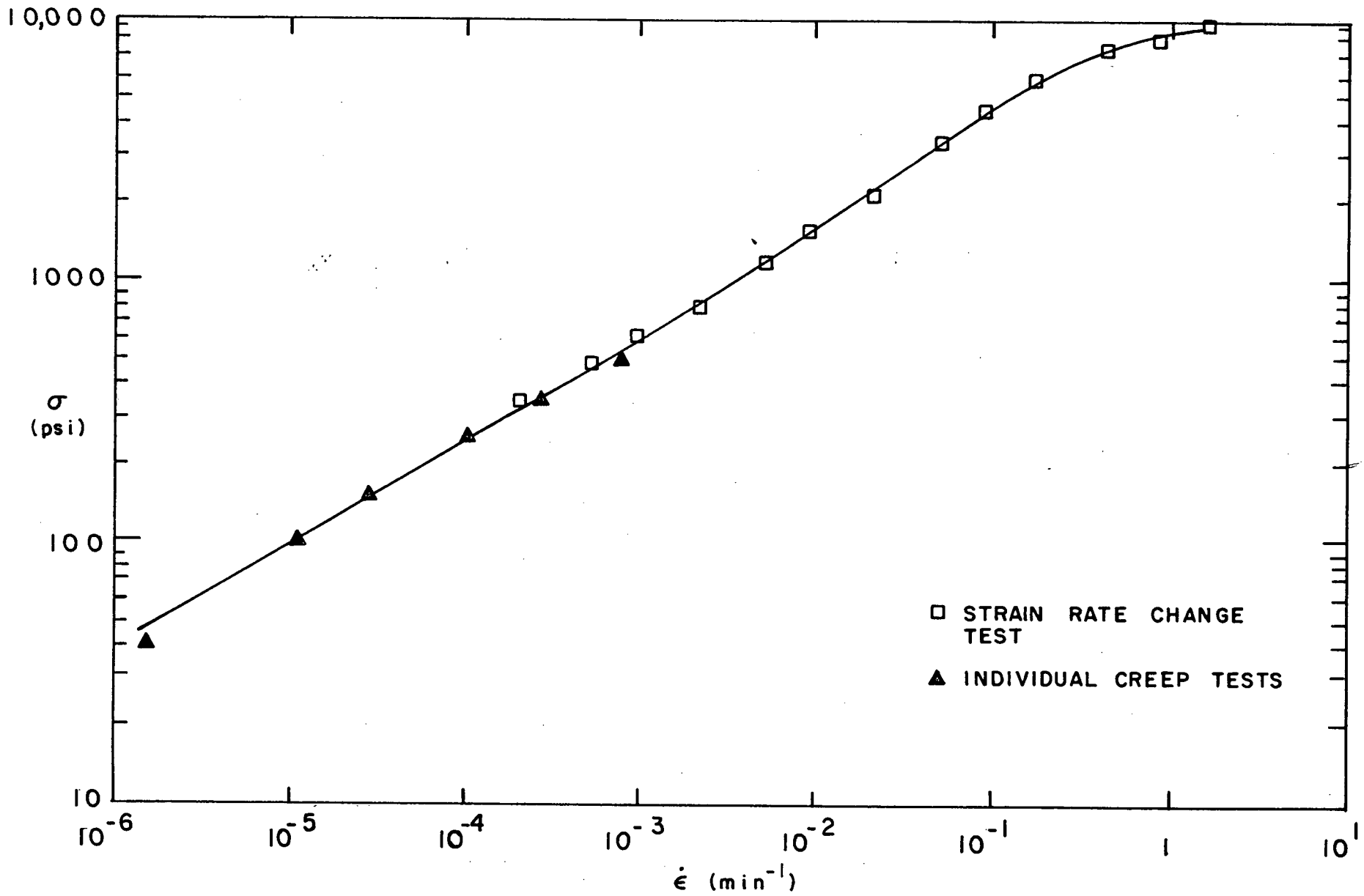


Fig.7. Comparison of Stress-Strain Rate Data Between Single Strain Rate Change Test and Individual Creep Tests.

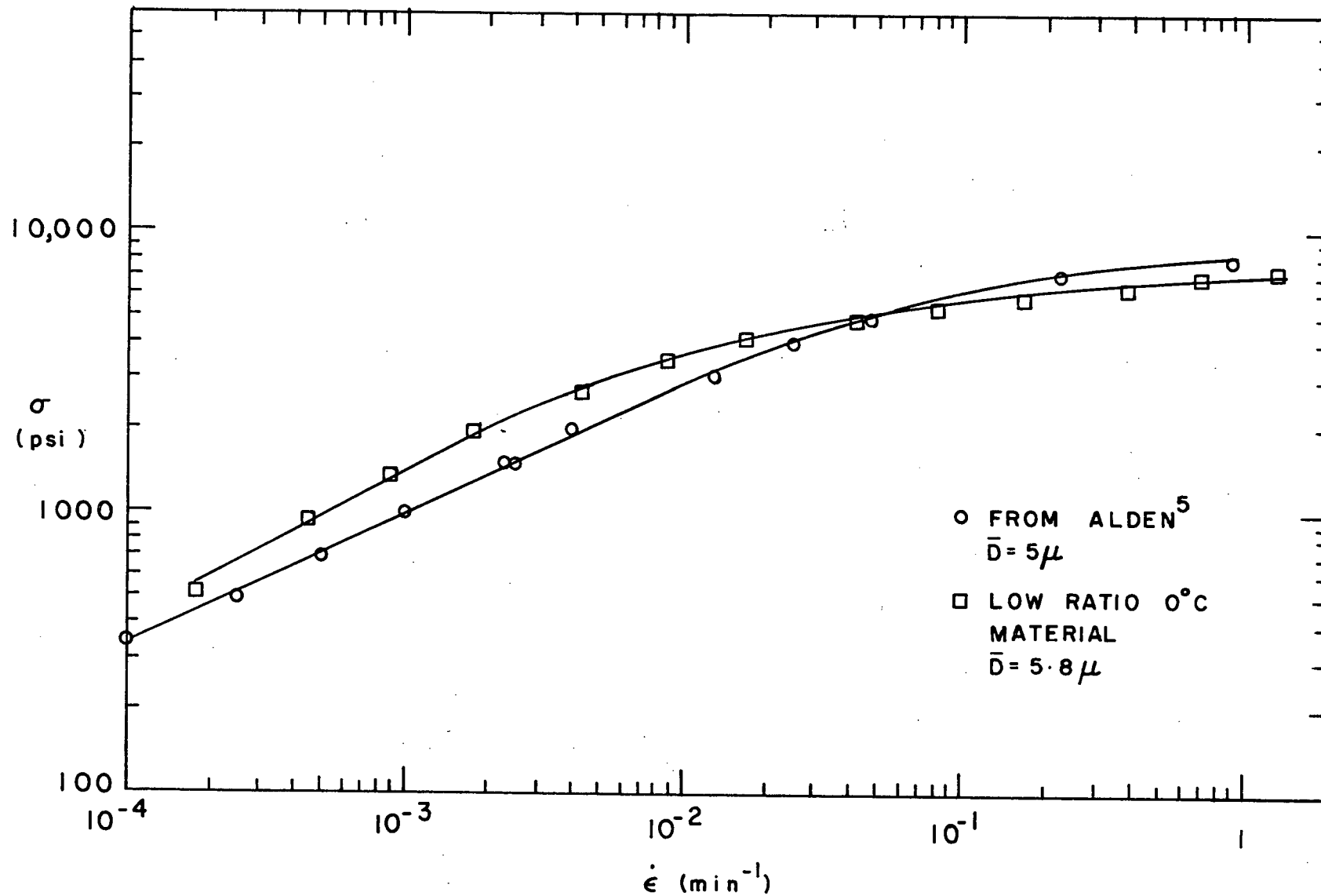


Fig.8. Comparison of Stress-Strain Rate Data Between Present and Previous Investigations.

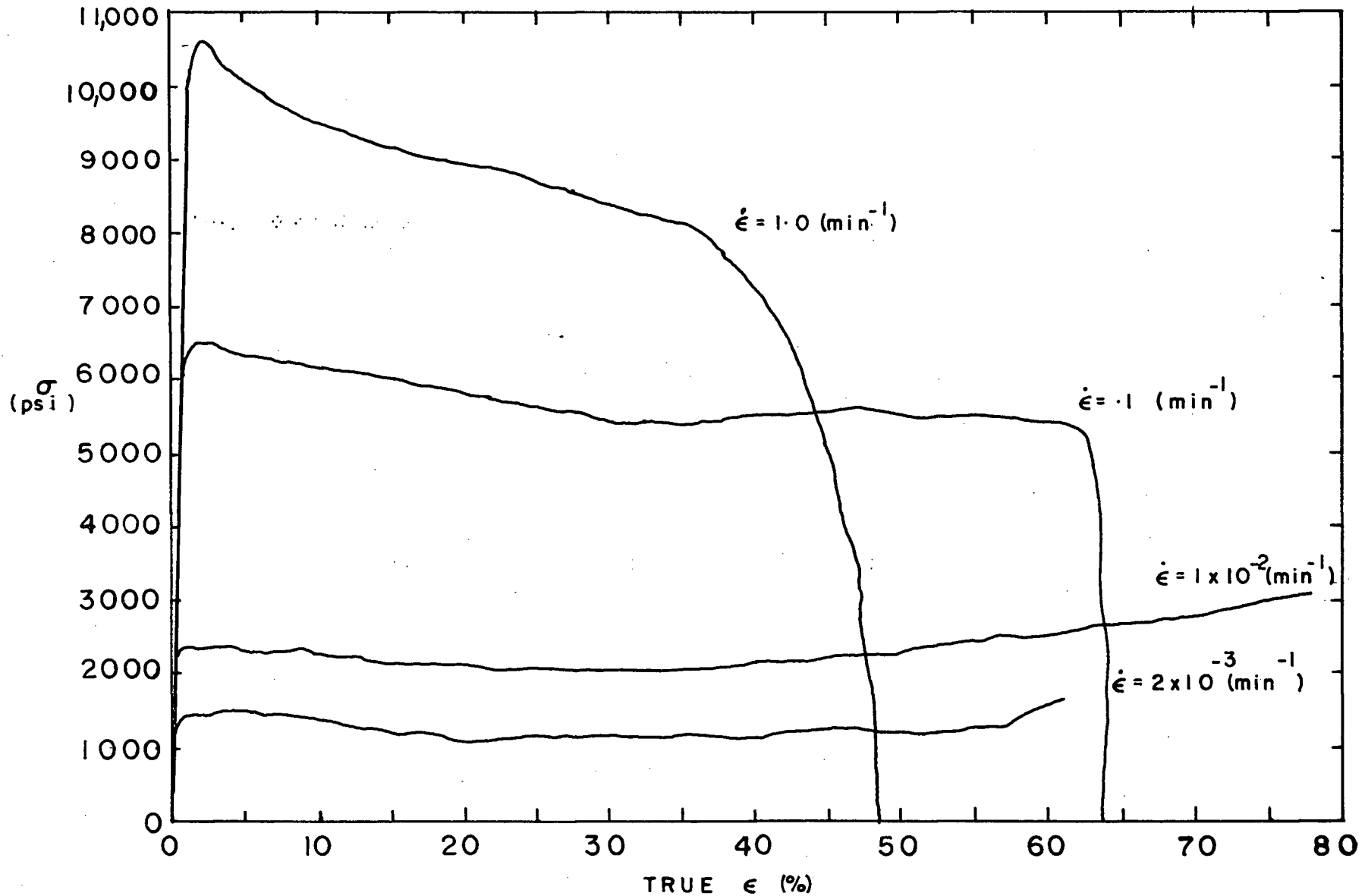


Fig.9. True Stress-True Strain Curves at Various Initial Strain Rates.

instead the flow stress continually decreases until failure. As the strain rate is decreased into the superplastic region the flow stress is maintained relatively constant. At the two lower strain rates in the Stage II region, following an initial decrease, the stress rises with increasing strain, despite the fact that the strain rate is continually decreasing during a constant crosshead speed test. This increase is likely the result of grain growth during the test.

During the low stress level creep tests the strain rate usually decreases continually with time (Figs.10 and 11). A decreasing strain rate with time can be indicative of either primary creep or increasing grain size. However, in the curves at stresses of 350 and 500 psi a steady state creep rate prevails after very low strains. At these stresses then, the transient or primary creep strain is small. Usually transient strain decreases with decreasing stress<sup>(42)</sup>, therefore, a primary region would not be expected also for the lower stress (< 250 psi) curves. The decreasing strain rate in these curves must be due to grain growth during the deformation. This effect is similar to the rising stress with strain in the constant extension rate tests.

### 3.2 - Grain Growth During Annealing

The grain growth kinetics during annealing at room temperature were studied by measuring the grain size on a plane perpendicular to the wire axis of the extruded rod. If the same sample was used for several determinations at different times it was remicrotomed before each measurement to eliminate any surface effects which could have affected the rate of grain growth. Grain size versus time curves were determined for three types of material; the low ratio material, extruded at room temperature and at 0°C and the high ratio material ex-

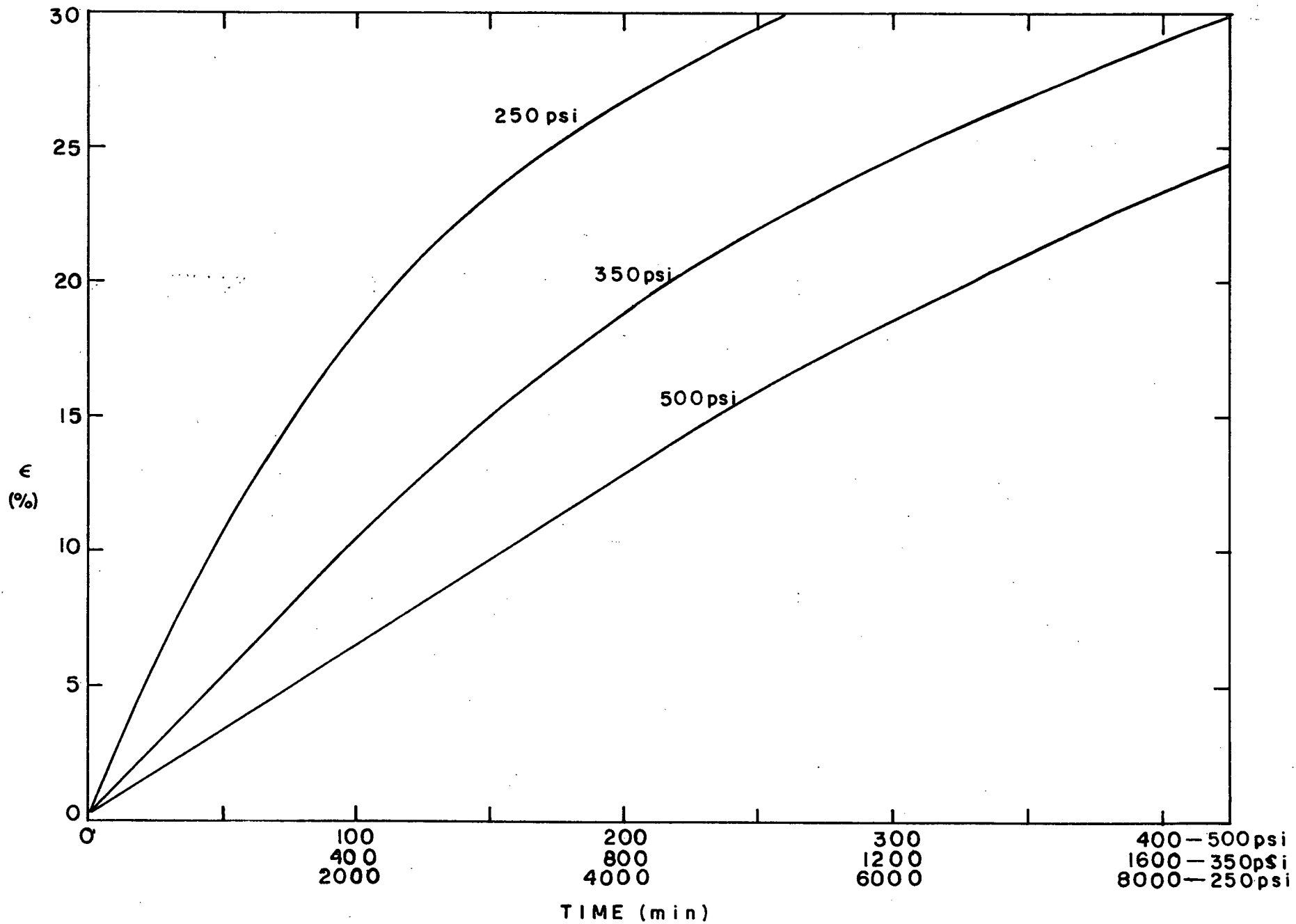


Fig.10. Creep Curves at Stresses of 500, 350 and 250 p.s.i.

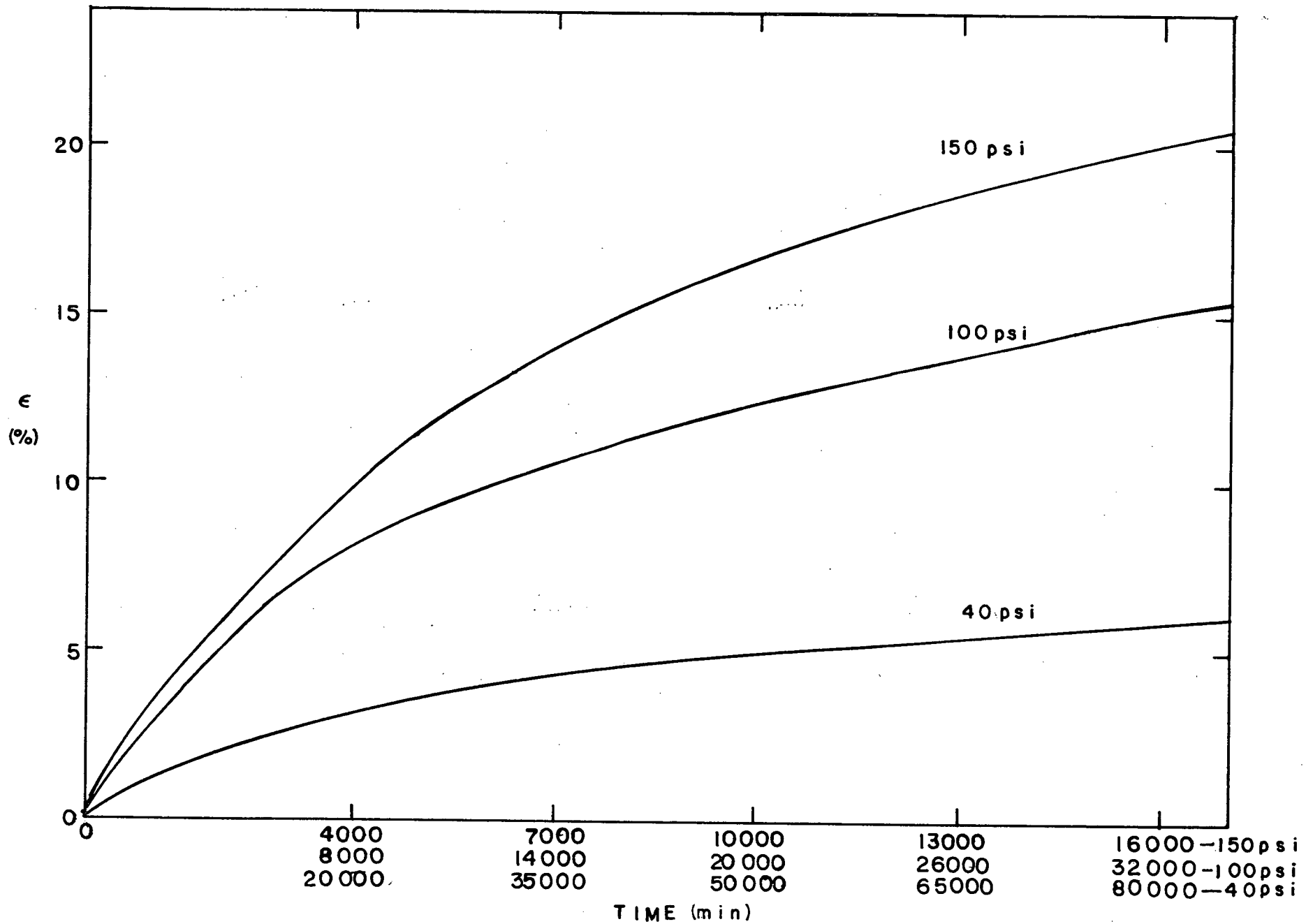


Fig.11. Creep Curves at Stresses of 150, 100 and 40 p.s.i.

truded at room temperature (Figs. 12 - 15). On the log - log scale the grain size - time curves are S-shaped with an approximately straight line central portion.

The points in the central region between the vertical lines were used to determine the constants,  $k$  and  $n$ , in a power law equation;  $\bar{D} = kt^n$ , by a least squares fitting program. The curved portions of the curves at short and long times were estimated visually. The constants,  $k$  and  $n$ , are presented in Table 1 along with the corresponding values of  $r$ , the correlation coefficient, an indication of the goodness of fit of the data. When  $r = 0$  there is no correlation. When  $r = \pm 1$  there is perfect correlation or a perfect fit.

TABLE 1 - Power Law Constants for Grain Size Versus Time Curves

Material	$k$	$n$	$r$
Low Ratio R.T. Extrusion	.0481	.546	.981
Low Ratio 0°C Extrusion	.1208	.455	.998
High Ratio R.T. Extrusion	.1207	.480	.879

In Fig.12, a "theoretical" curve (dashed line) of the form  $\frac{\bar{D}^2}{D_0^2} - \frac{\bar{D}_0^2}{D_0^2} = k^2 t$  is plotted. Several values of  $D_0$  and  $k$  were chosen and curves plotted until the best coincidence between the theoretical and experimental curves was obtained. The best fit was obtained for  $D_0 = 1.8 \mu$  and  $k = .067$ . This theoretical equation seems to represent the growth kinetics reasonably well except at long times and a small portion around 1000 minutes.

In Fig.15, where all three curves are compared without the

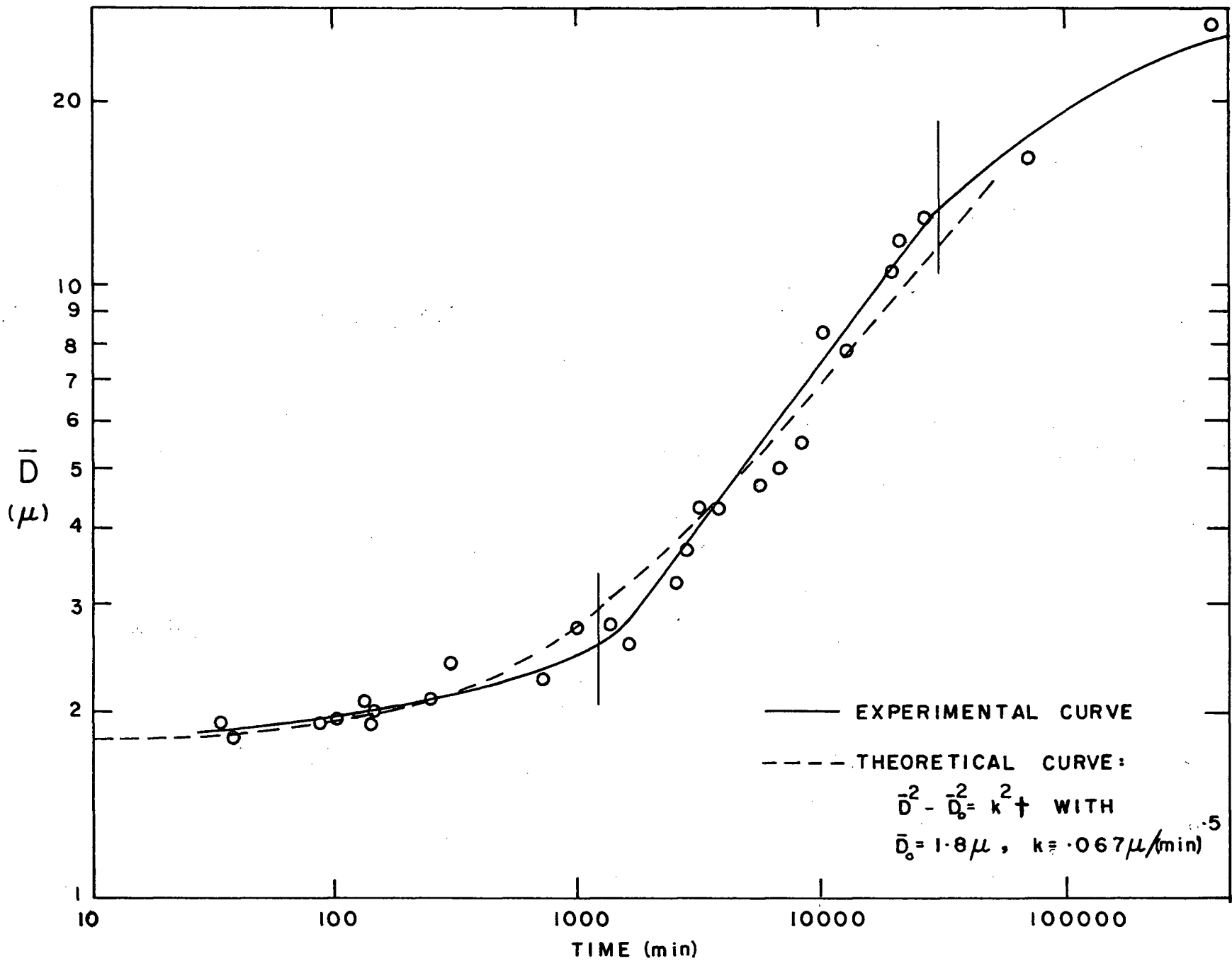


Fig.12. Grain Size versus Time During Static Annealing of Low Ratio Room Temperature Extrusion Material.

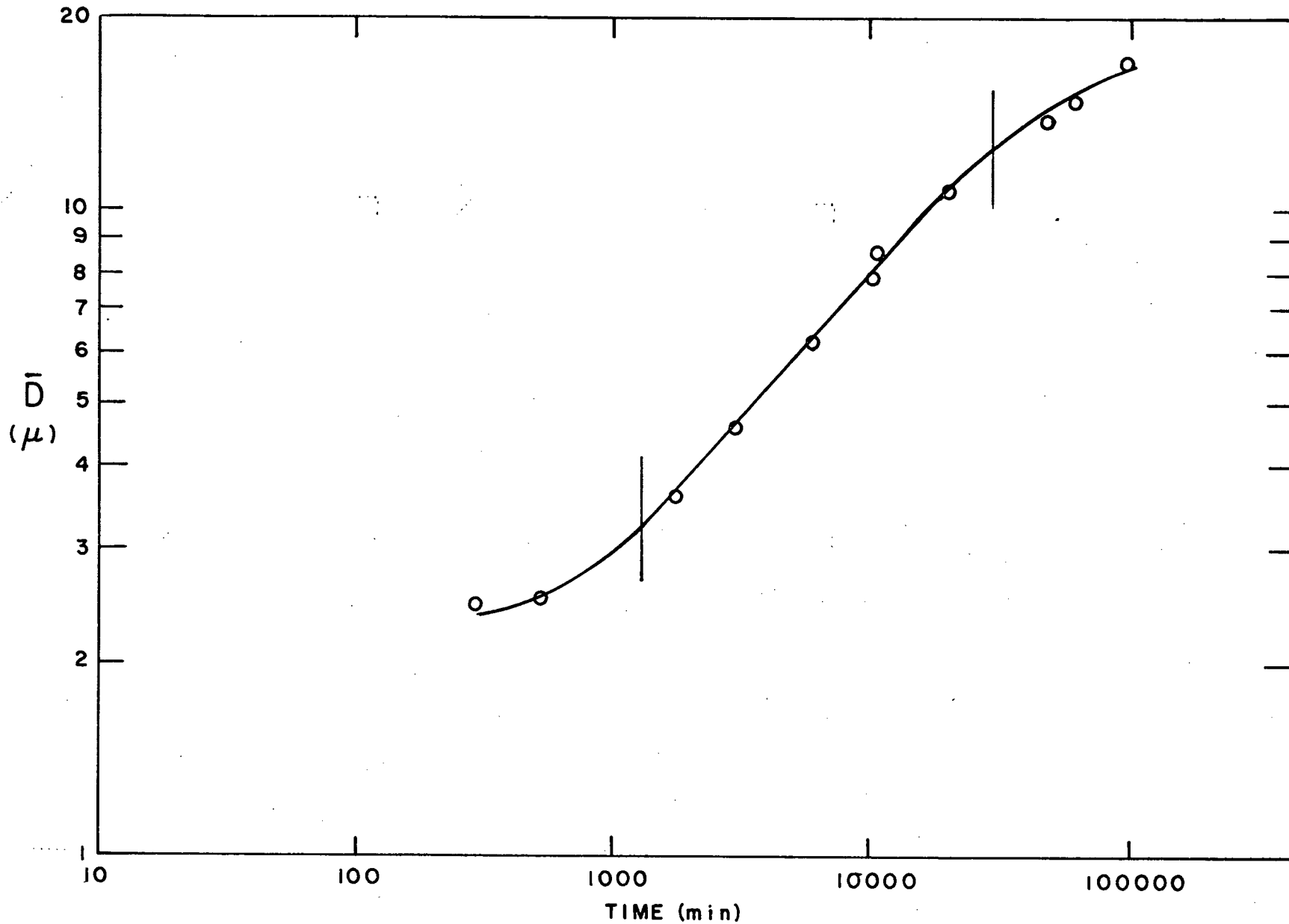


Fig. 13. Grain Size versus Time During Static Annealing of High Ratio Room Temperature Extrusion Material.

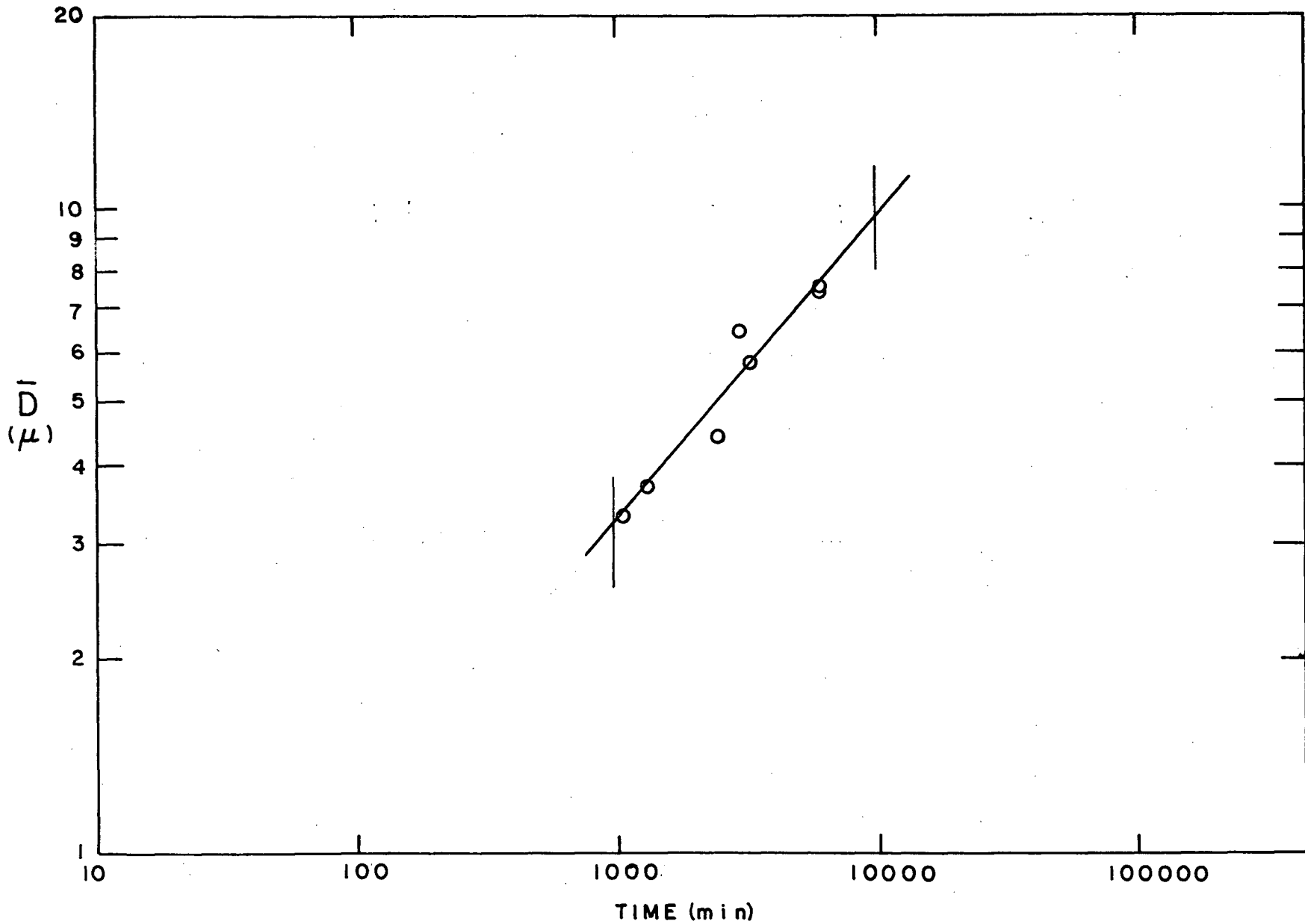


Fig.14. Grain Size versus Time During Static Annealing of Low-

Ratio-0°C Temperature Extrusion Material.

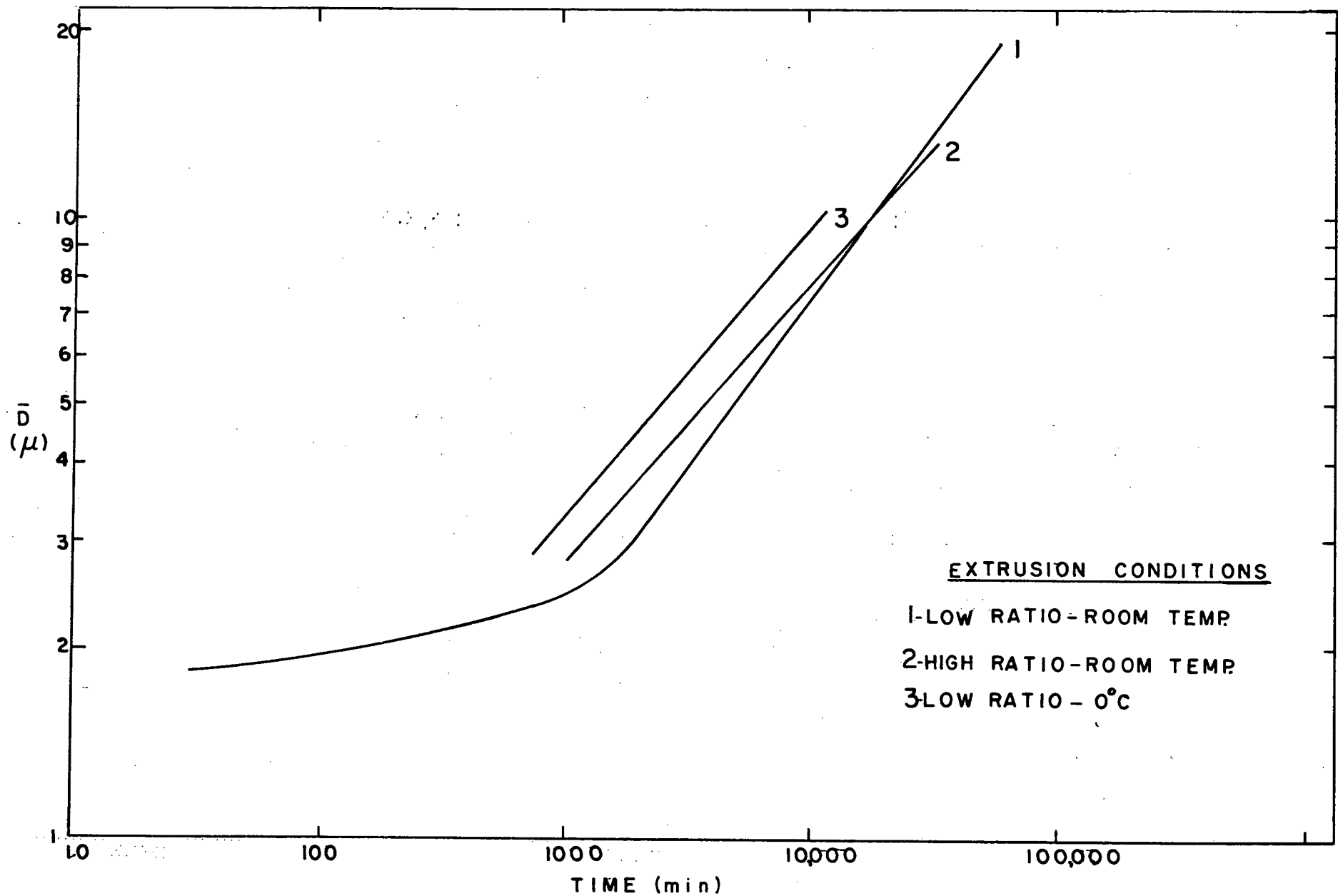


Fig.15. Grain Size versus Time for Different Processing Conditions.

experimental points it is seen that the processing variables had some effect on the grain growth kinetics. The higher extrusion ratio had a small effect causing a slightly lower  $n$  value and higher  $k$ . The lower extrusion temperature had a larger effect producing a higher  $\bar{D}$  than the other curves at the same time despite the fact that it would be expected to have a smaller recrystallized grain size ( $\bar{D}_0$ ).

### 3.3 - Grain Growth During Deformation.

#### 3.3.1 - Effect of Deformation Time

The grain size, as determined immediately after deformation will subsequently be referred to as "deformed grain size" and will be compared to the "annealed grain size" taken from the curves in Figs. 12 to 14 at the time required for the deformation.

One series of tests was performed on the room temperature extruded low ratio material using Instron tests at four different strain rates. A second series was carried out on the high ratio material using creep tests at several stress levels. In both series, at each stress level or strain rate, samples were tested to different amounts of strain and the grain size measured immediately after testing. In Figs. 16 and 17 the deformation grain size is plotted against the testing time for both series of tests along with the annealed grain size curves. All curves through the experimental points were drawn using regression analysis to the power law equation, except for the two lowest strain rates in Fig. 17. The constants,  $k$  and  $n$ , and the correlation coefficient  $r$  are presented in Table 2.

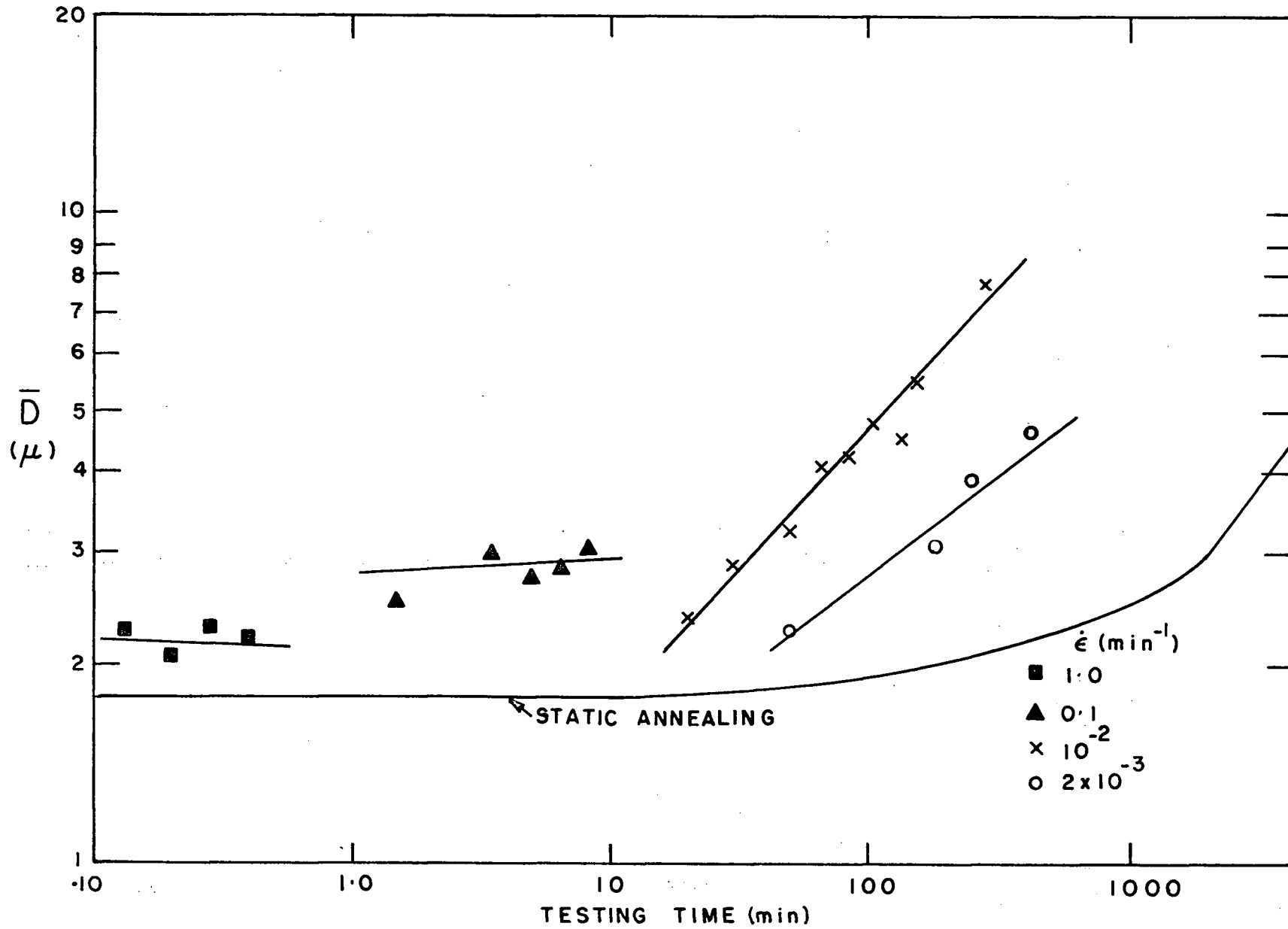


Fig.16. Grain Size versus Time During Instron Deformation

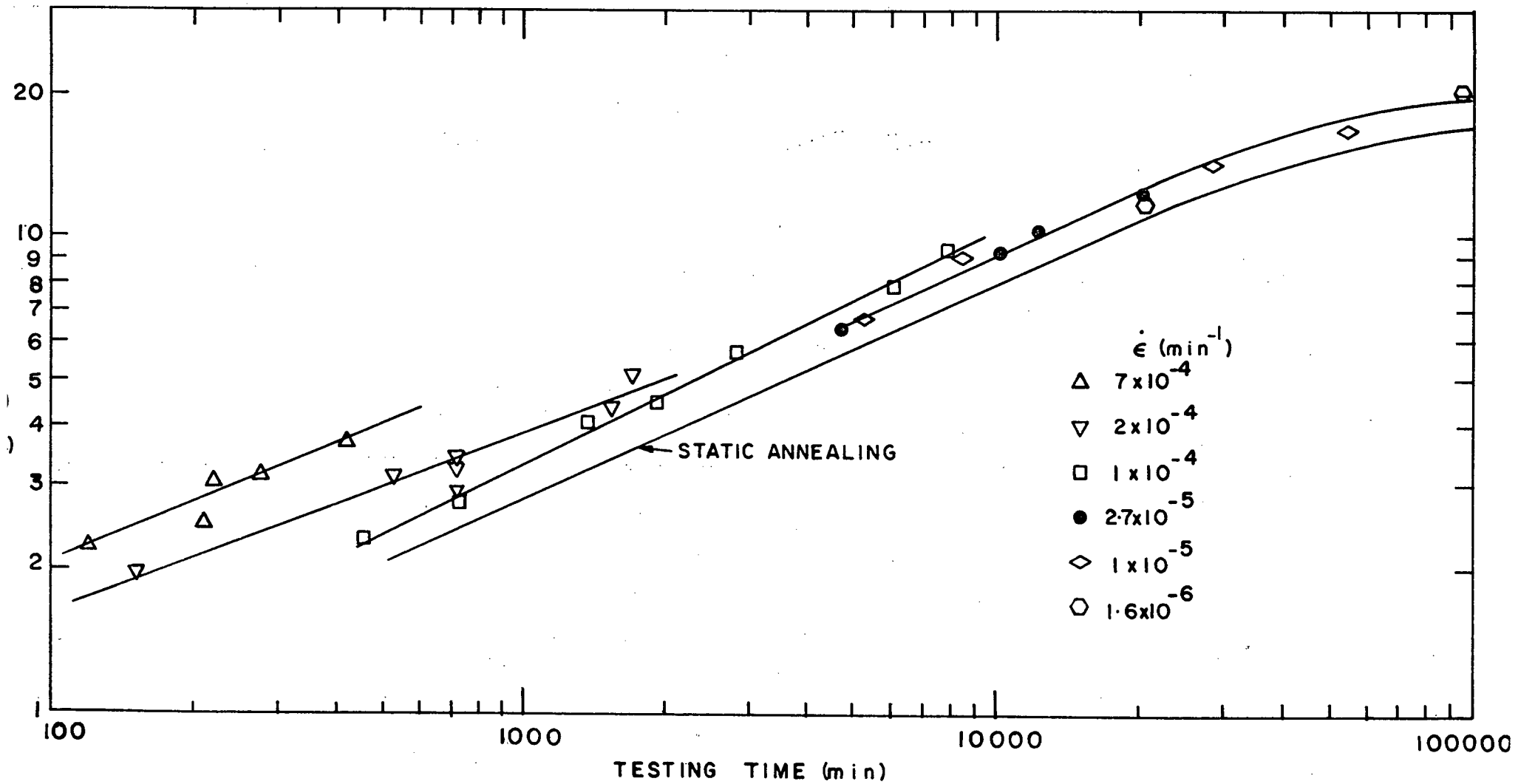


Fig.17. Grain Size versus Time During Creep Deformation.

TABLE 2 - Power Law Constants for Grain Size Versus Time Curves During Deformation

Strain Rate /min.	k	n	r
1.0	2.127	-.0162	-.211
.0	2.82	.0196	.152
$10^{-2}$	.640	.433	.985
$2 \times 10^{-3}$	.677	.308	.967
$7 \times 10^{-4}$	.353	.386	.868
$2 \times 10^{-4}$	.296	.374	.987
$1 \times 10^{-4}$	.108	.496	.998
$2.7 \times 10^{-5}$	.138	.454	.998

All strain rates produced an increase in the grain size. Except for the two highest strain rates, the "n" values remain between .3 and .5 regardless of strain rate. At strain rates below  $10^{-4}$ /min., the deformation causes an upward shift of the annealed curve independent of the strain rate and "k" remains constant. At the higher rates ( $> 2 \times 10^{-4}$ /min.) the value of "k" increases with strain rate.

### 3.3.2. Effect of Strain

The change in grain size with strain was also studied using these tests. In order to eliminate the effect of different amounts of annealed grain growth occurring at the different strain rates a value

$\frac{\Delta \bar{D}}{\bar{D}_A}$  was defined and plotted against true strain (Figs.18 and 19).

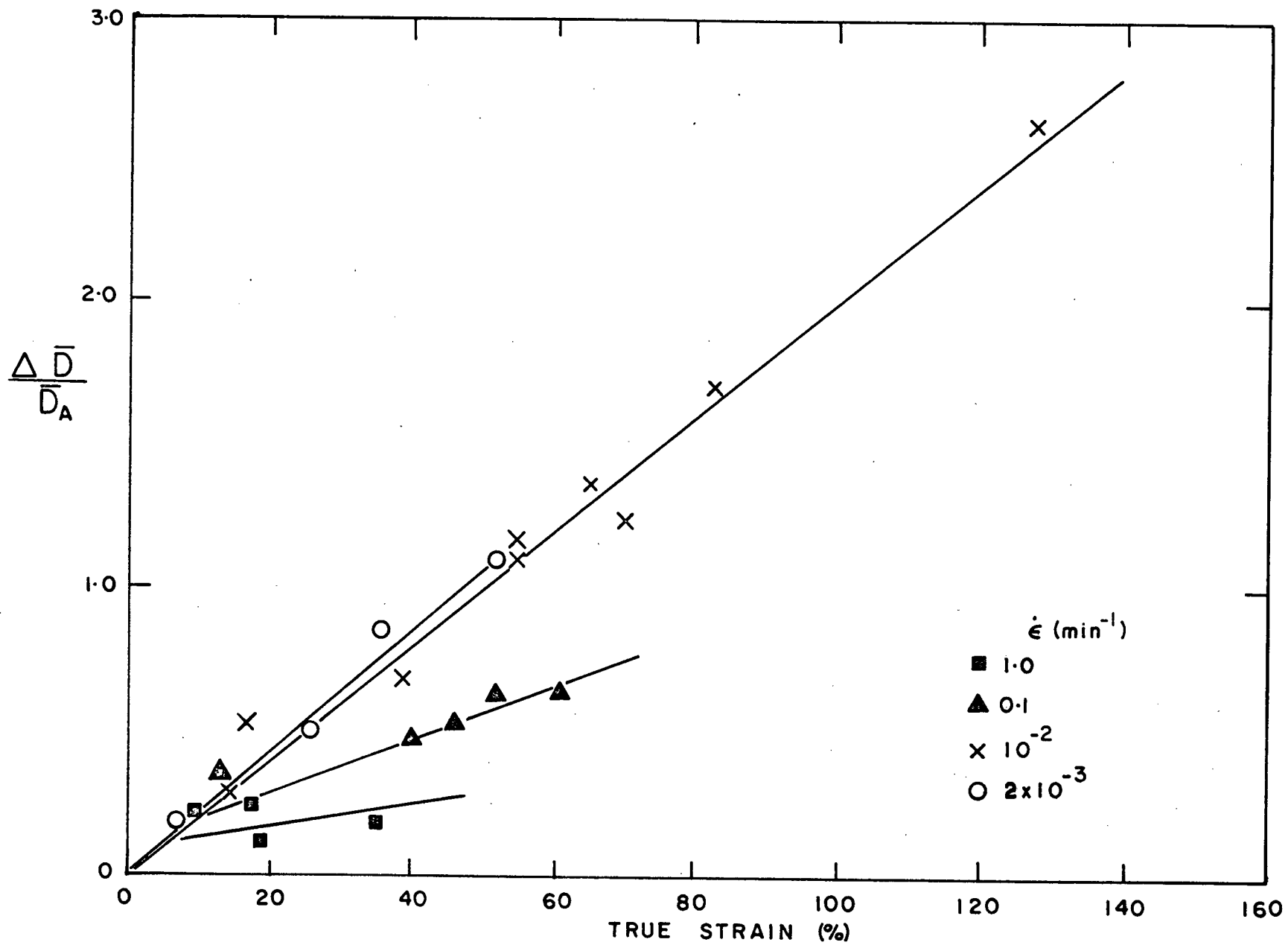


Fig.18. Relative Grain Size Change versus Strain During Instron Deformation.

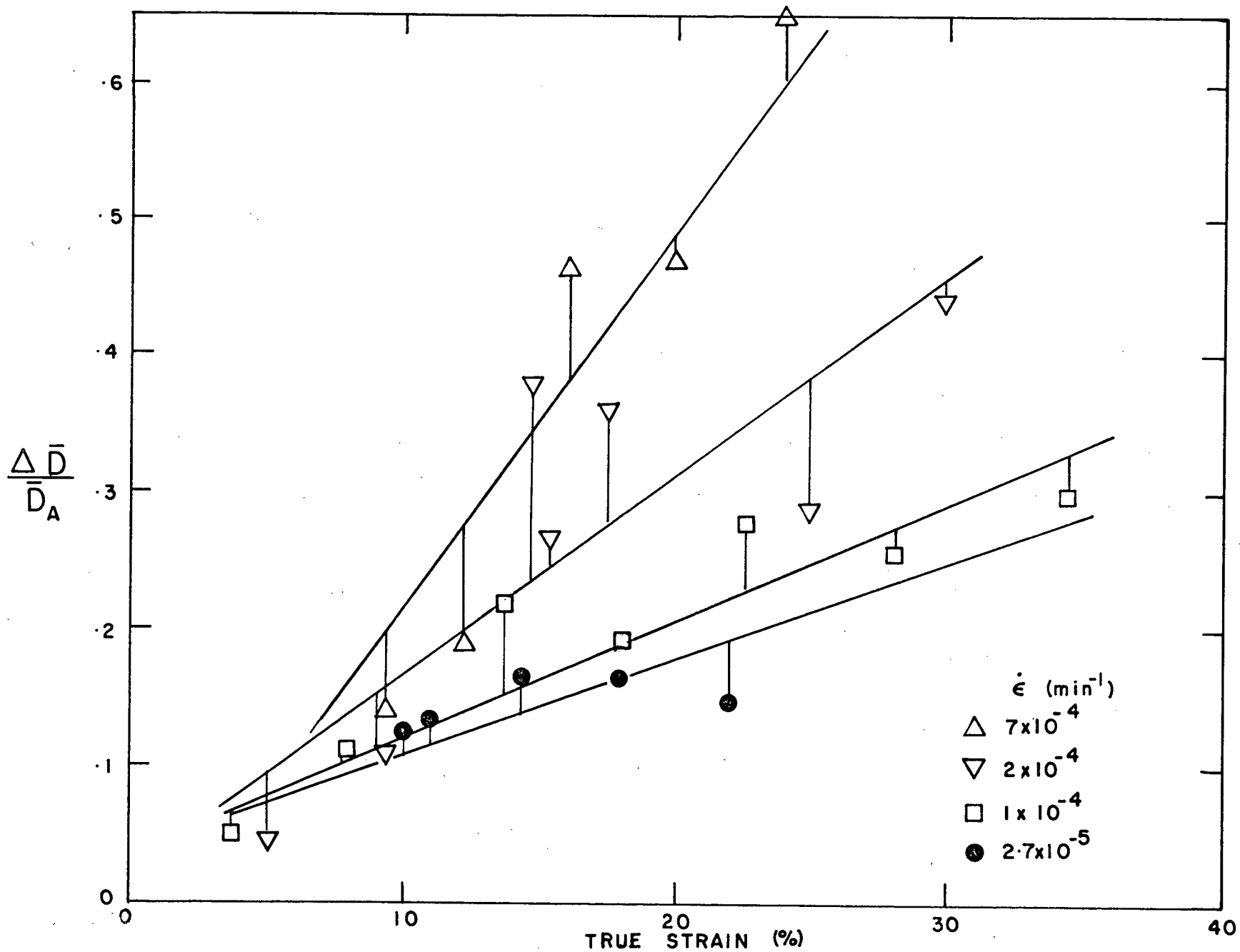


Fig.19. Relative Grain Size Change versus Strain During Creep Deformation.

$\overline{\Delta D}$  is defined as the difference between the deformation grain size,  $\overline{D}_D$ , and the annealed grain size,  $\overline{D}_A$ , after the time required for deformation. In other words  $\frac{\overline{\Delta D}}{\overline{D}_A}$  is the relative additional increase in grain size due to the deformation.

Regression analysis was used to determine the best fit straight lines at each strain rate. The constants, M and b, in the equation:

$$\frac{\overline{\Delta D}}{\overline{D}_A} = M \epsilon + b$$

and the correlation coefficient, r, are given in Table 3.

TABLE 3 - Straight Line Constants for Relative Grain Size Change Versus Strain Curves

$\dot{\epsilon}$ ( $\text{min}^{-1}$ )	M ( $\%^{-1}$ )	b	r
1.0	.004	.086	.537
.1	.0094	.100	.946
$10^{-2}$	.020	.015	.992
$2 \times 10^{-3}$	.021	.012	.994
$7 \times 10^{-4}$	.028	-.059	.959
$2 \times 10^{-4}$	.015	.020	.879
$1 \times 10^{-4}$	.009	.035	.944
$2.8 \times 10^{-5}$	.007	.032	.876

The amount of grain size enhancement at a given value of strain (25%) first increases, then decreases with continually decreasing strain rate (Fig.20). The error bars in Fig.20 indicate the standard error of

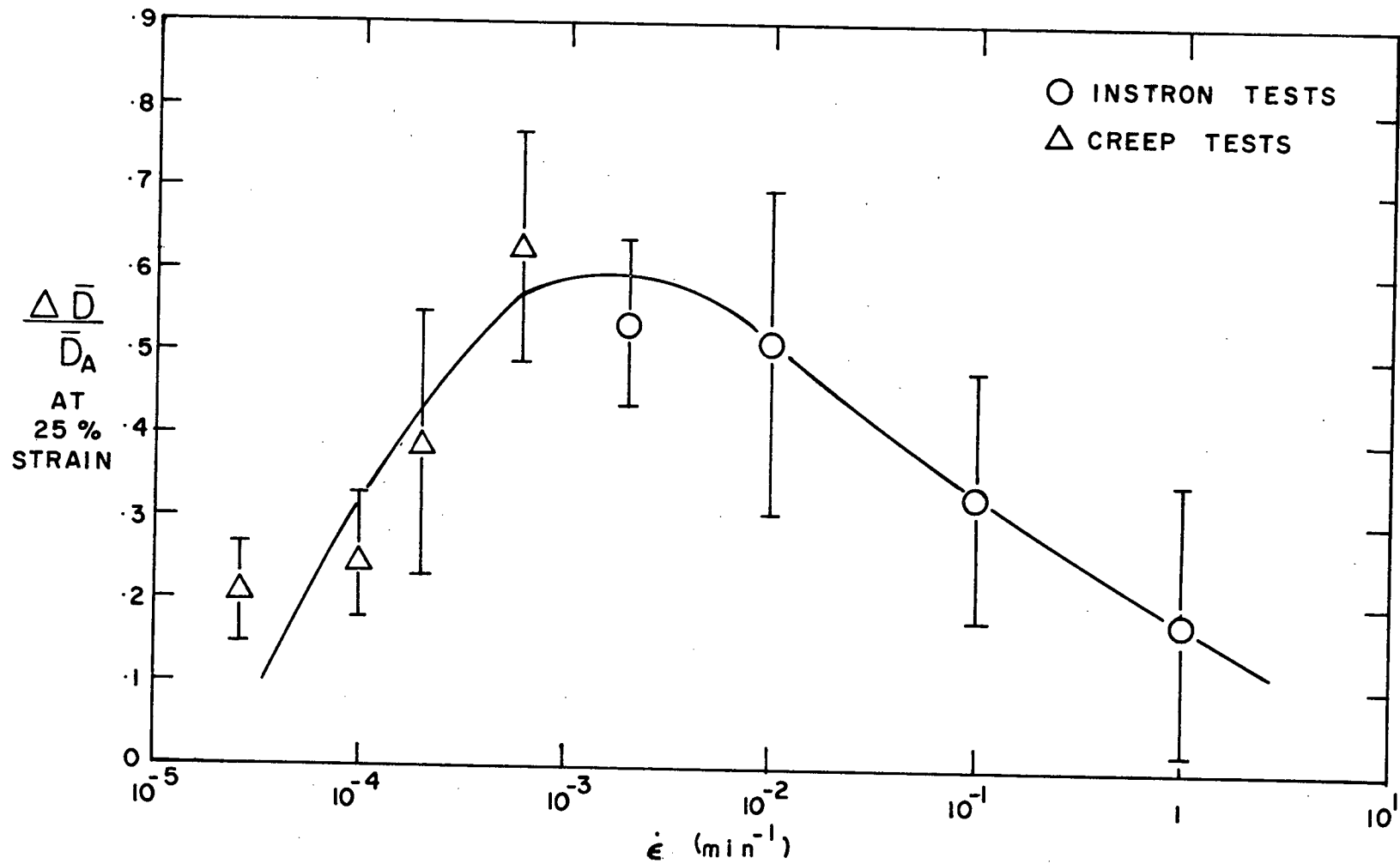


Fig.20. Relative Grain Size Change After 25% Strain versus Strain Rate.

estimate of the regression lines at the 95% confidence level. There is little correlation between the degree of grain size enhancement and "m" value, (Fig.21) in the high "m" regions. However,  $\frac{\Delta\bar{D}}{\bar{D}_A}$  does increase with "m" in the transition region between Stage II and Stage III.

### 3.3.3. - Grain Elongation

The grain size in the longitudinal direction ( $\bar{D}_L$ ) and the transverse direction ( $\bar{D}_T$ ) were determined for a series of specimen's deformed approximately 35% at different strain rates. Using Rachinger's<sup>(43)</sup> analysis, the amount of strain due to slip (or other grain elongation processes) can be calculated from the rate  $\bar{D}_L/\bar{D}_T$  by the formula:

$$\epsilon_{\text{slip}} = \left( \frac{\bar{D}_L}{\bar{D}_T} \right)^{\frac{2}{3}} - 1$$

The percentage of the deformation due to elongation processes can then be calculated (Fig.22). The contribution of grain elongation to the strain appears to increase with decreasing strain rate from the high m region ( $\dot{\epsilon} = 10^{-2}/\text{min.}$ ) to the lower m Stage I region. At the higher strain rates (Stage II - Stage III transition region) the contribution may also increase slightly.

### 3.3.4. - Alternating Tension - Compression

Tension-compression tests were carried out on the low extrusion ratio, 0°C extrusion temperature material. The specimens were annealed for 4 hours before testing while the epoxy used for gripping hardened. The stress-strain cycle used for the test is illustrated in Fig.23. The stress at 2% strain on each half cycle (Fig.23) remained fairly constant

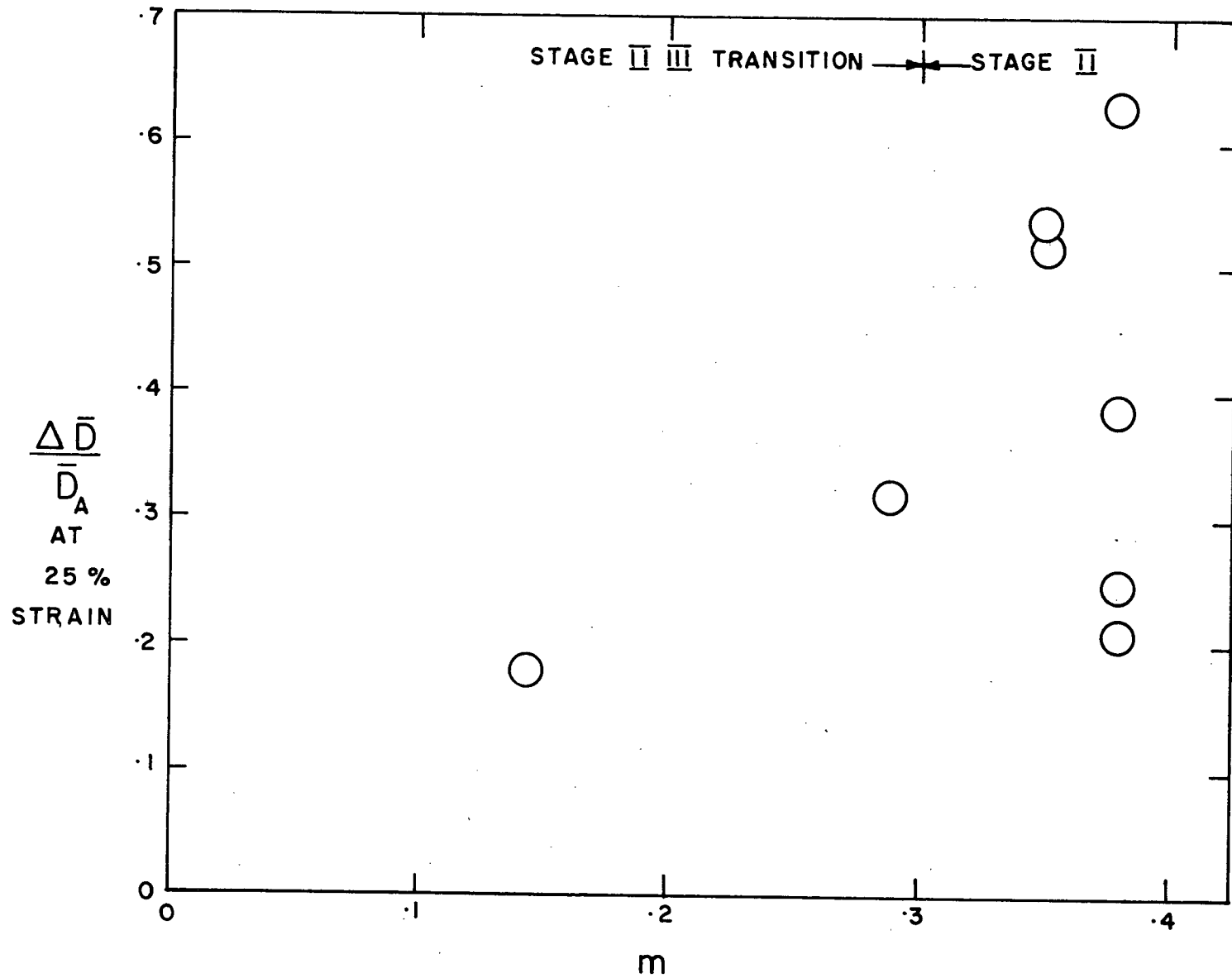


Fig.21. Relative Grain Size Change After 25% Strain versus "m".

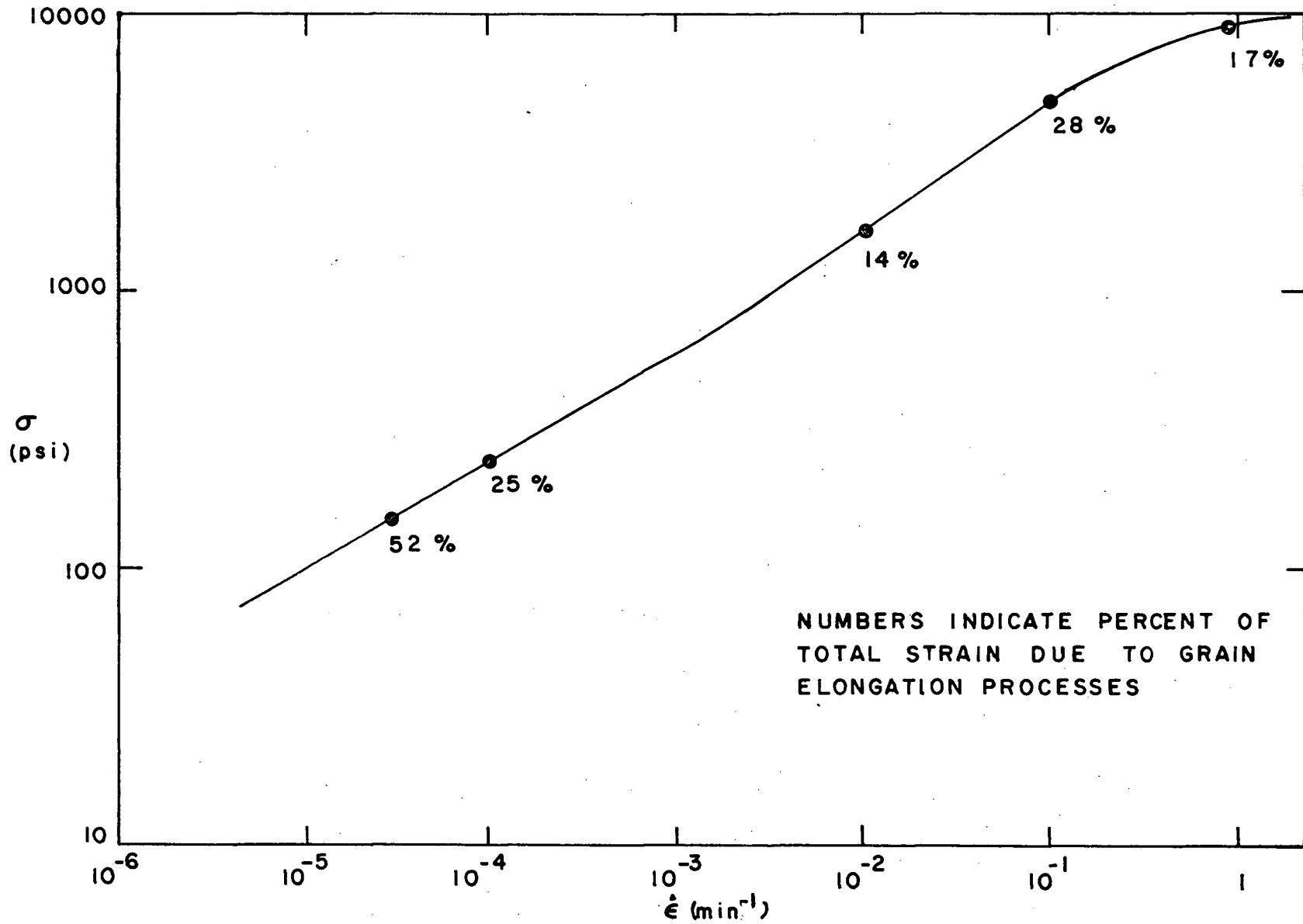
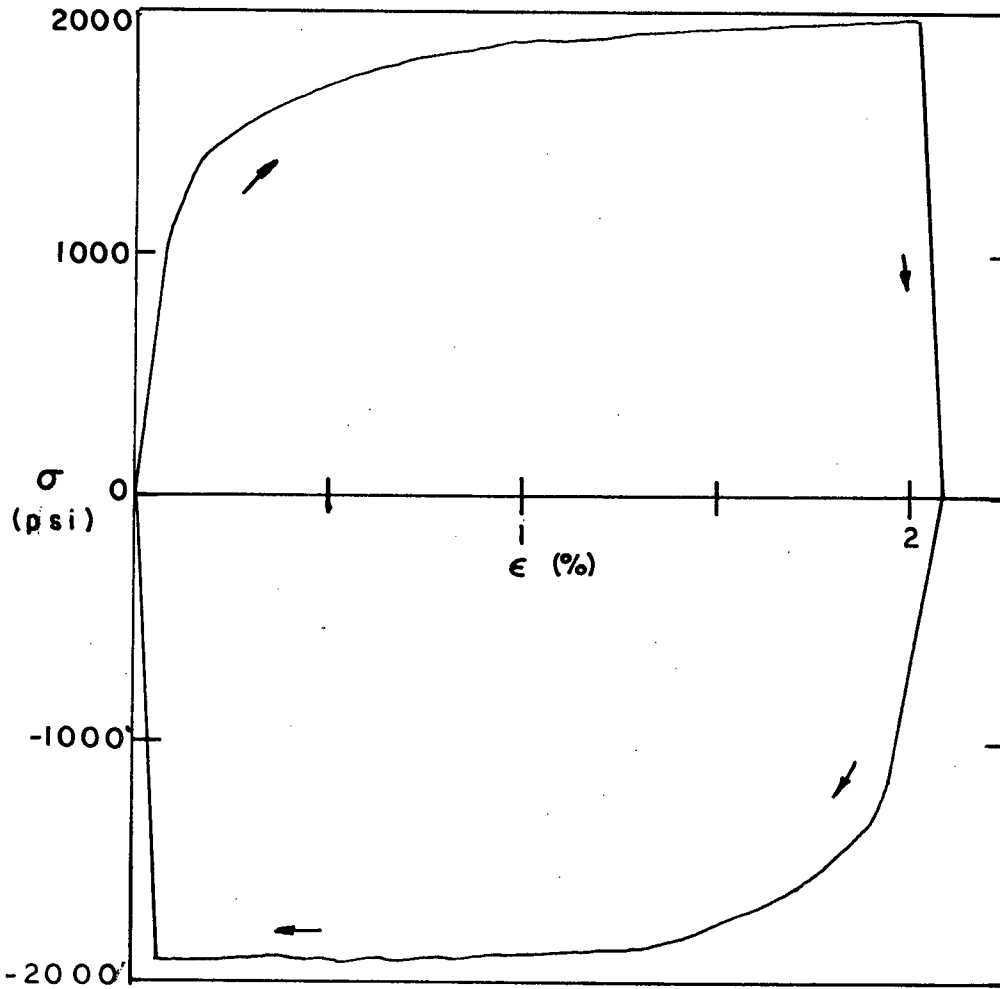
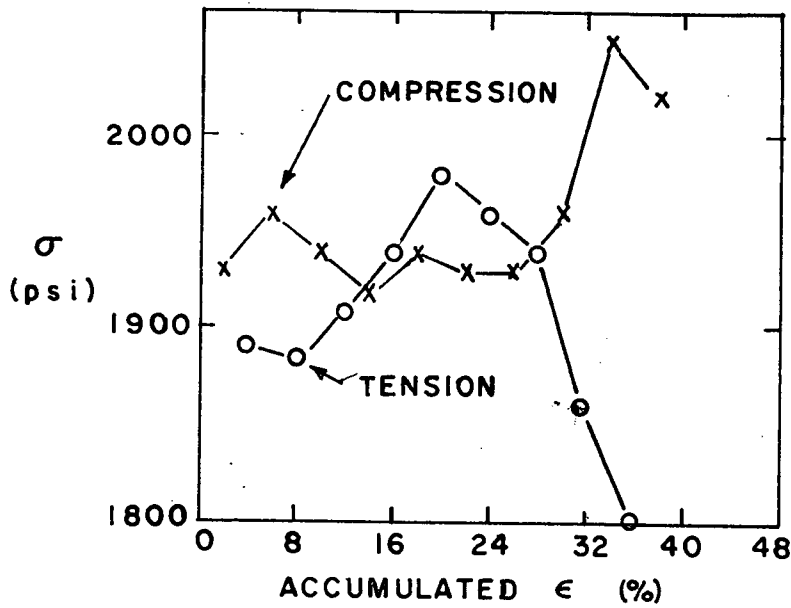


Fig.22. Degree of Grain Elongation After 35% Strain at Various Strain Rates.



a) TYPICAL CYCLE



b) FLOW STRESS AT END OF EACH CYCLE

Fig.23. Stress-Strain Relationships During Tension-Compression Testing.

with the accumulated strain until the last cycle when the specimen seemed to start slipping from the grips. The test was then terminated, grain size measured and X-rays taken.

Because several minutes were required to change the direction of the stress due to slack in the grips and testing machine, a control sample was needed for comparison. After the 4 hour anneal, the control sample was strained to 2% strain, in tension, unloaded to zero stress and annealed for the equivalent length of time needed to reverse the machine to the compression cycle. The 2% strain tension cycle was then repeated a number of times until the total time of testing and the strain cycles were the same as in the tension-compression test. The control sample had a total tensile strain of 38% whereas the tension-compression sample had a net tensile strain of only 2%. The measured grain size after testing was 3.70 microns for the tension-compression specimen compared to 3.30 microns for the control sample. Thus, it would appear that reversing the direction of the strain has little effect on the grain size enhancement.

### 3.3.5 - Grain Type Distribution

The grain "type" was defined as the number of sides possessed by an individual grain in the plane of examination. The distribution of types was determined by counting the number of sides of each grain inside a certain area. A sample was deformed in creep at an initial strain rate of  $2.8 \times 10^{-5}$ /min. to a strain of 14% and micrographs taken of the deformed section and the undeformed grip section. The grip section represents a static anneal of equivalent time (10,000 minutes). The grain sizes of the two sections were  $9.34 \mu$  for the deformed and  $7.9 \mu$

for the undeformed. Both distributions are of similar form (Fig.24) except for an increase in relative frequency of 8, 9 and 10 sided grains in the deformed specimen compared to the undeformed. Grains having less than 6 sides appeared slightly less frequently in the deformed material.

The cumulative frequency distributions (Fig.25) are plotted with the grain type on a logarithmic scale. Both curves are close to a straight line plotted in this fashion, although the deformed distribution departs slightly from the straight line at the upper end. A straight line relationship on these scales indicates a "log-normal" distribution in agreement with results of Feltham<sup>(44)</sup> on annealed aluminum. This form of the distribution appears to be typical of annealed materials where the driving force for grain growth is surface energy<sup>(45)</sup>.

A Chi-square test for comparing distributions was performed on these two distributions and showed that they differed significantly at the 97.5% confidence level. A difference of means test, performed on the two distributions showed that the distribution means differed at only the 57% confidence level.

### 3.3.6 - Grain Size Distributions

Grain size distributions were performed on the same samples used in Section 3.3.5 using the size grouping previously defined. The relative frequency distributions, plotted in Fig.26 show that the deformation has produced a shift of the curve to the right and an increase in the mean grain class. Calculations show a slightly greater dispersion in the distribution after deformation.

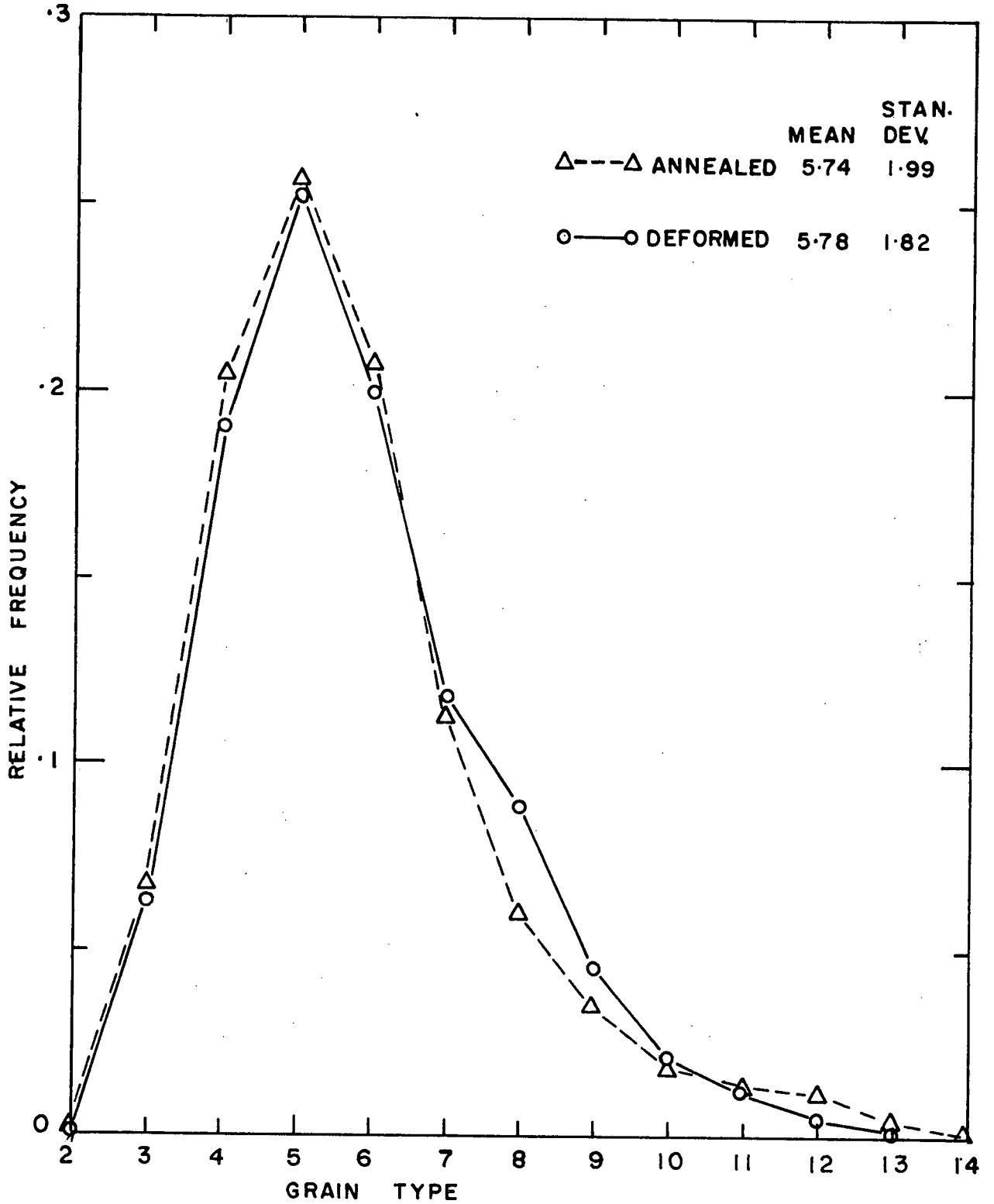


Fig.24. Grain Type Distribution for Annealed and Deformed Structure.

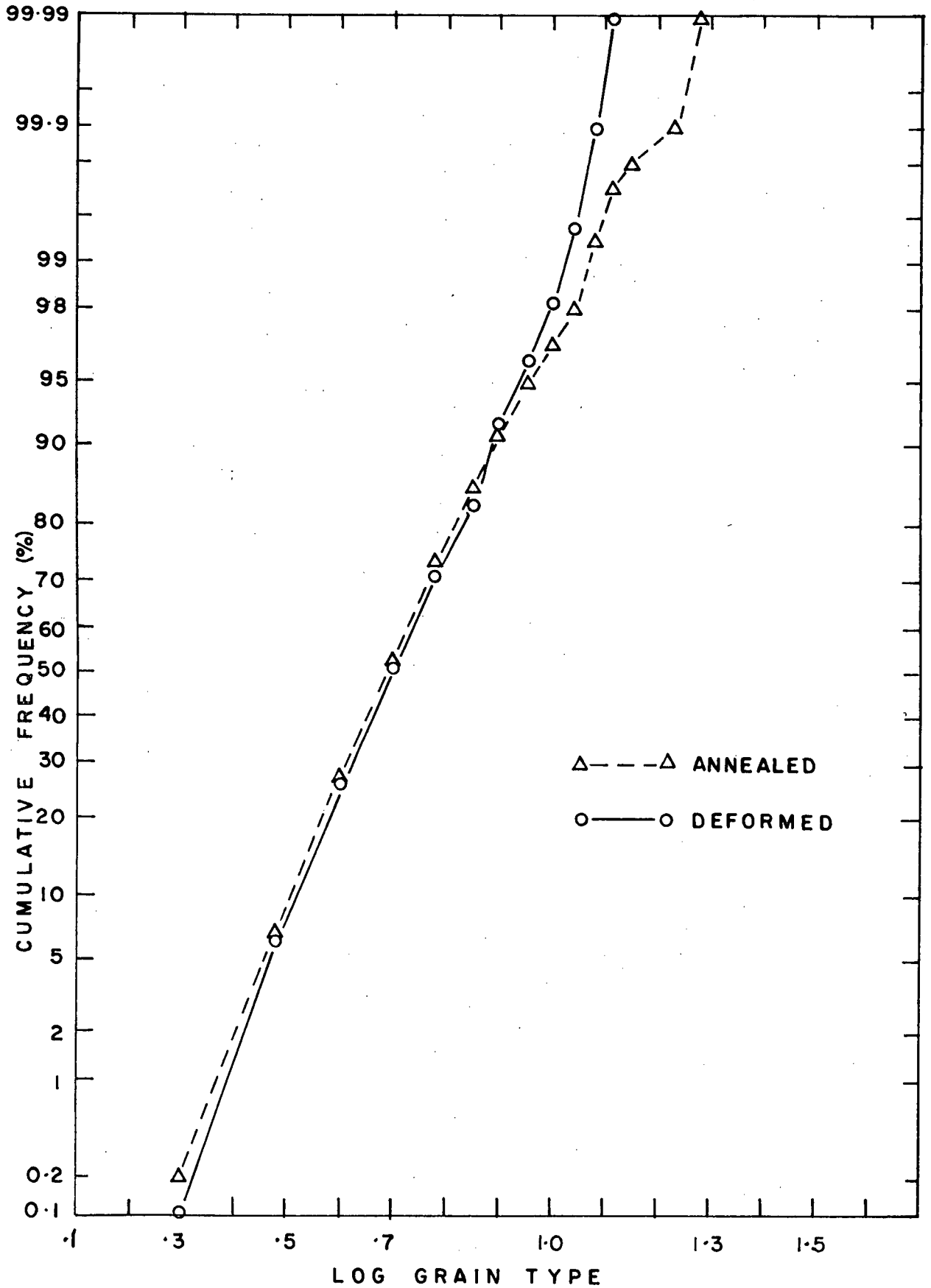


Fig.25. Cumulative Frequency Diagram for Grain Type Distribution of Fig.24.

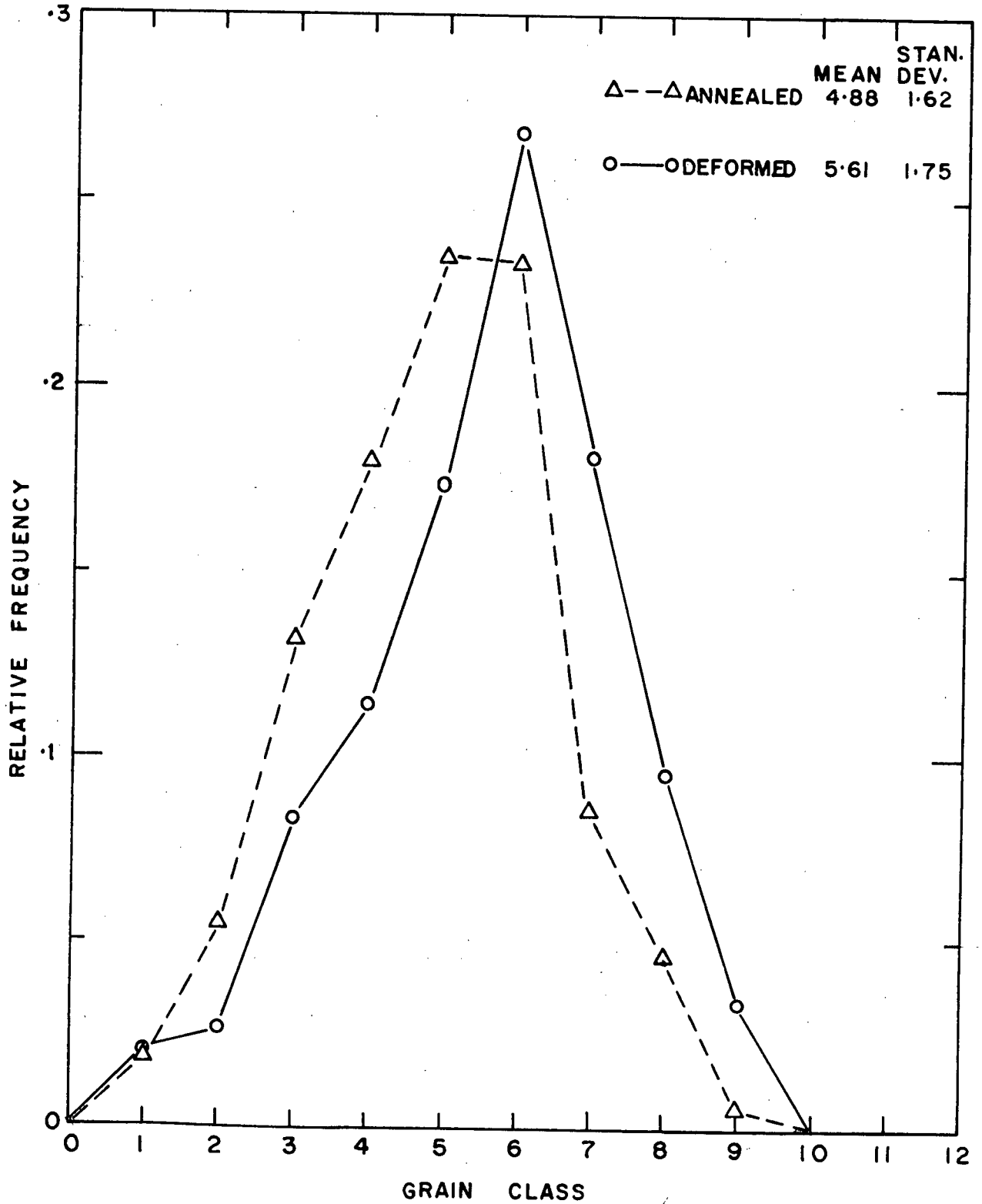


Fig.26. Grain Size Distribution for Annealed and Deformed Structures.

The means of these distributions can be related to the average lineal intercept which has been used as a measure of the grain size previously. The mean grain area in two dimensions<sup>(41)</sup>,

$$\bar{A} = \exp \left[ \ln \bar{A}_G + \frac{(\ln S_{GA})^2}{2} \right] \quad (2)$$

where  $\bar{A}_G$  is the geometric mean of the grain area and  $S_{GA}$  is the geometric standard deviation. Also

$$\ln \bar{A}_G = \bar{m} \ln 2 \quad (3)$$

and  $\ln S_{GA} = S_m \ln 2 \quad (4)$

where  $\bar{m}$  and  $S_m$  are the mean and standard deviation respectively of the grain classes. Thus, a value of  $\bar{A}$  can be calculated using the values of  $\bar{m}$  and  $S_m$  computed for Fig.26. The square root of  $\bar{A}$  can then be compared to  $\bar{D}$ . The calculated values of  $\sqrt{\bar{A}}$  were 10.1 and 7.4 microns for the deformed and annealed samples compared to 9.34 and 7.9 for  $\bar{D}$ . Agreement between the two grain size measuring methods is thus satisfactory.

The cumulative frequency distributions (Fig.27) for two samples again show that the size distributions are essentially log-normal. In order to see if the shapes of the size distributions had been changed by the deformation, distributions of an annealed and deformed sample of equivalent mean grain size should be compared. By shifting the annealed curve to the right to a position where it produced an average grain area or lineal intercept equivalent to the deformed sample such a comparison could be made. Although the dispersion of grain sizes is thought to increase somewhat with annealing<sup>(46)</sup>, it will be assumed that the standard deviation would not change appreciably for this change in

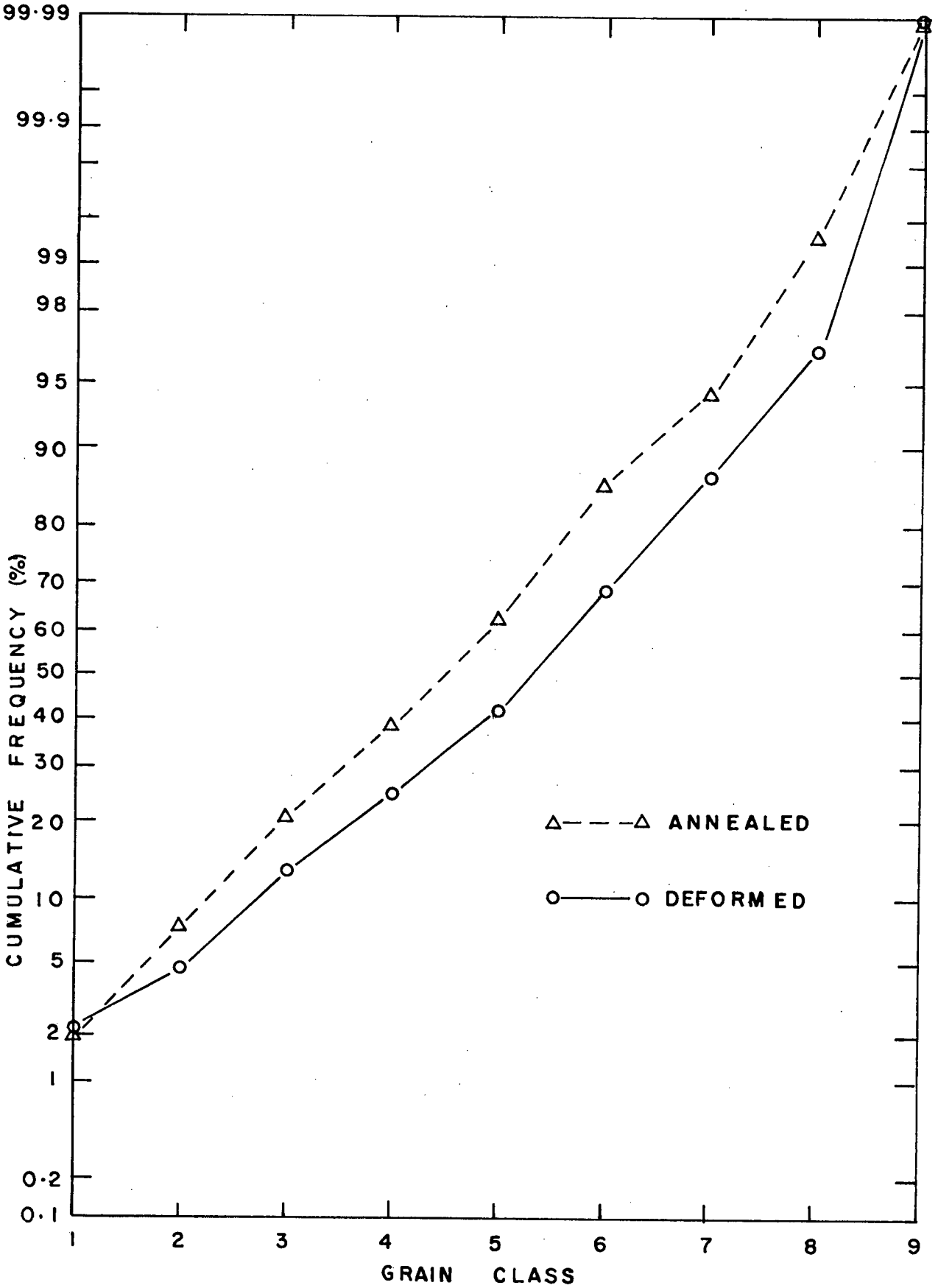


Fig.27. Cumulative Frequency Diagram for Grain Size Distribution of Fig.26.

average grain size (7.4 to 10.1  $\mu$ ). From equation<sup>(2)</sup> a new value of  $\bar{m}$ , the mean grain class, was calculated to give a  $\sqrt{A}$  of 10.1  $\mu$ . The difference between this new  $\bar{m}$  of 5.76 and the old  $\bar{m}$  for the annealed sample (4,88) was the amount that each point on the annealed cumulative frequency plot was shifted to the right. This procedure produced a new annealed distribution with a mean grain class of 5.74 and a standard deviation of 1.63. From the points of this shifted curve a relative frequency distribution was calculated and compared to the deformed frequency distribution curve (Fig.28). These two curves then represent two samples with the same lineal intercept of 10.1, one having been deformed and the other annealed.

Although the deformed sample seems to possess a higher proportion of class 6 sizes no other trends are evident and both curves are basically the same shape. The grain size distribution appears to be unchanged by the deformation process.

### 3.4 - X-Ray Analysis

In the back reflection photographs, a variation in intensity around the circumference of some of the Debye rings was observed (Fig.29) indicating that a texture was present in the as-extruded material. In order to determine the orientation of the fiber axis, the X-ray pattern was first indexed using Bunn charts. It was found that the rings with the most prominent evidence of texture corresponded to reflections from the (442) and (640) planes. By measuring the angle  $\alpha$  (Fig.29) at the centre of the arcs on these rings, the angle  $\rho$  was calculated from the formula<sup>(36)</sup>:

$$\cos \rho = \cos \theta \cos \alpha$$

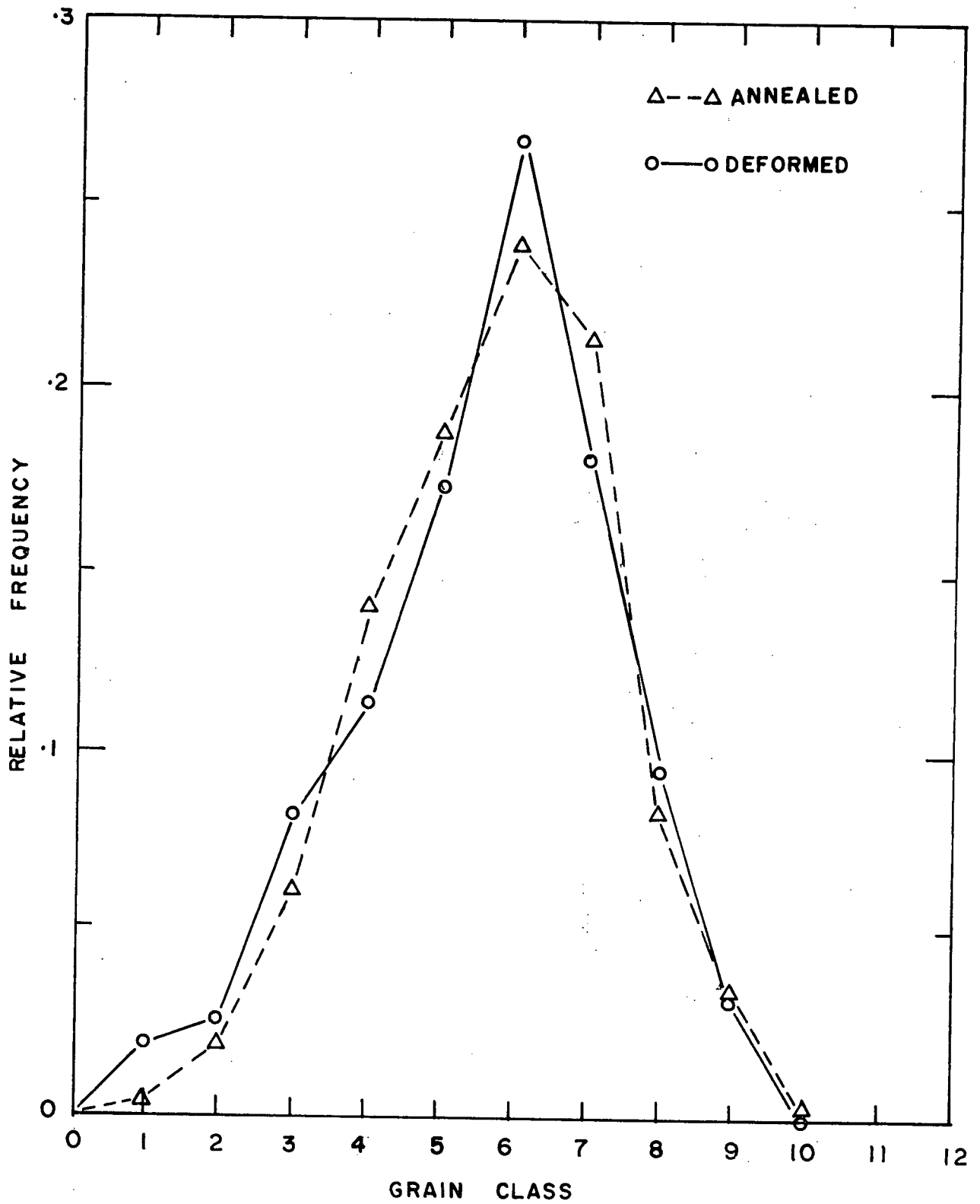


Fig.28. Grain Size Distribution for Annealed and Deformed Structures of Equivalent Mean Grain Size.

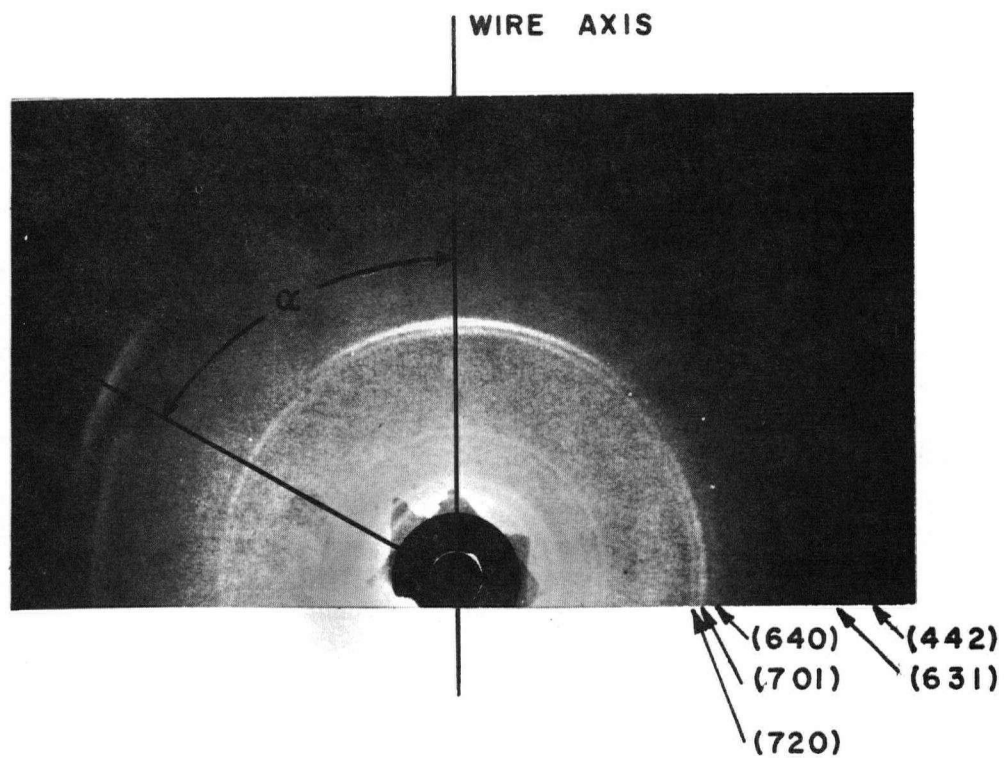


Fig.29. Back Reflection Pattern for Extruded Rod.

where  $\rho$  is the angle between the normal to the plane in question, and the fiber axis. By a graphical method (Fig.30), the location at the fiber axis was then found to be within  $14^\circ$  of a  $[\bar{1}\bar{1}0]$  pole of the crystal (Fig.30). In other words, a large proportion of the crystals were aligned with a  $[110]$  pole almost parallel to the direction of the wire axis.

A  $[110]$  pole figure was plotted in Fig.31, with the solid lines representing the location of two of the  $[110]$  poles calculated from the centre of the Debye arcs. The dotted lines are the locations of the poles at the point where the intensity of the Debye arc falls to one half of the peak intensity. These dotted lines then indicate the strength or degree of perfection of the texture.

The strength of the texture was measured with the microdensitometer by determining the relative intensity of the arc of the (640) reflection as a function of the angle  $\alpha$ , with  $\alpha = 0^\circ$  at the peak intensity position (Fig.32).

The extrusion ratio had little effect on the degree of the texture (Fig.32(a)). Annealing of the extruded rod also had little effect (not shown). Deformation did appear to influence the texture however, (Fig.32(a)). Only the highest strain rate used (1.0/minute) produced a strengthening of the texture (Fig.32(b)). All other strain rates produced a weakening of the texture to about the same degree except for  $\dot{\epsilon} = .1/\text{minute}$  which produced a slightly greater effect. These results indicate that during superplastic deformation random grain rotation is taking place as a result of grain boundary sliding causing a decrease in the texture.

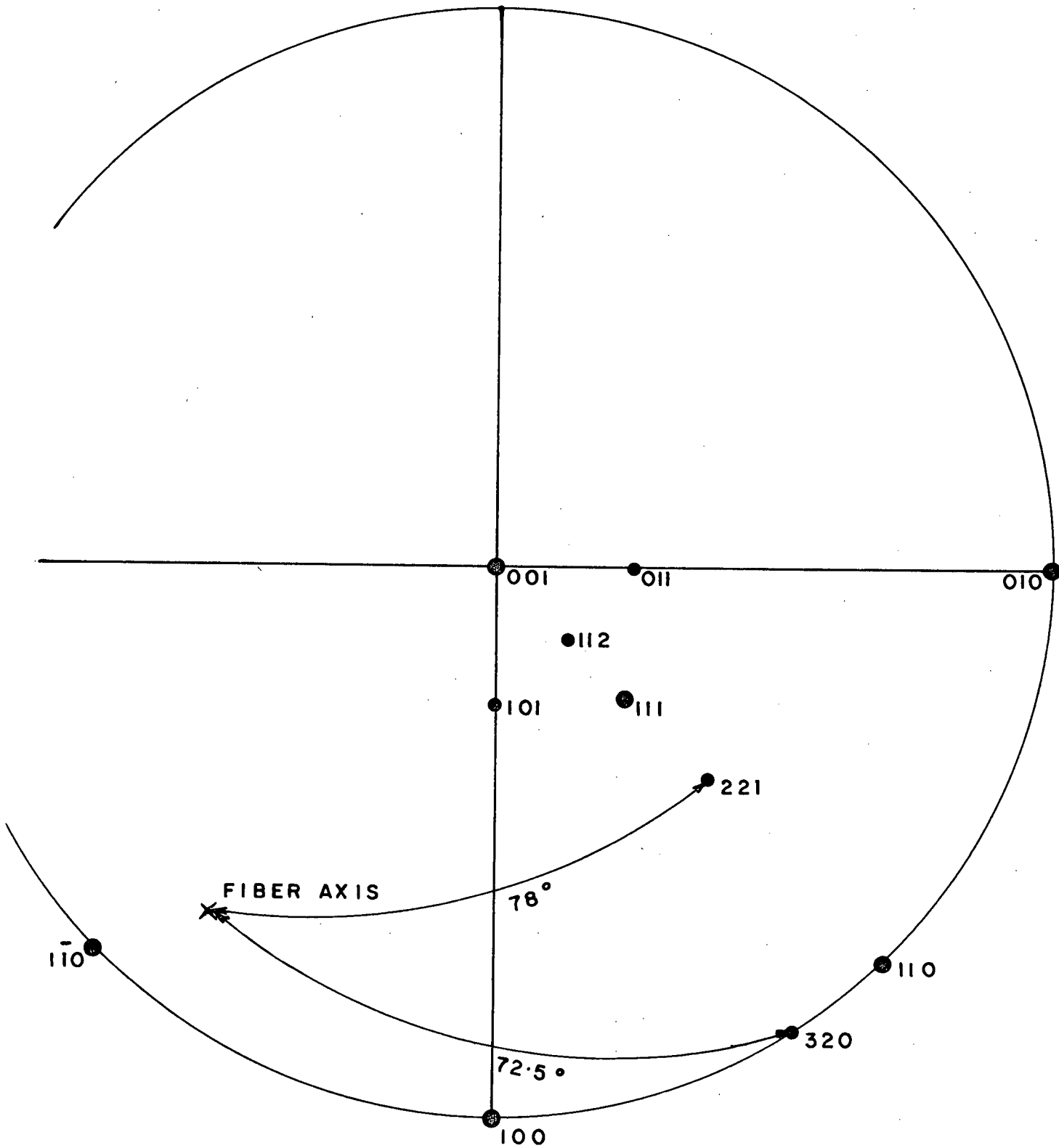


Fig.30. Location of Fiber Axis on Standard Stereographic Projection of Tin.

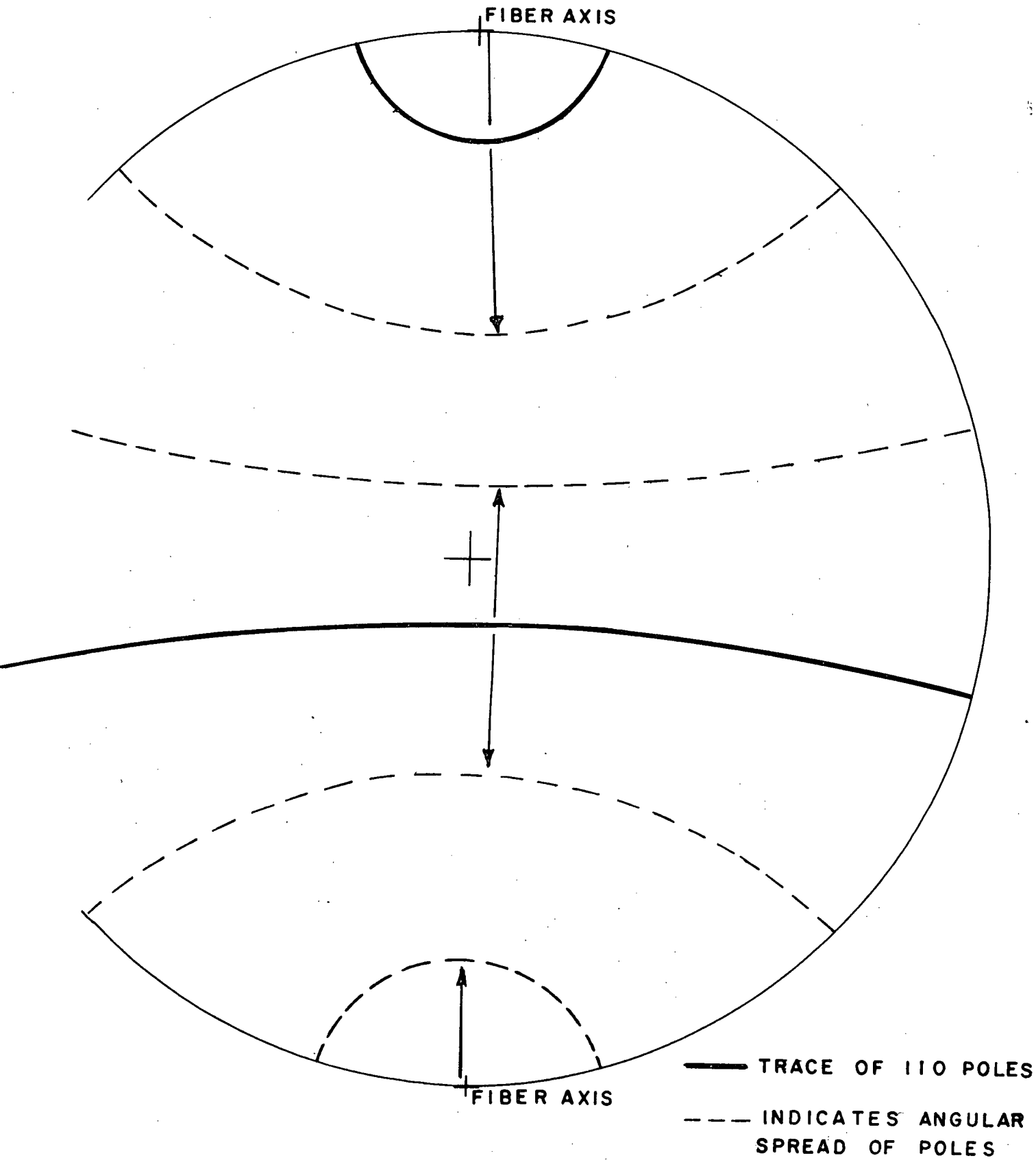
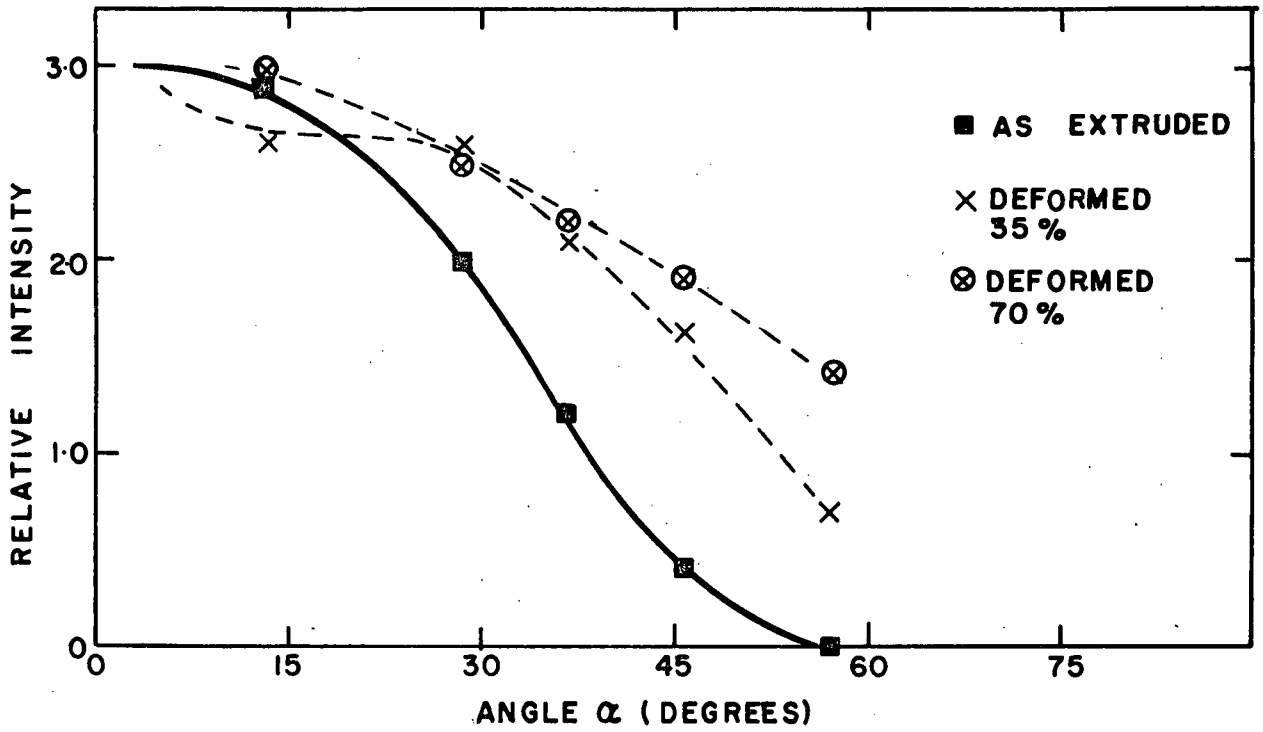
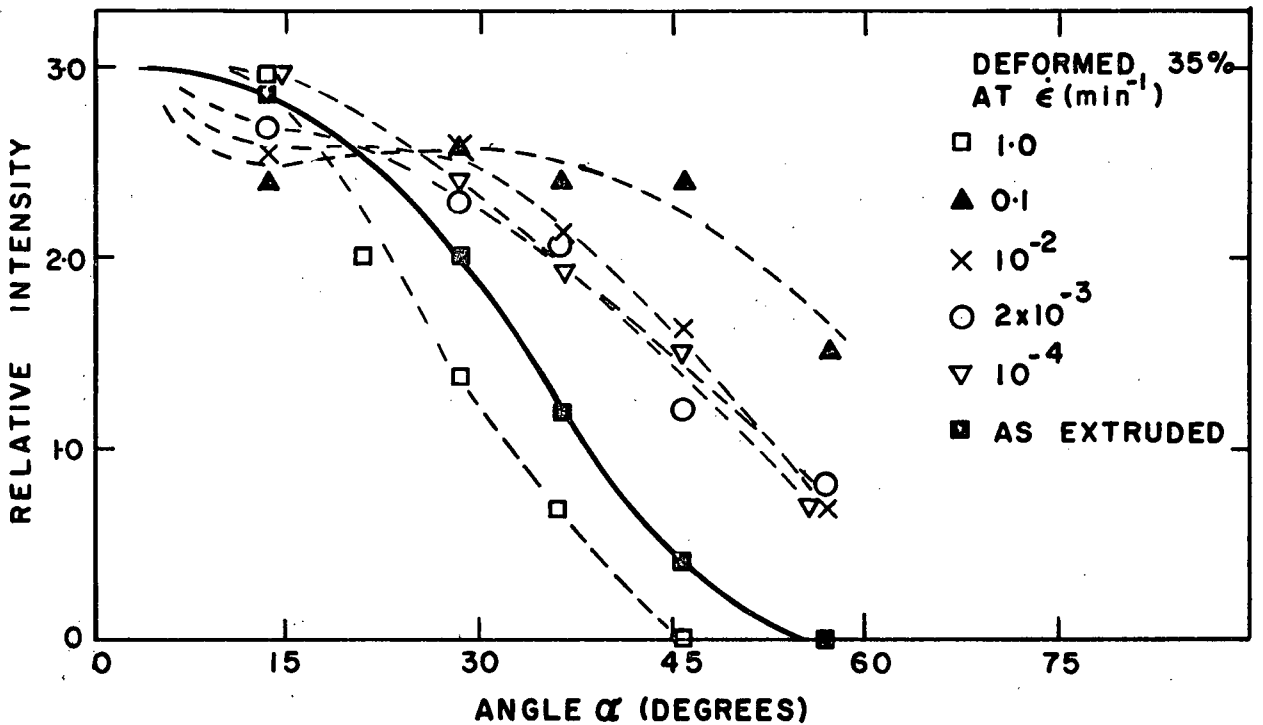


Fig.31. (110) Pole Figure for Extruded Rod.



a) EFFECT OF STRAIN ON DEGREE OF TEXTURE



b) EFFECT OF STRAIN RATE ON DEGREE OF TEXTURE

Fig.32. Degree of Texture Before and After Deformation.

### 3.5 - Grain Growth After Deformation

#### 3.5.1 - Growth by Annealing

To determine if any factors affecting grain growth were changed by deformation, samples were deformed then annealed at room temperature. The grain size variation with time during and after deformation at a strain rate of  $10^{-2}$ /min. is plotted in Fig.33 along with the static annealing curve for this material. Immediately after the stress is removed, the growth rate is lower. It is interesting to note that after deformation and considerable post deformation annealing, the grain size is actually less than that of a sample statically annealed for the equivalent length of time. Similar post deformation annealing curves (Fig.34) for different amounts of strain suggest that the rate of growth after deformation is a function of strain; small strains are followed by a faster growth rate than large strains. Further illustration is afforded by Figs.35 and 36 where two curves of Fig.34, for 70% strain and 6.9% strain are replotted along with sections of the static annealing curve with the time axis shifted; the time to reach an annealed grain size equivalent to the deformation grain size is taken as zero time. In this way, it is possible to compare growth rates of two samples having reached the same grain size by two routes; annealing and deformation. These curves confirm that the post deformation growth rate is less than the static annealing rate but only after large amounts of straining.

#### 3.5.2 - Growth Enhanced by Deformation

The deformation seemed to be producing some change in the material structure which, in turn, caused a reduction in the grain

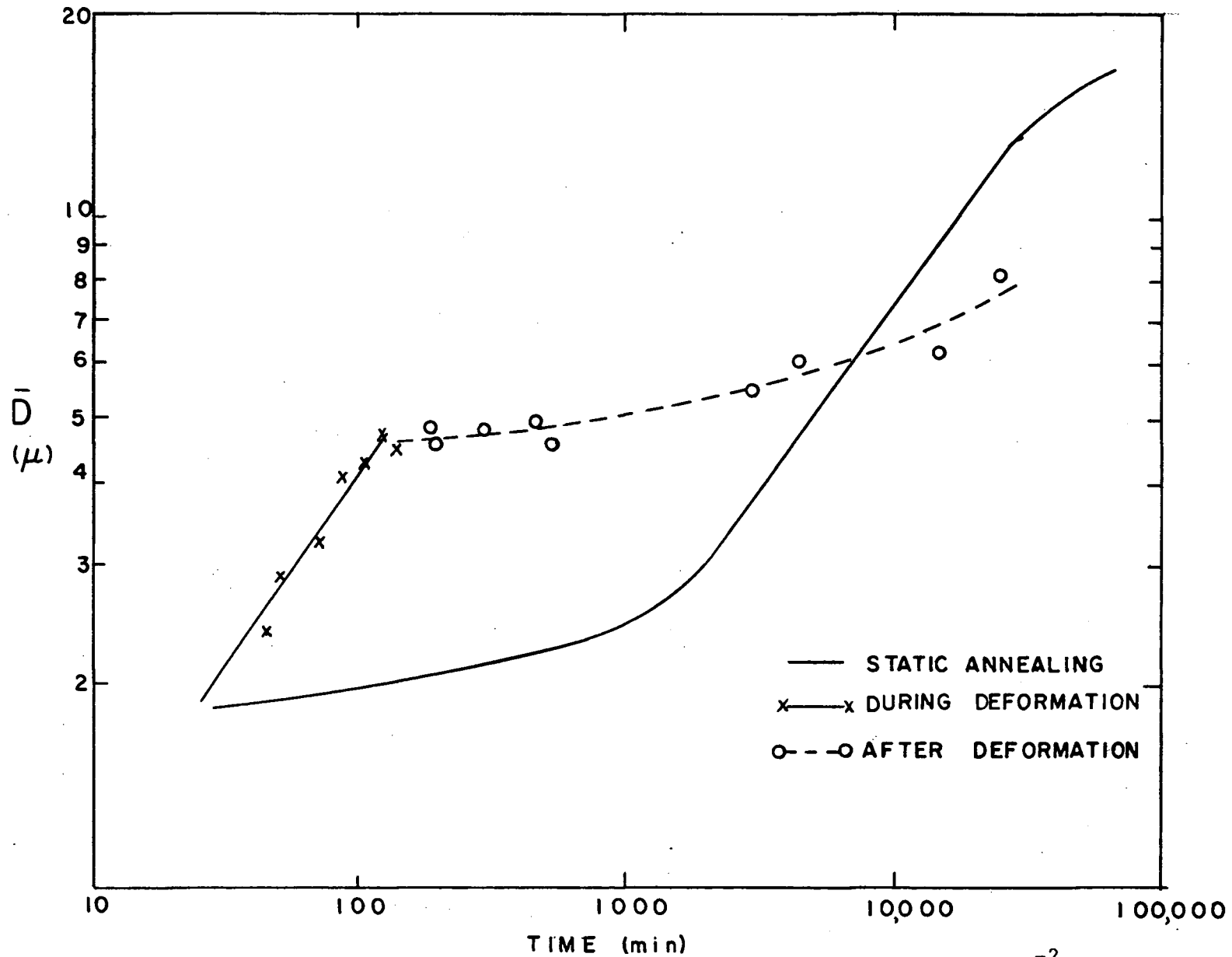


Fig.33. Grain Size versus Time During and After Deformation at  $\dot{\epsilon} = 10^{-2}/\text{min}$ .

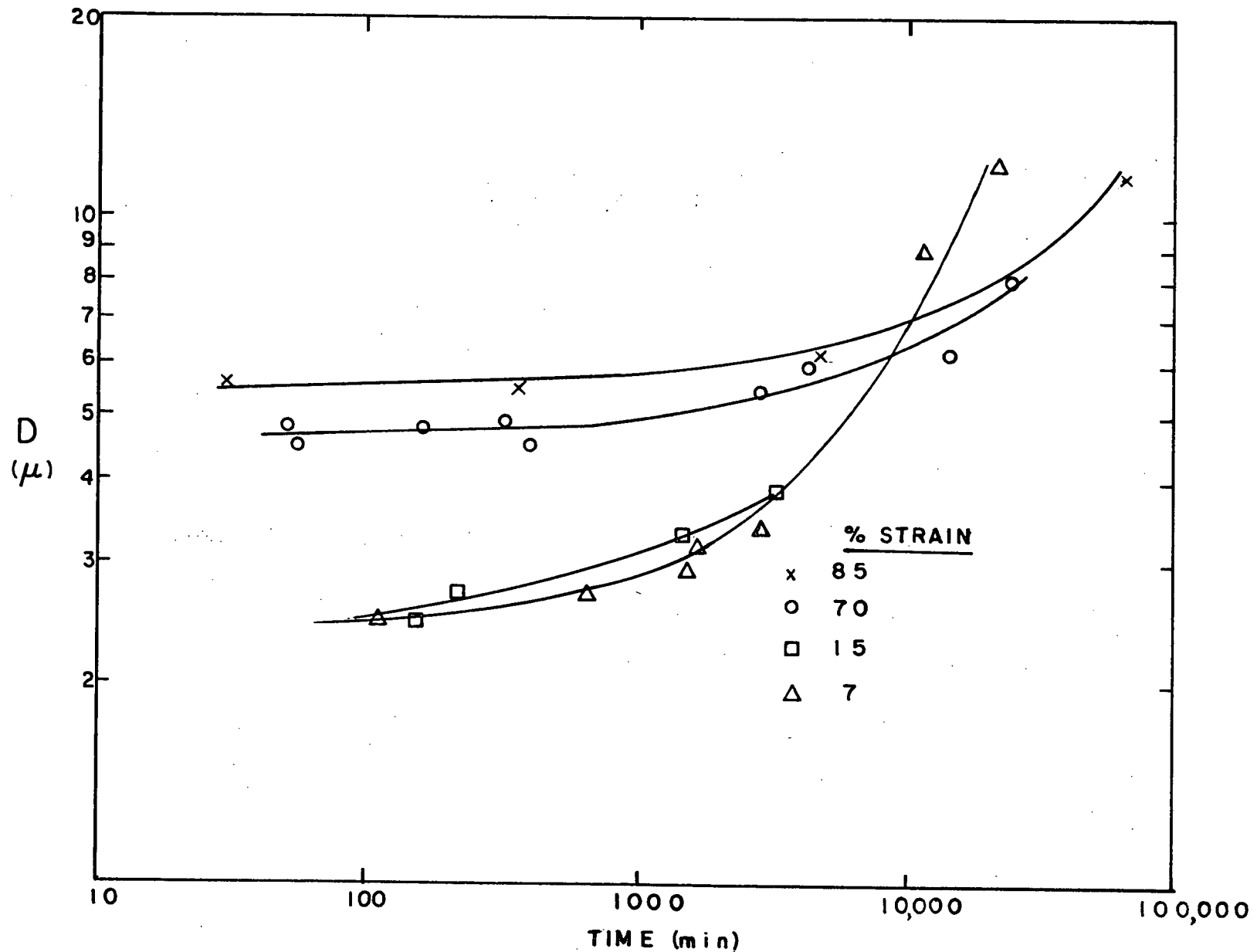


Fig.34. Effect of Strain on Grain Size versus Time Curves After Deformation.

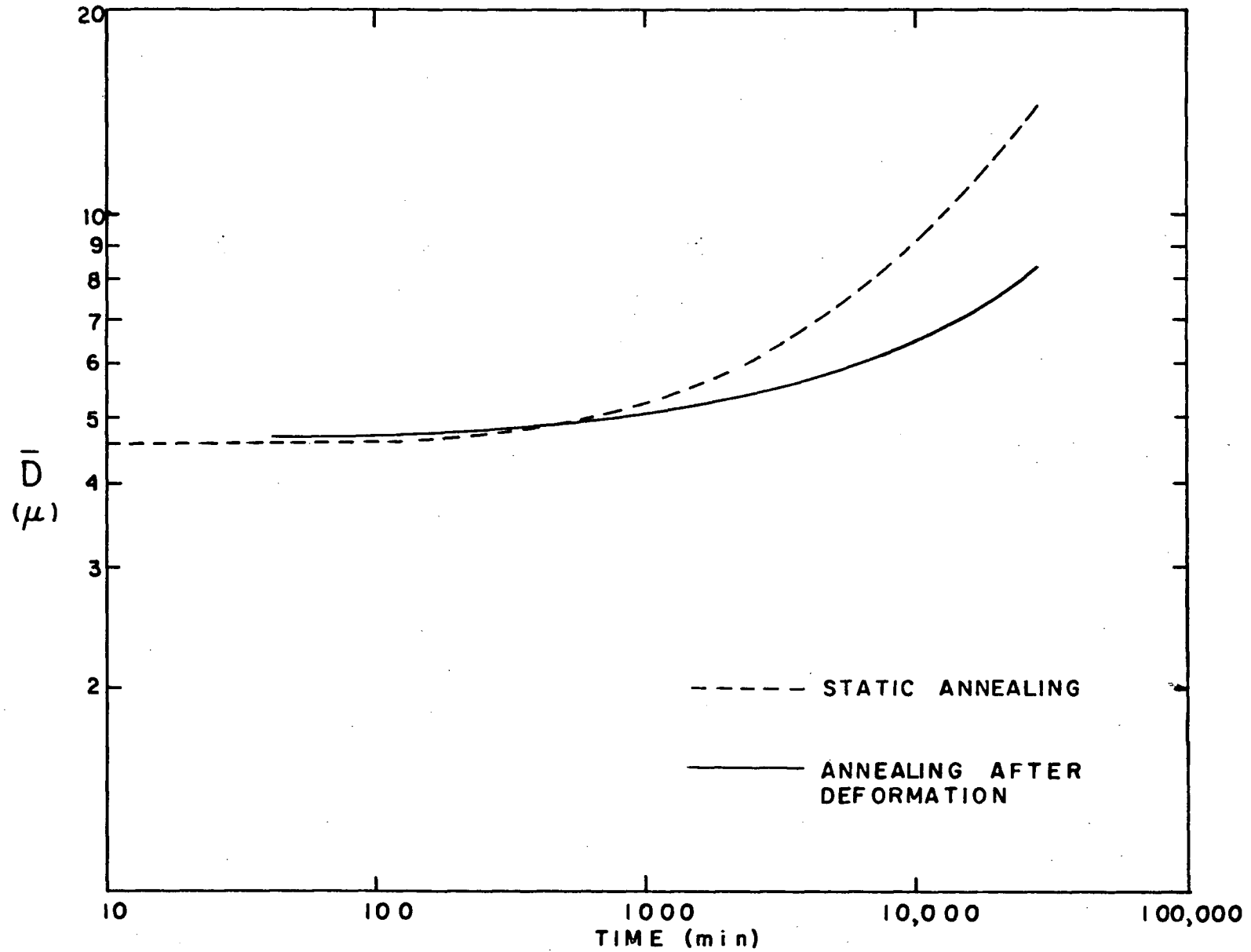


Fig.35. Comparison of Grain Size versus Time Curves for Static Annealing and Annealing After Deformation of 70% Strain.

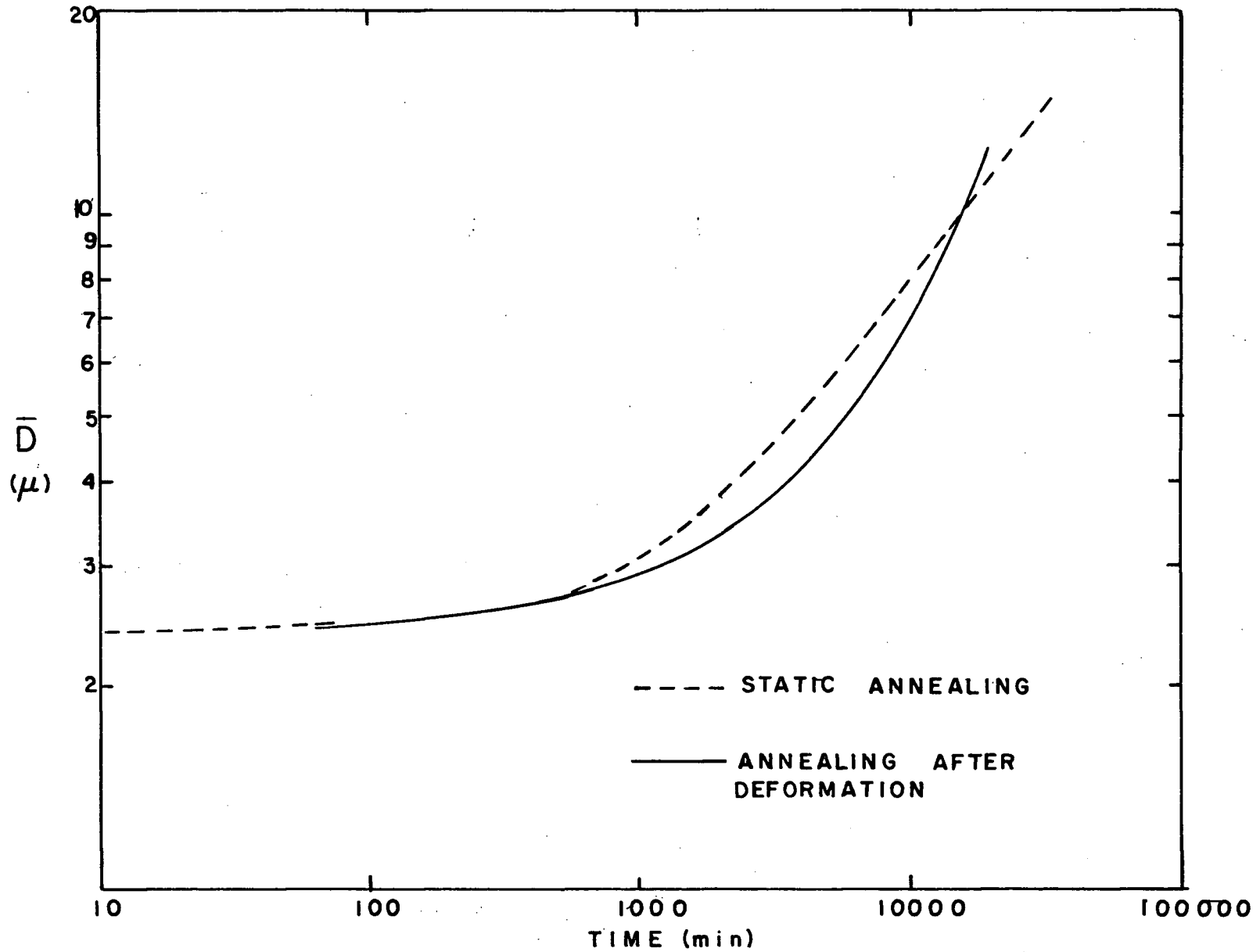


Fig.36. Comparison of Grain Size versus Time Curves for Static Annealing and Annealing After Deformation of 7% Strain.

growth rate. To determine if this structural change affected the stress-strain rate relationships, the following experiment was performed. A sample of the low ratio 0°C extrusion temperature material was deformed in the Instron to 85% true strain at a strain rate of  $10^{-2}$ /min. The grain size after deformation was 5.5 microns. A piece of the same material was annealed to a grain size of 5.8 microns and the two samples used to perform an incremental strain rate change test (Fig.37).

The deformed material behaved very similarly to the annealed material although the deformed material had a slightly higher "m" value at the low strain rates. The structural changes produced by the prior deformation had little effect on the stress-strain rate relationships.

To see if the change had any effect on the growth kinetics during further deformation, another set of experiments was performed. Two samples were again deformed to 85% strain (at  $\dot{\epsilon} = 10^{-2}$ /min.) and a grain size of 5.5 microns. One of these was then annealed to a grain size of 6.2 microns to see if the structural changes might be altered by an annealing treatment. Two other samples were annealed to similar grain sizes (5.8 and 6.5 microns) for comparison. All four samples were then deformed at  $\dot{\epsilon} = 6.7 \times 10^{-4}$ /min. to a strain of approximately 15% and the grain sizes measured.

The initial and final grain sizes are presented in Fig.38 as a function of the deformation time at  $\dot{\epsilon} = 6.7 \times 10^{-4}$ /min. The annealed samples had a much greater increase in grain size than the previously deformed samples; the annealed sample had a relative enhancement  $\left(\frac{\bar{D}}{D_A}\right)$  of 60% compared to only 30% for the deformed sample.

The structural change produced by deformation had the same

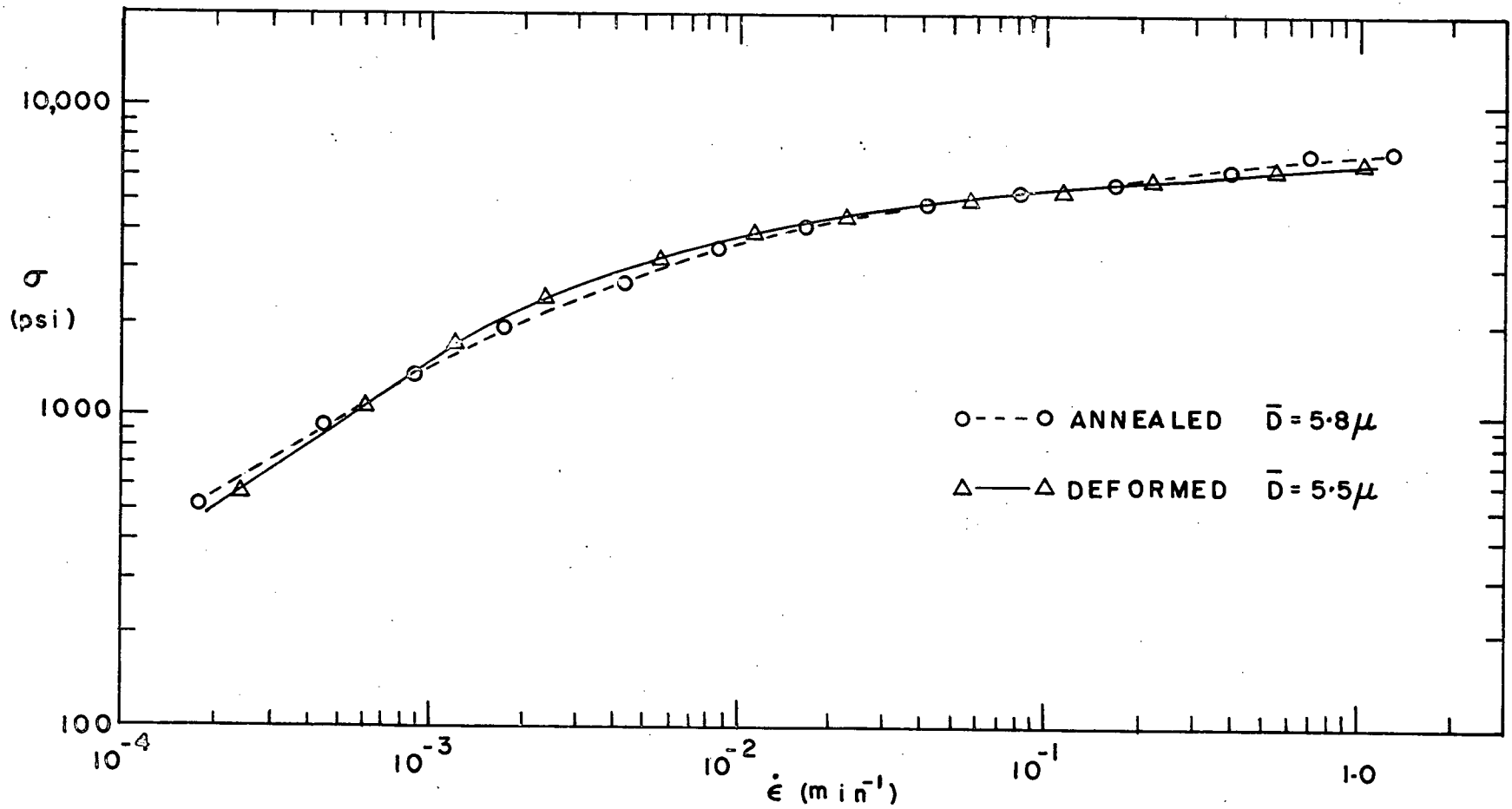


Fig.37. Comparison of Stress-Strain Rate Data for Annealed and Deformed Material.

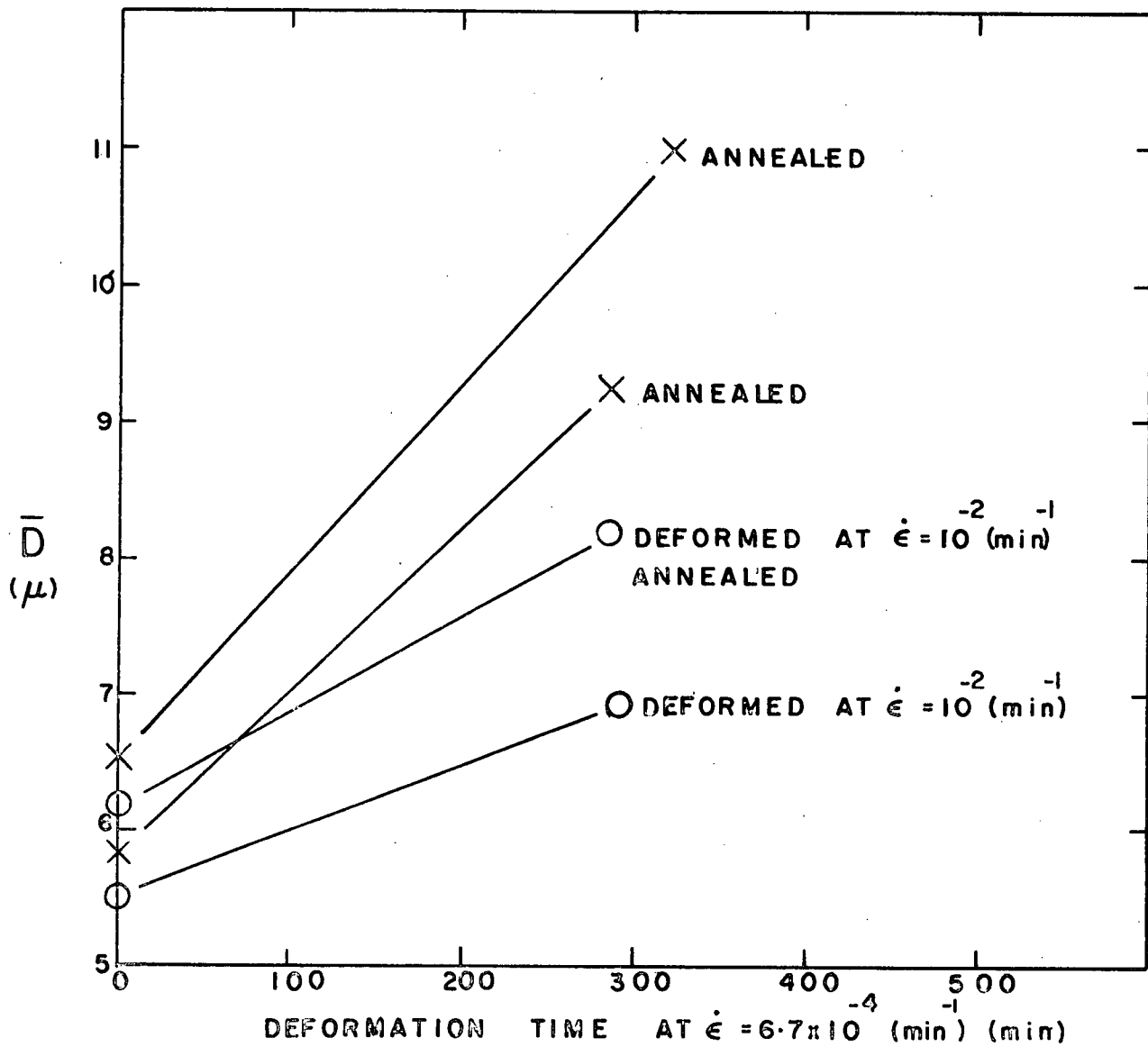


Fig.38. Effect of Pre-Deformation on Grain Size Increase During Deformation.

effect in this case as it did on post deformation annealing, i.e. it reduced the grain growth kinetics as compared to undeformed material.

In other words, deformation in the superplastic region causes a reduction in subsequent grain growth rates exclusive of whether this growth is produced by annealing or by further deformation.

## DISCUSSION

### 4.1 - Superplasticity

Evidence has been presented to suggest that the Sn-1% Bi alloy used in this study is superplastic. The phenomenological basis of superplasticity requires a strong dependence of the flow stress on strain rate. The Sn-Bi alloy does possess high "m" regions (Figs. 4 and 5). The characteristic three-stage curve typical of most superplastic alloys was not obtained, despite the use of very low stress creep tests (Fig.7). A slight reduction in "m" can be seen in Fig.7 but mainly in the creep test region. The decreased "m" could be due to the change in testing procedure rather than a different mechanism characteristic of Stage I deformation.

Elongation values from alloys regarded as superplastic range from 300 to 2000%. The maximum value obtained for this alloy was slightly greater than 300%. Elongation values reported by Alden on the same alloy with similar strain rates ranged from 450 to 500%. A possible reason for this difference could be differences in impurity content<sup>(12)</sup>. A higher maximum value of "m" was obtained by Alden (Fig.8), lending support to this supposition.

After large amounts of deformation the grains of the Sn-Bi alloy remained equiaxed, a prominent feature of superplastic alloys. The ratio of the average linear intercepts measured in the longitudinal and transverse directions ( $\bar{D}_L/\bar{D}_T$ ) was found to be 1.15 after 300% elongation.

On the basis of these results it is concluded that the Sn - 1% Bi alloy under study is superplastic.

#### 4.2 - Grain Growth

An equation can be derived for the growth of cells in a soap froth where the surface energy of the film is the driving force. A pressure difference exists across each curved cell wall, the pressure being greater on the concave side and proportional to the curvature of the wall. The pressure difference causes diffusion from the high to the low pressure side resulting in movement of the walls toward the centre of curvature. The rate of motion of the walls and hence the rate of increase of the average cell diameter  $(\frac{d\bar{D}}{dt})$  will be proportional to the curvature,  $C$ .

In an equiaxed structure the curvature can be assumed proportional to the inverse of the average cell diameter so that:

$$\frac{d\bar{D}}{dt} = K'C = \frac{K}{\bar{D}} \quad (5)$$

Integration of this equation and evaluation of the constant of integration yields;

$$\bar{D}^2 - \bar{D}_0^2 = 2 Kt \quad (6)$$

where  $\bar{D}_0$  is the average cell size at  $t = 0$ .

Experimental observations have confirmed that this equation adequately describes the growth of cells in a soap froth<sup>(47)</sup>.

The growth of grains in a metal can be represented by a similar type of equation except that the exponent is usually found to be greater than 2 and can change with temperature, purity of the metal, and the presence of impurities. It was shown (Fig.12) that the room temperature grain growth of the Sn-Bi could be approximated by an equation similar to (6). Therefore one may conclude that grain growth during static annealing

is driven by the reduction of surface energy of the grain boundaries.

Lücke and Detert<sup>(48)</sup> and Gordon and Vandermeer<sup>(49)</sup> proposed similar atomistic theories to explain the migration rates of grain boundaries in which the segregation of impurity atoms to the boundary control the movement. Both theories depend on the fact that the equilibrium concentration of the impurity in the region of the grain boundary will be different from the concentration in the bulk of the material. The lattice distortion caused by the impurity atom is less if it is placed in the already distorted boundary region instead of in the interior crystal lattice. Thus, if a force acts on the grain boundary tending to separate it from the array of excess impurity atoms, the free energy of the system will be increased. The boundary will have to climb an energy hill which is equivalent to a restraining force exerted by the impurities on the boundary.

If the force acting to move the boundary is large enough to overcome the maximum restraining force, the boundary will break away from the impurity array and migrate at a rate that depends only on the net rate of atom transfer across the boundary. If however, the driving force is not sufficient to cause this breakaway the boundary will tend to move away from the impurity array a short distance until the restraining force just equals the driving force. The boundary will then move with a constant velocity with the impurity array trailing behind. The rate of migration will then be controlled by the diffusion of the impurity atoms in the distorted region adjacent to the boundary.

The rate of grain boundary migration can be written as:

$$G = M \frac{dF}{dx} \quad (7)$$

where  $M$  is the mobility of the rate determining step.

$F$  is the free energy per atom

and  $x$  is the distance co-ordinate in the direction of boundary migration.

The mobility is related to a diffusion coefficient by the equation:

$$M = \frac{D^i}{kT} \quad (8)$$

where  $D^i$  is the diffusion coefficient for the impurity atoms in the region adjacent to the boundary when the rate is impurity dependent.

Lücke and Detert consider that the impurity atoms will trail so far behind the boundary that they can be considered as diffusing in the undistorted bulk material and  $D^i$  will be equal to that for lattice diffusion of the impurity. In contrast Gordon and Vandermeer suggest that the impurity atoms will be diffusing closer to the boundary in a much more distorted area.  $D^i$  then could be significantly greater than that for lattice diffusion.

Vandermeer and Gordon developed an equation for  $\frac{dF}{dx}$  by assuming that in grain growth the surface energy is the driving force:

$$\frac{dF}{dx} = \frac{2\gamma_s V_m}{N \lambda \bar{D} C_B} \quad (9)$$

where  $\gamma_s$  is the specific grain boundary energy

$V_m$  is the molar volume of the parent material

$N$  is Avogadro's number

$\lambda$  is the width of the grain boundary

$\bar{D}$  is the average grain diameter

$C_B$  is the equilibrium concentration of impurity in the grain boundary.

They also assumed that the boundary migration rate was equal to the rate of change of the average grain diameter. By combining equation 7, 8 and 9 and substituting for  $C_B$  and  $D^i$  the following equation was developed:

$$\frac{d\bar{D}}{dt} = \left[ \frac{2\gamma_s V_m D_o^i \exp\left(-\frac{Q^i+E}{RT}\right)}{RT \lambda A C_o} \right] \cdot \frac{1}{\bar{D}} \quad (10)$$

where  $D_o^i$  and  $Q^i$  are the pre-exponential factor and activation energy per mole for diffusion of solute in the region near the boundary

A is a vibrational entropy factor

$C_o$  is the atomic fraction of solute

E is the internal energy gain per mole of solute atoms transferred to the boundary from the bulk material.

This equation is identical to equation (5):

$$\frac{d\bar{D}}{dt} = \frac{K}{\bar{D}}$$

with the bracketed term equal to K.

Holmes and Winegard<sup>(45)</sup> made estimates of the values of the terms in equation (10) for dilute Sn-Bi alloys (Table 4).

TABLE 4 - Estimated Values for Terms of Equation (10)<sup>(45)</sup>

Term	Value
$\gamma_s$	$10^{-5}$ cal/cm <sup>2</sup>
$V_m$	16.3 cm <sup>3</sup>
$D_o^i$	72 cm <sup>2</sup> /sec.
$\lambda$	$5 \times 10^{-8}$ cm.
A	$\frac{1}{4}$

They were then able to calculate a value of 22,000 cal for  $Q^i + E$  from experimentally determined grain growth curves.

Using the values of Table 4 calculations for the three grain growth curves (Fig.15) yielded an average value for  $Q^i + E$  of 24,000 cal. which compares favourably with Winegard's result. Since Winegard's data was shown to be consistent with the impurity dependent migration model<sup>(35)</sup>, it can be concluded that the boundary migration in the Sn-1% Bi alloy is also controlled by the diffusion of the solute Bi atoms.

Various mechanisms by which deformation can increase the average grain size at a given time will now be discussed.

#### 4.3 - Mechanisms of Deformation Enhanced Grain Growth

##### 4.3.1 - Grain Coalescence

Grain boundaries in a single phase metal exist because of different crystallographic orientations of the grains (Fig.39a). If one of the adjacent grains rotates (Fig.39b) in a direction so that the misorientation is eliminated (Fig.39c), then the boundary itself will have been eliminated and the two original grains will have coalesced into one. After the coalescence some local migration of the surrounding boundaries will probably occur (Fig.39d). It is obvious that operation of this mechanism will produce an increased grain size. Li<sup>(50)</sup> proposed that a similar phenomenon occurred with subgrains and used the mechanism as an explanation for the origin of recrystallization nuclei.

During superplastic or creep deformation grain boundary sliding is accompanied by a rotation of the grains with respect to

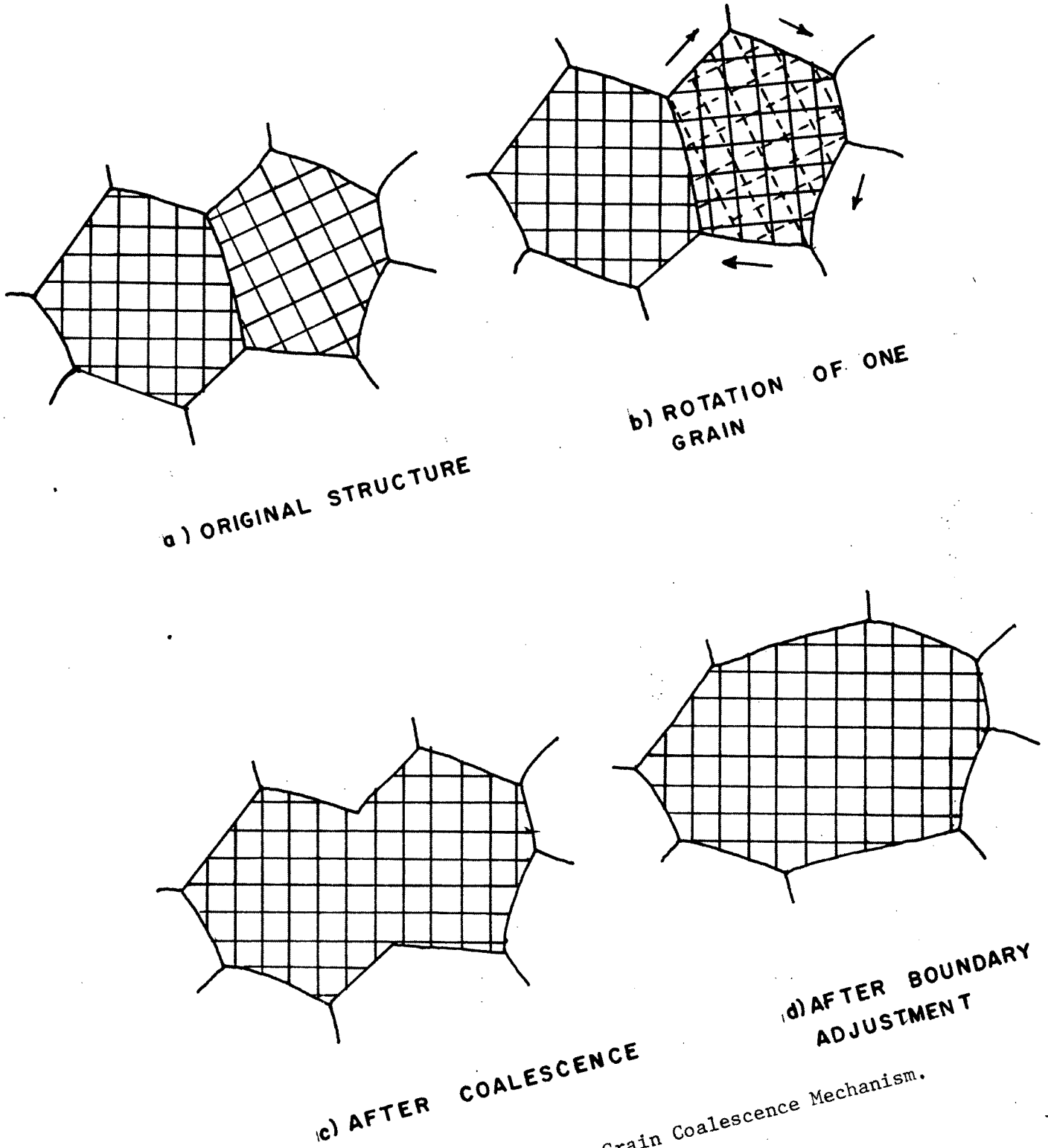


Fig. 39. The Grain Coalescence Mechanism.

each other. The amount of rotation can be quite large i.e. 25-30° after 45% extension<sup>(7)</sup>. Thus, stress-induced rotation could produce coalescences in a similar fashion to Li's mechanism.

In creep deformation it is generally found<sup>(51)</sup> that a linear relationship exists between the amount of sliding and the total strain. The amount of grain rotation and the number of coalescence reactions should also increase continually with strain. If these relationships are assumed true for superplastic materials, the grain coalescence mechanism predicts qualitatively the curves of Figs.18 and 19 where the grain size enhancement increases with strain.

The effects of strain rate are also consistent with the mechanism. The grain elongation measurements show that as the strain rate is lowered from the high "m" region the percentage of the total deformation due to grain boundary sliding decreases. Thus, for a given amount of strain, the lower strain rates would have experienced less grain rotation and should show a smaller rate of grain growth. In fact, the results show that, in the superplastic region, the lower the strain rate the lower the relative enhancement for a given amount of strain (Fig.19).

However, the results of the alternating tension-compression tests are not explained. The alternating stress-strain cycles would be expected to approximately reverse the direction of the grain rotations so that the large net rotations needed to produce a significant number of coalescences would not occur. Thus, this type of deformation should produce very little grain enhancement. In fact, the alternating deformation produced slightly more grain growth than the corresponding tension only control sample.

In order to attempt to theoretically predict the effects of the coalescence mechanism on the grain type and size distributions the analysis of Appendix I was carried out. The calculations show that the slight changes in the grain type distribution curves can be accomplished if 6% of the original grains coalesced during deformation. However, this 6% coalescence was not sufficient to account for the observed changes in the grain size distribution.

It is therefore concluded that the distribution calculations and the tension-compression experiments show that the grain coalescence mechanism cannot be the cause of the grain size enhancement during deformation.

#### 4.3.2 - Increased Driving Force

It appears more likely that the grain size enhancement is a result of a "speeding up" of the normal grain growth processes caused by increased boundary migration rates. Deformation could increase either the mobility or the driving force. Mechanisms affecting the driving force will be considered in this section.

##### 4.3.2.1 - Recrystallization

Recrystallization taking place continuously during the deformation could produce an increased grain size. Continuous recrystallization has been suggested by some authors (17,18,20,26,52) to be associated with superplastic deformation. The recrystallized grains would be equiaxed thus explaining the observed lack of directionality in grain shape after deformation. Recrystallization would be initiated by stress concentrations at triple lines or at local distortions around

sliding grain boundaries.

However, it does not seem likely that recrystallization during deformation could be the cause of the increased grain size in superplastic metals. Studies of recrystallization during creep deformation of large grained metals (Pb<sup>(53,54)</sup>, Ni<sup>(55)</sup> and Mg<sup>(56)</sup>) show that the grain size after recrystallization occurs can be either larger or smaller than the original size. Theories<sup>(53,55)</sup> of the origin of recrystallization during creep require a dislocation or subboundary network to provide the nuclei and the driving force for growth. However, one of the main characteristics of superplastic deformation is the lack of dislocation networks during deformation. Recrystallization is also difficult to imagine in a two phase superplastic system since simultaneous recrystallization and growth of both phases would be required.

#### 4.3.2.2 - Grain Boundary Sliding

Since grain boundary sliding is observed in all superplastic alloys its effects on grain boundary migration must be considered. Studies of grain boundary sliding in polycrystals and bicrystals have shown that boundary migration is often connected with sliding. However, an important conclusion of the bi and tricrystal studies<sup>(57-59)</sup> is that migration does not necessarily accompany sliding. Migration depends on the configuration of the sample<sup>(60,61)</sup> and the relationship<sup>(62)</sup> between the surface examined and the direction of sliding. There appear to be two types of migration associated with bicrystal sliding. The first type<sup>(62,60)</sup> occurs when sliding produces a step on the crystal surface and the boundary migrates to the low

energy position with respect to this new surface (Fig.40). The second type appears to be caused by the build up of dislocations at the boundary as a result of the sliding process (62,61).

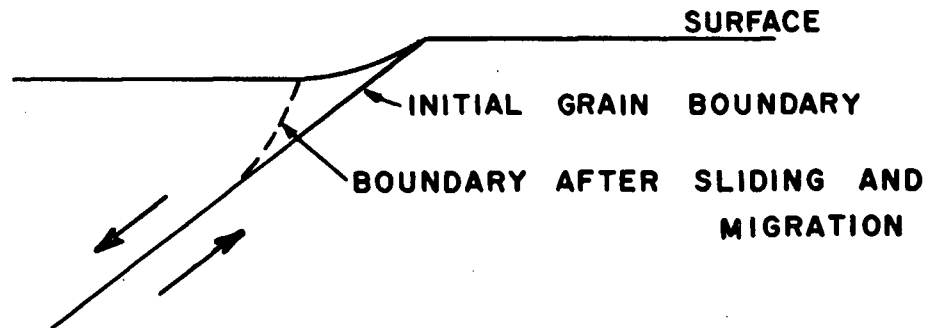


Fig.40 Surface Grain Boundary Migration Associated with Internal Boundary Sliding.

Studies on polycrystals (63-67) also suggest that migration is not a necessary result of grain boundary sliding. Almost all observations were made on the surface of the specimens so that the migration may be attributed to the surface step effect or to another surface effect investigated by Bell and Langdon (63) and Gittins and Gifkins (64). They observed that grain boundaries intersecting the surface tended to orient themselves at  $90^\circ$  to the surface during annealing and during creep. If samples were annealed prior to creep so that most of the angles approached  $90^\circ$  the amount of migration during the deformation was greatly reduced. Surface observations also do not suggest a mechanism for a grain size increase since the migration occurs both away from and toward the centre of curvature of the boundaries (65-67).

However, Ishida, et al<sup>(68)</sup>, using an internal marker method, found simultaneous migration and sliding in the interior of samples and concluded that some migration could be driven by strain energy. The strain energy could be present in two forms; as dislocation arrays<sup>(67)</sup> adjacent to the sliding boundary and produced directly by the shearing process, or as arrays at triple points<sup>(65,68)</sup> produced by local deformation to relieve stress concentrations.

A model of stress induced grain growth based on the first type of array was suggested by Cook<sup>(21)</sup>. A difference in dislocation density across a shearing boundary was postulated with the larger grains containing the higher density. The boundaries would then migrate in such a way as to decrease the size of the larger grains and increase the size of the smaller. In normal grain growth the larger grains grow at the expense of the smaller. The operation of this model is thus in direct opposition to the normal growth process and would only decrease the size dispersion of the grain structure and not produce an increase in average grain size. Changes in the grain size dispersion were not observed experimentally in the Sn-1% Bi alloy.

If the dislocation structure was arranged so that migration toward the centre of curvature tended to decrease the stored strain energy, the normal growth process could be enhanced. The results of the alternating tension-compression test appear to disprove this type of model. The dislocation pile-ups produced in the tension cycle would probably be counteracted by similar pile-ups on the opposite side of the boundary when the stress reverses in the compression cycle. Thus, a large net build up of dislocations on one side of a shearing boundary would be unlikely in this type of experiment. Hence, a large

net increase in the grain growth rate would not be expected, contrary to experiment.

The local deformation structure at triple points also seems an unlikely mechanism to promote growth since the induced migration is equally likely to be toward or away from the centre of curvature of the blocking grain<sup>(68)</sup>.

#### 4.3.2.3 - Grain Elongation

An elongated grain must possess greater boundary curvature than one of equivalent volume but with an equiaxed shape. An increase in local curvature should produce an increase in boundary migration. Some grain elongation did take place in the alloy studied and could have been caused by either slip processes or Nabarro-Herring diffusion.

However, it is difficult to see how grain elongation can lead to a net increase in grain size. The increased curvature causes migration in a direction to restore the original equiaxed shape without an increase in grain volume. Also, if an elongated grain structure was responsible for the grain size enhancement, the accelerated rate of growth during deformation would be expected to continue after the deformation ceased until the elongation was removed. Measurements revealed that very long post deformation annealing times were required before the equiaxed shape was restored. Figure 32, however, reveals a sharp decrease in growth rate as the deformation ends.

#### 4.3.2.4 - Grain Boundary Width

An increase in the driving force term could be effected by a decrease in the boundary width (Equation (9)). Since accurate

measurements of grain boundary width are not available and controversy still exists as to the exact nature of the high angle boundary it is difficult to assess the effects of deformation on the boundary width. If grain boundary sliding tended to smooth the boundary, the width could be reduced, However, some experimental evidence<sup>(63,62)</sup> suggests that sliding boundaries become corrugated.

#### 4.3.3 - Mobility Enhancement

The only way the mobility of the grain boundaries can be increased by deformation is through the diffusion coefficient (Equation (8)).

Strain enhanced diffusion has been a subject of considerable controversy in the literature. Most experimental work has been concerned with either self diffusion coefficients or bulk coefficients of a major alloying element. Several investigators<sup>(69-71)</sup> have reported large increases in the self diffusivity of Ag after deformation. Increases by factors of 10 to 15 were found in Ag, Fe<sup>(72,73)</sup> and Cu<sup>(74)</sup>. These results have been questioned however, on theoretical and experimental grounds by a number of writers<sup>(75-77)</sup>. Contradictory experimental evidence has also been presented for Ag<sup>(78)</sup>, in which maximum enhancements of only 2 times were obtained. Other systems, such as Zn-Al<sup>(79)</sup>, S-Ni<sup>(80)</sup>, Cu-Ag<sup>(82)</sup> and Ni-Fe<sup>(81)</sup> showed little increase with deformation.

Excess vacancies produced by the motion of dislocations during deformation have been used to explain the apparent enhancement. However, theoretical arguments showed that this mechanism was insufficient to account for the larger enhancements. A dislocation pipe model appeared more plausible, the increased dislocation density pro-

viding faster paths for the diffusing atoms. Despite the controversial nature of this subject, it seems reasonable to conclude that some increase in the bulk diffusion coefficient is possible. The effect is highly dependent on conditions of temperature, and strain rate.

The effects of deformation on the grain boundary diffusivity have not received widespread attention. Bhat and Vitovec<sup>(83)</sup> studied the diffusion of zinc in copper with superimposed fatigue straining and found no significant enhancement of the volume diffusion coefficient. However, they did find increased diffusion along grain boundaries which, they postulated, might be due to damage resulting from grain boundary sliding. Blackburn and Brown<sup>(84)</sup> measured the grain boundary diffusion coefficients of Ag diffusing in copper bicrystals. Tests on static and sliding boundaries showed a slight increase (30%) in grain boundary diffusivity when the boundaries were sliding. The results cannot be taken as conclusive since the number of measurements was small and the observed increase was within the experimental error.

Thus, there is some suggestion that grain boundary diffusion coefficients can also be increased by deformation and in particular by grain boundary sliding. Processes of grain boundary sliding, such as climb-glide of dislocations or Nabarro-Herring migration of grain boundary bumps, which involve motion of vacancies, could conceivably produce an excess of vacancies in the grain boundary region and increase the diffusion coefficient. Since the controlling factor in grain boundary migration is the diffusion of the Bi atoms in a distorted region close to the boundary a local increase in the vacancy concentration in this region would lead to faster grain boundary migration.

If the production rate of vacancies is proportional to the strain rate and the annealing rate of vacancies is proportional to the excess vacancy concentration, then the equation governing the vacancy concentration<sup>(85)</sup> is:

$$dn_x = K_1 \dot{\epsilon} dt - n_x K_2 dt \quad (11)$$

where  $n_x$  = atomic fractions of vacancies due to strain

$K_1$  = constant such that  $K_1 \dot{\epsilon}$  is the rate of vacancy production

$\dot{\epsilon}$  = strain rate

$K_2$  = constant equal to  $\frac{1}{\tau}$  where  $\tau$  is the average lifetime of a vacancy.

Integration of this equation yields:

$$n_x = \frac{K_1 \dot{\epsilon}}{K_2} (1 - \exp(-K_2 t)) \quad (12)$$

where  $t$  is the time to reach a value of strain at the given strain rate. If diffusion takes place by a vacancy mechanism, the diffusivity is proportional to the total atomic fraction of vacancies. Thus, the diffusivity in a strained system will be proportional to  $(n_x + n_v)$  where  $n_v$  is the equilibrium vacancy concentration (mole fraction).

In preceding sections it was shown that during annealing:

$$\frac{d\bar{D}}{dt} = M \frac{dF}{dx}$$

where  $M$  was proportional to the diffusivity and  $\frac{dF}{dx}$  was proportional to  $\frac{1}{D}$ . Combining these factors yields:

$$\frac{d\bar{D}}{dt} = \frac{k' n_v}{\bar{D}} \quad (13)$$

when the vacancy concentration is in thermal equilibrium and:

$$\frac{d\bar{D}}{dt} = \frac{k' (n_x + n_v)}{\bar{D}} \quad (14)$$

when excess vacancies are generated. Substituting for  $n_x$  from equation (12) gives:

$$\frac{d\bar{D}}{dt} = \frac{k' \left( \frac{K_1 \dot{\epsilon}}{K_2} (1 - \exp(-K_2 t)) + n_v \right)}{\bar{D}} \quad (15)$$

Integration of this equation gives the grain size variation with time during deformation:

$$\bar{D}^2 - D_o^2 = 2k' \left[ \left( \frac{K_1}{K_2} \dot{\epsilon} + n_v \right) t - \frac{K_1}{K_2} \dot{\epsilon} \left( \frac{1 - \exp(-K_2 t)}{K_2} \right) \right] \quad (16)$$

This equation can be compared to the integrated form of equation (13):

$$\bar{D}^2 - D_o^2 = 2 k' n_v t \quad (17)$$

If the values of the various constants can be estimated, theoretical grain size versus time curves during deformation can be calculated. An approximate value of  $n_v$  of  $10^{-9}$  was obtained from<sup>(86)</sup>:

$$n_v = \exp - \Delta H_f / RT \quad (18)$$

where  $\Delta H_f$ , the activation energy for formation of vacancy, = 11.8 kcal/mole<sup>(87)</sup>. Then  $k'$  was determined from the  $k$  value for the theoretical unstrained grain growth curve (Fig.12).

The constant  $K_2$  will depend upon the nature of the vacancy sinks in the material. The most effective sink in this case will probably be the grain boundary. Girifalco and Grimes<sup>(85)</sup> have shown that

for a plate-like sink:

$$K_2 = \frac{2D_v}{L^2} = \frac{2D_o}{L^2} \exp(-\Delta H_m/RT) \quad (19)$$

where  $D_v$  is the vacancy diffusion coefficient

$\Delta H_m$  is the activation energy for vacancy motion = 15.7 kcal/mole <sup>(87)</sup>

$D_o$  is the frequency factor for vacancy diffusion = 9.7 cm<sup>2</sup>/sec. <sup>(88)</sup>

and  $L$  is the perpendicular distance from the sink.

An accurate value for the distance  $L$  cannot be determined since it depends on the boundary shear process that produces the vacancies. A value of  $L = 100A^\circ$  was taken as a reasonable estimate which yielded  $K_2 \approx 10^3/\text{min}$ .

To determine  $K_1$ , values of  $D$ ,  $t$  and  $\dot{\epsilon}$  for one experimental point were inserted in equation (16) along with the values of the other constants. The theoretical curves were thus constrained to pass through only this one point and could be used for comparison with experimental points at other strain rates. The point chosen was:

$$\bar{D} = 4.7 \mu \text{ at } t = 100 \text{ minutes and } \dot{\epsilon} = 10^{-2}/\text{min.}$$

which gave  $K_1 = 4.1 \times 10^{-3}$ . Barry and Brown <sup>(89)</sup> estimated  $K_1 = 10^{-3}$  for strain enhanced bulk diffusion.

Equation (16) was now used to calculate a series of grain size versus time curves for different strain rates (Fig.41). The experimental points from Figs. 16 and 17 and the unstrained annealing curve are shown in Fig.41 for comparison. Agreement of the experimental points with the theoretical curves is satisfactory from strain rates from 1.0/minute to  $7 \times 10^{-4}$ /minute. The lower strain rate curves do not agree quite so well. It should be remembered that the points for these low strain rates were determined by creep testing the high ex-

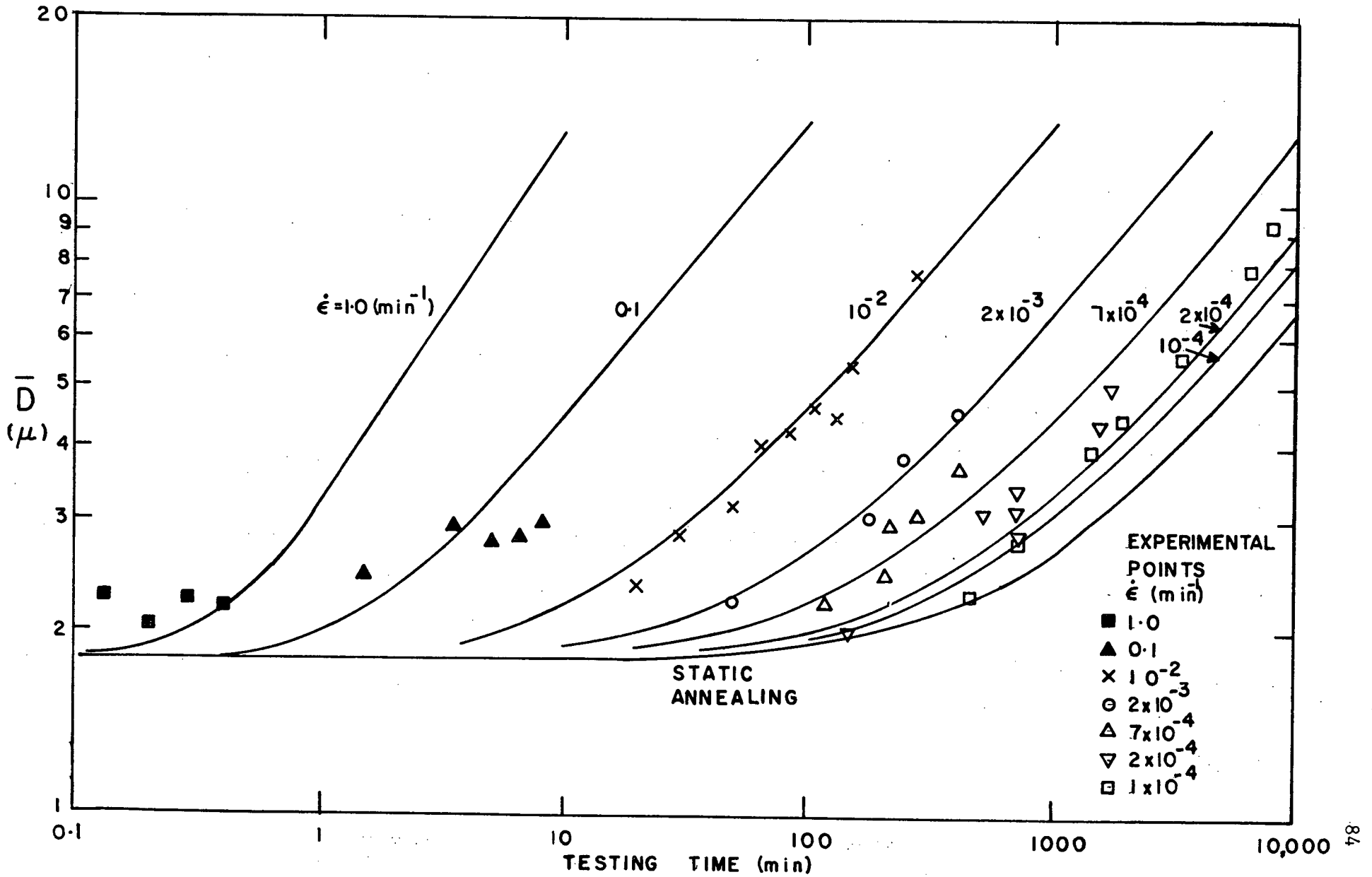


Fig.41. Comparison of Theoretical and Experimental Grain Size versus Time During Deformation Curves.

trusion ratio material which seemed to possess slightly different grain growth characteristics from the lower extrusion ratio material (Fig.15).

The same equation (16) can be used to calculate theoretical  $\frac{\Delta \bar{D}}{\bar{D}_A}$  versus strain curves by computing the time required to reach a certain value of strain and inserting it in the equation (Fig.42). Again agreement is good for the high strain rates shown. The trend to lower  $\frac{\Delta \bar{D}}{\bar{D}_A}$  values with decreasing strain rate in the superplastic region is also predicted. Theoretical  $\frac{\Delta \bar{D}}{\bar{D}_A}$  values at 25% true strain for all strain rates were calculated and compared to the experimental points from Fig.21 (Fig.43). The experimental trend is again predicted by the theory.

Predictions of the annealing behaviour after deformation can also be made. When excess vacancies are no longer produced  $K_1$  equals zero. The excess vacancies that were present at the end of the deformation will continue to influence the grain growth until they anneal out. If the deformation ends at time  $t_1$ , the excess vacancies present,  $n_{x_1}$ , will be given by:

$$n_{x_1} = \frac{K_1}{K_2} \dot{\epsilon} (1 - \exp(-K_2 t_1)) \quad (20)$$

The loss rate of the excess vacancies is given by:

$$\frac{d n_x}{dt} = - n_x K_2 \quad (21)$$

Integration of this equation yields:

$$n_x = n_{x_1} e^{-K_2 (t_1 - t)} \quad (22)$$

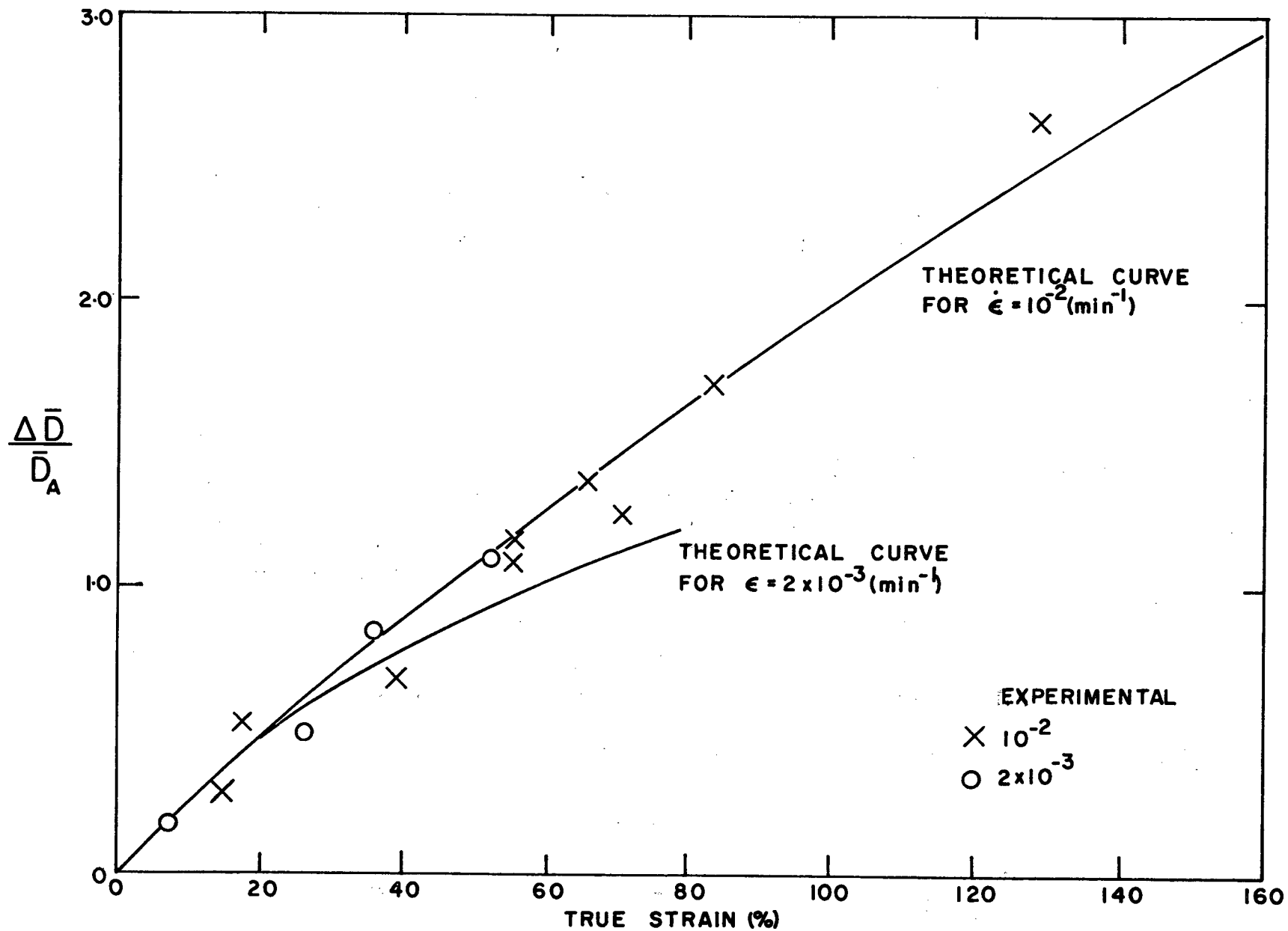


Fig.42. Comparison of Theoretical and Experimental Relative Grain Size Change versus Strain Curves.

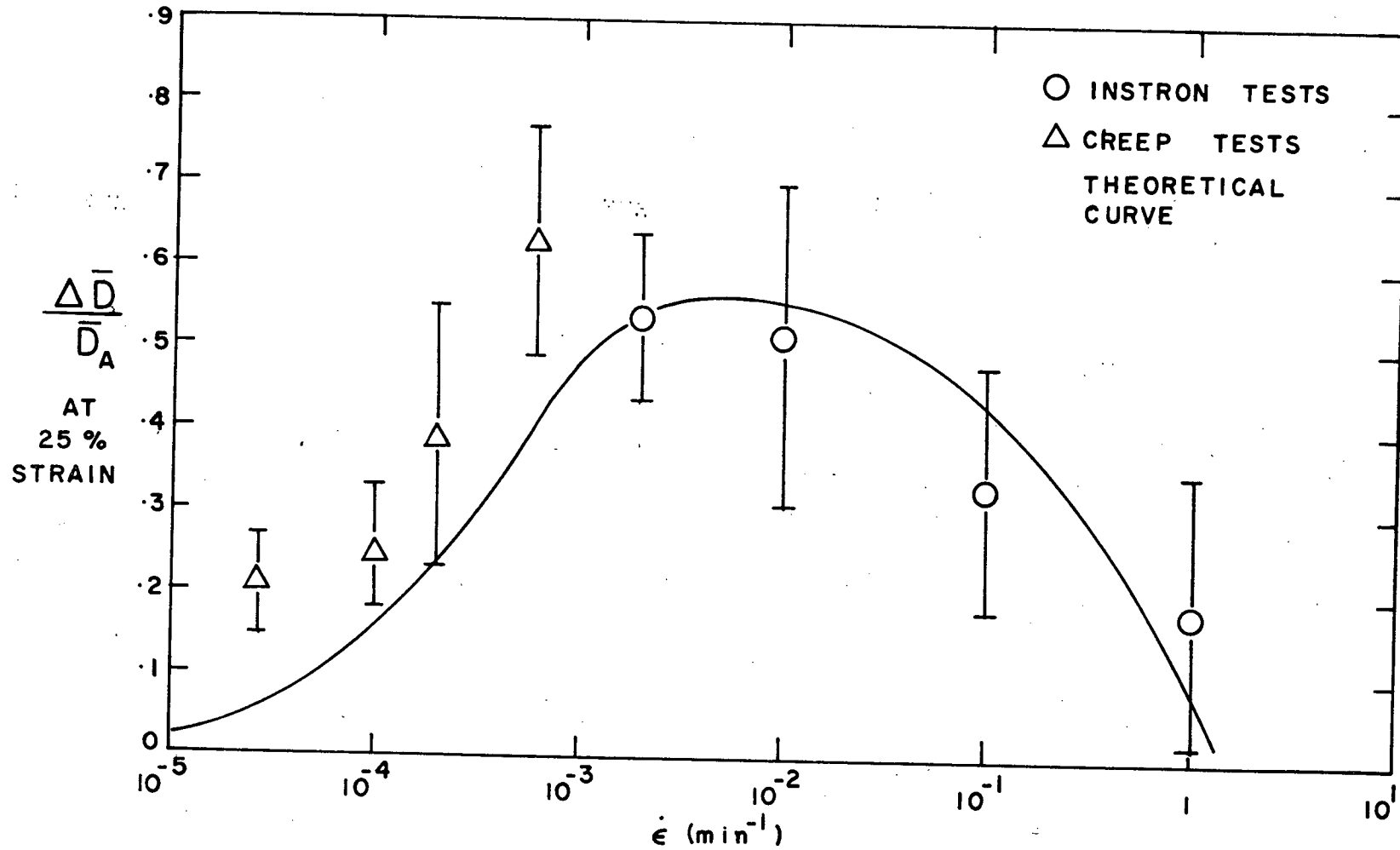


Fig.43. Comparison of Theory and Experiment for the Relative Grain Size Change After 25% Strain.

where  $n_x$  is the atomic fraction of excess vacancies at time  $t$  after deformation ceases.

Substituting equation(20)into equation (14) gives:

$$\frac{d\bar{D}}{dt} = \frac{k' (n_{x1} e^{K_2(t_1 - t)} + n_v)}{\bar{D}} \quad (23)$$

If  $\bar{D}_1$  is the grain size at time  $t_1$  integration of this equation gives the time dependence of the grain size after deformation:

$$\bar{D}^2 - \bar{D}_1^2 = 2k' n_v (t - t_1) + \frac{2k' n_{x1}}{K_2} (1 - \exp (K_2 (t_1 - t))) \quad (24)$$

A curve was calculated from this equation with  $t_1 = 120(\text{min.})$  and  $\bar{D}_1 = 4.6 \mu$  and compared to the corresponding experimental curve (Fig. 44). The theory correctly predicts the sharp transition in the curve after deformation, but does not predict the actual grain size after long periods of post deformation annealing. The theoretical curve coincides with the static annealing curve of Fig.35 rather than the actual post deformation curve. These decreased growth rates after deformation can be explained by a mechanism involving the effects of deformation on texture.

Neilsen<sup>(46)</sup> has discussed a coalescence-type mechanism which occurs as a consequence of grain "encounters" during normal grain growth. Normal grain growth occurs by the disappearance of the small grains of few sides. In a typical sequence a four sided grain (Fig.45a No.5) shrinks until the upper two triple points meet (b)

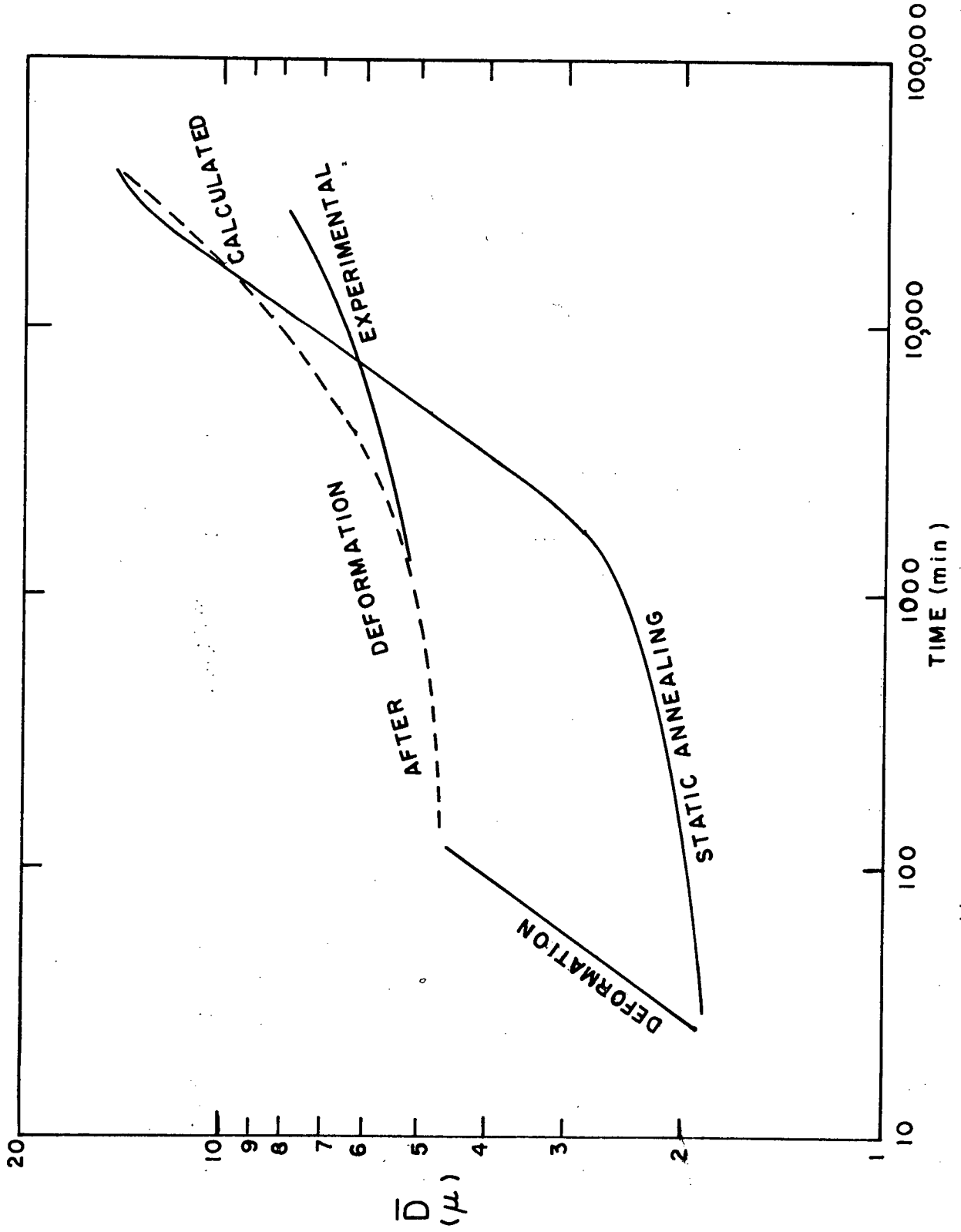


Fig. 44. Comparison of Theory and Experiment for Post Deformation Annealing.

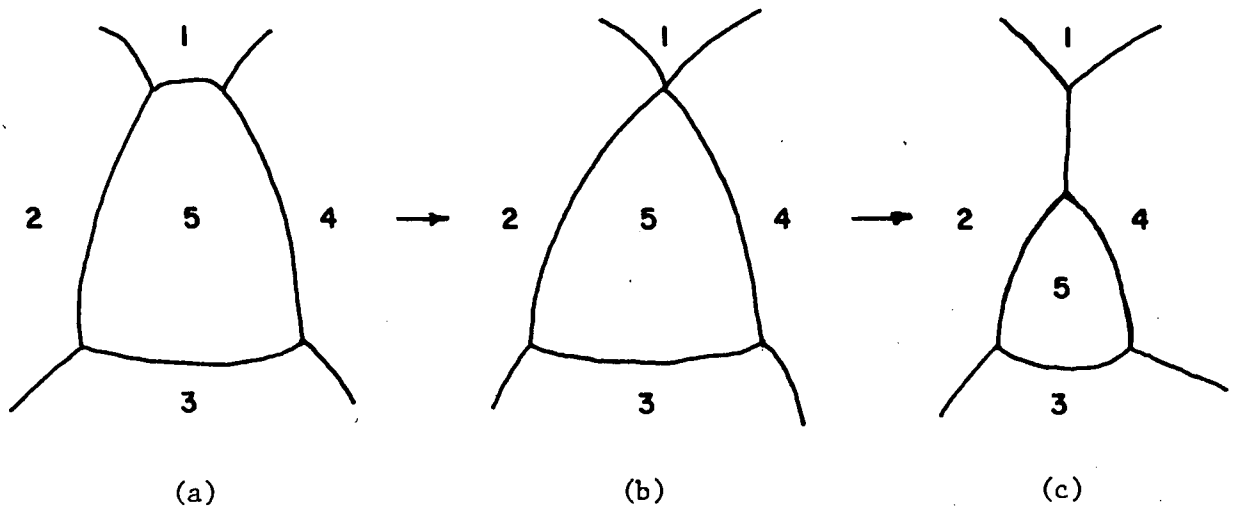


Fig.45. Illustration of Grain "Encounter" During Grain Growth.

This unstable configuration changes to the more stable one (c) and grain 5 has lost a side. In the process grains 2 and 4 have "encountered" or formed a new boundary between them. Nielsen proposed that if grains 2 and 4 were of like orientation or slightly misoriented a grain boundary would not form between them. They would have coalesced to form a larger grain and increased the average grain size.

The frequency of encounters that lead to a coalescence will depend on the relative number of like-oriented grains present in the structure. Compared to a random structure, a textured material will have a higher proportion of these like orientations and consequently a higher grain growth rate. Since superplastic deformation causes a randomization of the original texture the growth rate after deformation should be less than a statically annealed sample as is observed.

The grain size distribution analysis and the tension-compression experiment are also consistent with the diffusivity enhancement model. Since the deformation causes only a speeding up of the normal growth processes, equivalent grain size samples should possess the same size distributions regardless of the path taken to reach that grain

size. The curves of Fig.28 show that the grain size distributions are indeed identical. In the tension-compression experiment reversal of the stress direction should still produce a vacancy excess in the grain boundary region. As long as the boundaries are sliding, vacancies will be generated and the mobility increased regardless of the sliding direction. Experimentally the stress direction had little effect on the grain size enhancement produced.

Since all of the experimental results are consistent with the diffusivity enhancement model, it seems the most likely cause of the deformation induced grain growth.

SUMMARY AND CONCLUSIONS

- 1) Superplastic deformation of Sn - 1% Bi was found to produce considerable increases in grain growth rates. During annealing the grain size kinetics could be described by an equation of the form  $\bar{D}^2 - D_0^2 = k^2 t$ . The effect of deformation was to increase the value of the constant k.
- 2) The grain growth enhancement was most pronounced at high strain rates in the superplastic region. Reduction of strain rate produced a lessening of the growth rates.
- 3) The relative grain size change,  $\frac{\Delta \bar{D}}{\bar{D}_A}$ , was found to depend linearly on strain.
- 4) The grain growth rates on annealing after deformation were less than static rates.
- 5) Grain type and grain size distributions were similar in deformed and annealed structures.
- 6) A mechanism involving the production of excess vacancies in the grain boundary region leading to increased boundary mobility was found to be consistent with all experimental observations.

APPENDIX AEffect of Coalescence Mechanism on Grain Type  
and Size Distributions

If the coalescence mechanism is responsible for the grain size increase during deformation, changes in the grain type and size distributions would be expected. In this section an attempt will be made to calculate the expected distributions after deformation from the static annealing distributions.

It will be assumed that the distribution curves (Figs. 24 and 26) for static annealing are representative of the actual distributions at any time during annealing. This assumption is usually made in theoretical considerations of grain growth<sup>(44)</sup> although some changes in the size distribution may occur on extended annealing<sup>(46)</sup>. Since it has been shown that the distribution curves taken from a random 2 dimensional section and the actual spatial distribution are similar in form<sup>(41,44)</sup> the analysis will be done in 2 dimensions.

When a boundary coalesces, the local distribution of grain types is affected. In a perfect 6 sided network (Fig.46), when grains 1 and 2 undergo a coalescence so that the indicated boundary disappears, the combined 1-2 grain will have 8 sides. The adjacent grains (5 and 9) have become 5 sided.

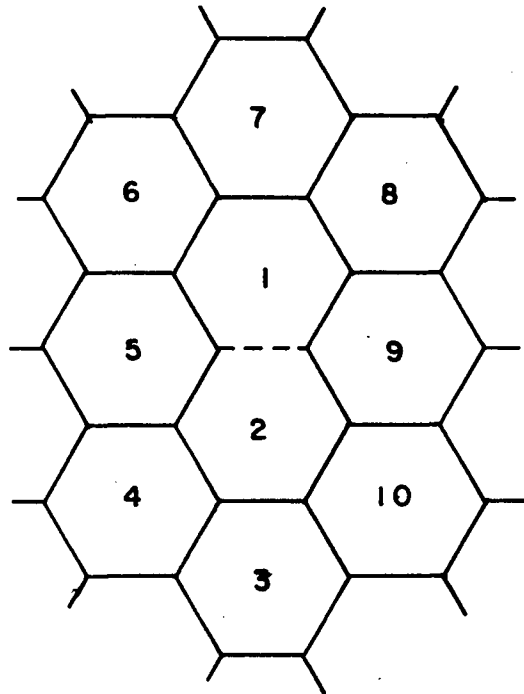


Fig.46. Effect of a Grain Boundary Coalescence.

In general when a boundary separating grains having  $m$  and  $n$  sides disappears, a combined grain is produced with sides numbering  $(m + n) - 4$  and the two adjacent grains have each lost a side. In addition, the total number of grains has been reduced by one.

The probability of any one grain taking part in a coalescence will depend on its number of sides ( $m$ ) and also on its relative frequency in the structure ( $f_m$ ). The frequency  $f_m$  will be defined as  $X_m/X_t$  where  $X_m$  is the number of  $m$  sided grains in a given area and  $X_t$  is the total number of grains in the same area. The probability of an  $(m + n)$  coalescence taking place will vary as  $m f_m \cdot n f_n$ . The probability of producing an adjacent grain having  $p-1$  sides will equal the probability of finding a  $p$  sided grain in an adjacent site. The

probability of finding a  $p$  sided grain in any site in the structure will vary as its relative frequency ( $f_p$ ). Therefore, for each coalescence that occurs there will be produced in the adjacent positions:

$$\begin{aligned} & 2 f_p \text{ grains of } p-1 \text{ sides} \\ & + 2 f_m \text{ grains of } m-1 \text{ sides} \\ & + 2 f_n \text{ grains of } n-1 \text{ sides} \\ & \quad \cdot \quad \quad \quad \cdot \\ & \quad \cdot \quad \quad \quad \cdot \\ & \quad \cdot \quad \quad \quad \cdot \end{aligned}$$

To simplify the calculations, coalescences will be restricted to the most frequently occurring grains, the 4, 5, 6 and 7 sided grains. In addition  $m$  will be restricted to values from 3 to 13.

If a number of coalesced grains ( $X_c$ ) are produced by a given amount of strain, the total will be composed of the number formed from each combination i.e.

$$X_c = a + b + c + d + e + f + g + h + i + j \quad (25)$$

where  $a \equiv$  number of 4-4 coalescence

$b \equiv$  " " 4-5 "

$c \equiv$  " " 4-6 "

$d \equiv$  " " 4-7 "

$e \equiv$  " " 5-5 "

$f \equiv$  " " 5-6 "

$g \equiv$  " " 5-7 "

$h \equiv$  " " 6-6 "

$i \equiv$  " " 6-7 "

$j \equiv$  " " 7-7 "

The ratio  $a:b:c: \dots$  will be proportional to the probability of occurrence of each combination ( $m f_m \cdot n f_n$ ) i.e.

$$a:b:c: \dots = 4 f_4 : 4 f_4 ; 4 f_4 5 f_5 ; 4 f_4 6 f_6 : \dots \quad (26)$$

If  $X_c$  is known and is small compared to  $X_t$  then values of  $a, b, c, \dots$  can be calculated from the original frequency distribution. The number of grains of side  $m$  after a number of coalescences have occurred will be defined as  $X'm$ .

For one (4-4) coalescence  $X_4$  will be reduced by two

$$X'_4 = X_4 - 2$$

However, a coalesced grain has been produced having sides equal to  $m + n - 4$  (=4)

$$X'_4 = X_4 - 2 + 1$$

Also  $2 f_5$ , 4 sided grains have been produced in the adjacent position

$$X'_4 = X_4 - 2 + 1 + 2 \frac{X_5}{X_t}$$

Finally,  $2 f_4$ , 4 sided grains have lost a side in the adjacent position

$$X'_4 = X_4 - 2 + 1 + 2 \frac{X_5}{X_t} - 2 \frac{X_4}{X_t} \quad (27)$$

This equation will apply for every 4-4 coalescence that occurs, therefore, for "a" 4-4 coalescences:

$$X'_4 = X_4 - a + \left( 2 \frac{X_5}{X_t} - 2 \frac{X_4}{X_t} \right) a \quad (28)$$

The frequency of the other grains will be affected only by the adjacent grain reactions:

$$X'_5 = X_5 + \left( 2 \frac{X_6}{X_t} - 2 \frac{X_5}{X_t} \right) a$$

$$X'_6 = X_6 + \left( 2 \frac{X_7}{X_t} - 2 \frac{X_6}{X_t} \right) a$$

⋮  
⋮  
⋮

The 13 sided grains will only lose by the adjacent grains since 14 sided grains were not permitted originally:

$$X'_{13} = X_{13} - 2 \frac{X_{13}}{X_t} a$$

A 2 sided grain is possible by the adjacent mechanism but is unstable and will disappear very quickly. It will be included in the calculations however:

$$X'_2 = 2 \frac{X_3}{X_t} a$$

For each of these "a" coalescences the total number of grains has been reduced by one:

$$X'_t = X_t - a$$

This analysis can be extended to the other combinations.

For example for "a" 4-4 and "b" 4-5 coalescences the equations will be:

$$X'_2 = 2 \frac{X_3}{X_t} (a + b)$$

$$X'_3 = X_3 + \left( 2 \frac{X_4}{X_t} - 2 \frac{X_3}{X_t} \right) (a + b)$$

$$X'_4 = X_4 + \left( 2 \frac{X_5}{X_t} - 2 \frac{X_4}{X_t} \right) (a + b) - (a + b)$$

$$X'_5 = X_5 + \left( 2 \frac{X_6}{X_t} - 2 \frac{X_5}{X_t} \right) (a + b) + b - b$$

$$X'_6 = X_6 + \left( 2 \frac{X_7}{X_t} - 2 \frac{X_6}{X_t} \right) (a + b)$$

⋮  
⋮  
⋮

$$X'_{13} = X_{13} + \left( 2 \frac{X_{13}}{X_t} \right) (a + b)$$

$$X'_+ = X_t - (a + b)$$

The equations obtained after all possible combinations are considered are:

$$X'_2 = X_2 + \left( 2 \frac{X_3}{X_t} \right) (a + b + c \dots)$$

$$X'_3 = X_3 + \left( 2 \frac{X_4}{X_t} - 2 \frac{X_3}{X_t} \right) (a + b + c \dots)$$

$$X'_4 = X_4 + \left( 2 \frac{X_5}{X_t} - 2 \frac{X_4}{X_t} \right) (a + b + c \dots) - (a + b + c + d)$$

$$X'_5 = X_5 + \left( 2 \frac{X_6}{X_t} - 2 \frac{X_5}{X_t} \right) (a + b + c \dots) - (2e + f + g)$$

$$X'_6 = X_6 + \left( 2 \frac{X_7}{X_t} - 2 \frac{X_6}{X_t} \right) (a + b + c \dots) - (f + 2h + i) + e$$

$$X'_7 = X_7 + \left( 2 \frac{X_8}{X_t} - 2 \frac{X_7}{X_t} \right) (a + b + c \dots) - (g + i + 2j) + f$$

$$X'_8 = X_8 + \left( 2 \frac{X_9}{X_t} - 2 \frac{X_8}{X_t} \right) (a + b + c \dots) + g + h$$

$$X'_9 = X_9 + \left( 2 \frac{X_{10}}{X_t} - 2 \frac{X_9}{X_t} \right) (a + b + c \dots) + i$$

$$X'_{10} = X_{10} + \left( 2 \frac{X_{11}}{X_t} - 2 \frac{X_{10}}{X_t} \right) (a + b + c \dots) + j$$

$$X'_{11} = X_{11} + \left( 2 \frac{X_{12}}{X_t} - 2 \frac{X_{11}}{X_t} \right) (a + b + c \dots)$$

$$X'_{12} = X_{12} + \left( 2 \frac{X_{13}}{X_t} - 2 \frac{X_{12}}{X_t} \right) (a + b + c \dots)$$

$$X'_{13} = X_{13} + \left( \quad - 2 \frac{X_{13}}{X_t} \right) (a + b + c \dots)$$

$$X'_t = X_t - (a + b + c + \dots)$$

By taking successive increments for  $X_c$  and knowing the original distribution, the new distribution can be calculated from the equations. Three increments of  $X_c$  were taken, each increment being 2% of the total number of grains ( $X_t$ ). The calculated distribution after the 6% coalescence could then be compared with the deformed distribution (Fig.47). The theory predicts the observed decrease in the frequency of the 4, 5 and 6 sided grains as compared to the annealed state. It also predicts the observed frequency increase in the 8, 9 and 10 sided grains. However, disagreement is not obtained for the 2, 3, 7, 11, 12 and 13 sided grains. It seems reasonable to conclude however, that the theory predicts the general trend of the distribution changes and that only approximately 6% of the grains need coalesce to produce the degree of change observed.

In order to determine if this 6% coalescence could also produce the observed changes in the grain size distribution a similar analysis can be performed. First, it is necessary to estimate the most probable area of each type of grain. Feltham<sup>(44)</sup> has shown that a one-one relationship exists between the type and size distributions i.e. the smaller grains would, in general, be those with few sides and the larger grains those with many sides. This relationship was suggested by the log-normal distributions of the grain sizes and types. To prove the relationship, the actual size distributions for each type of grain were measured. The mean diameter of each type varied linearly with the number of sides. It has been shown that the size and type distributions of the Sn - 1% Bi are also log-normal so it will be assumed that the same linear relationship is valid.

By comparing the two distribution curves for the annealed

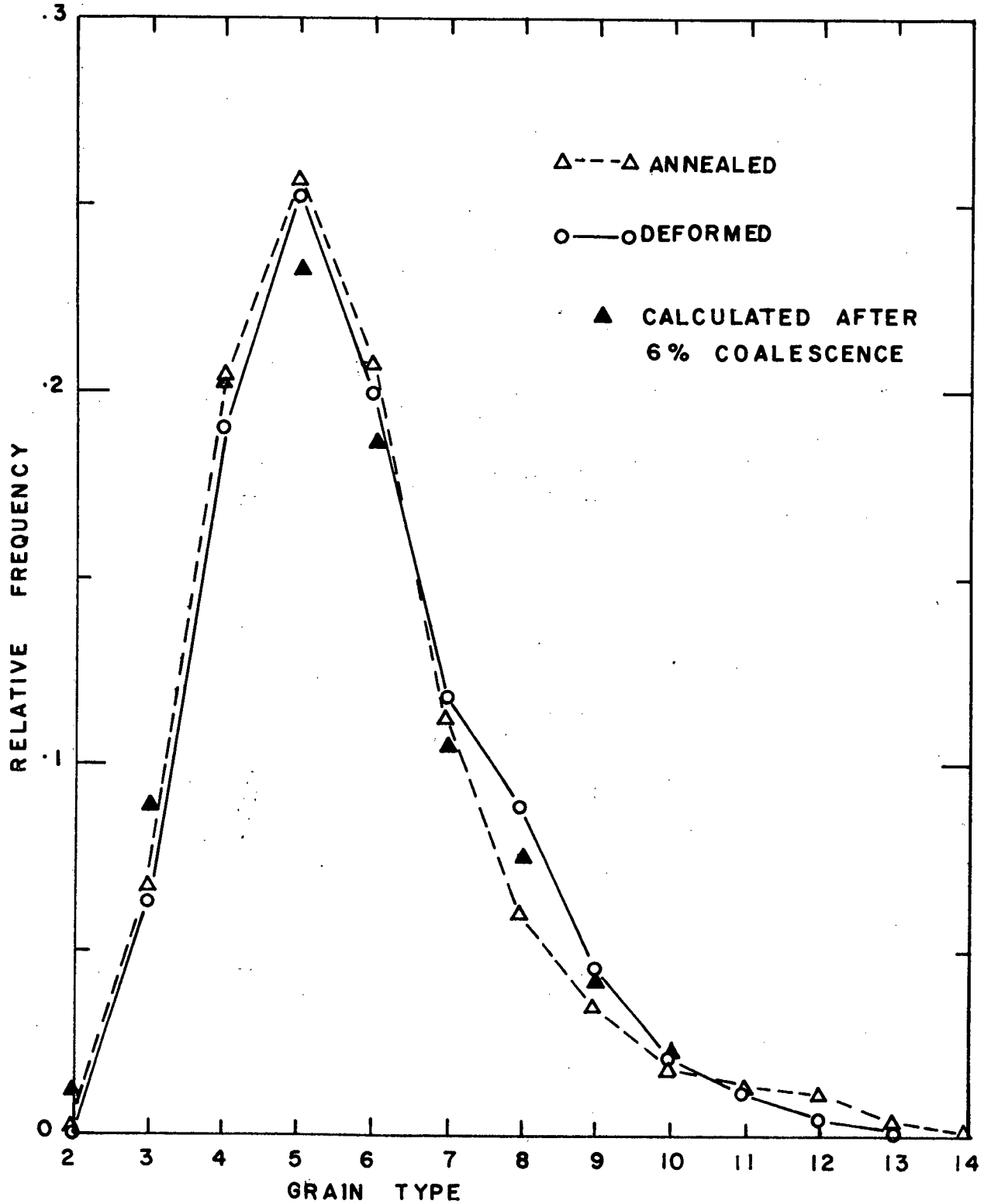


Fig.47. Comparison of Calculated and Experimental Grain Type Distributions.

material it seemed that the three sided grains should have mean diameters corresponding to grain classes 1 and 2, 4 sided grains to 3 and 4 classes, 5 sided grains to class 5, 6 sided to class 6 and 7 sided to class 7. The most probable diameters of the 3, 4, 5, 6 and 7 sided grains were thus taken to be 1.9, 3.8, 6.4, 9, and 12.8  $\mu$  respectively. The areas corresponding to these diameters are 2.8, 11, 32, 64 and 128 ( $\mu^2$ ) respectively.

Again only the coalescences between the 4, 5, 6 and 7 sided grains will be considered. For one  $m + n$  coalescence a new grain is formed having an area which is the sum of the areas of the combining grains. At the same time the number of grains in the  $m$  sided grain class has been reduced by one. Similarly the number of grains in the class of the  $n$ -sided grain has been depleted by one.

The possible combinations are listed in Table 5, along with the area of the coalesced grains.

TABLE 5 - Areas of Coalesced Grains

Combination	No. of Combinations	Area of the Coalesced Grain ( $\mu^2$ )	Grain Class to which Coalesced Grain belongs
4 - 4	a	22	4
4 - 5	b	43	5
4 - 6	c	75	6
4 - 7	d	139	7
5 - 5	e	64	6
5 - 6	f	96	7
5 - 7	g	160	7
6 - 6	h	128	7
6 - 7	i	192	8
7 - 7	j	256	8

When all these combinations take place the number of grain in class 6 has been increased by  $c + e$  but at the same time has been decreased by all those reactions involving a 6 sided grain i.e.  $c, f, 2h$  and  $i$  grains have been lost. If  $N_p$  is the number of grains originally in grain class  $p$  and  $N'_p$  is the number after  $(a + b + c \dots)$  coalescences have occurred then the following equation can be written:

$$N'_5 = N_5 - 2e - b - f - g + b$$

$$N'_6 = N_6 - c - f - 2h - i + c + e$$

$$N'_7 = N_7 - d - g - i - 2j + d + f + g + h$$

$$N'_8 = N_8 + i + j$$

It will be assumed that the grains lost from grain classes 3 and 4 by the reactions involving 4 sided grains will be equally divided between the two classes:

$$N'_4 = N_4 - \frac{(2a + b + c + d)}{2} + a$$

$$N'_3 = N_3 - \frac{(2a + b + c + d)}{2}$$

Using the experimental values for  $N_3, N_4$  etc. (Fig.26) and taking  $X_c$  in steps of 2% of the total number of grains the size distributions after coalescence can be calculated. When the results for a total of 6% coalescence are compared to the actual as deformed distribution (Fig.48), it is seen that the predicted changes are very small compared to the actual measured results.

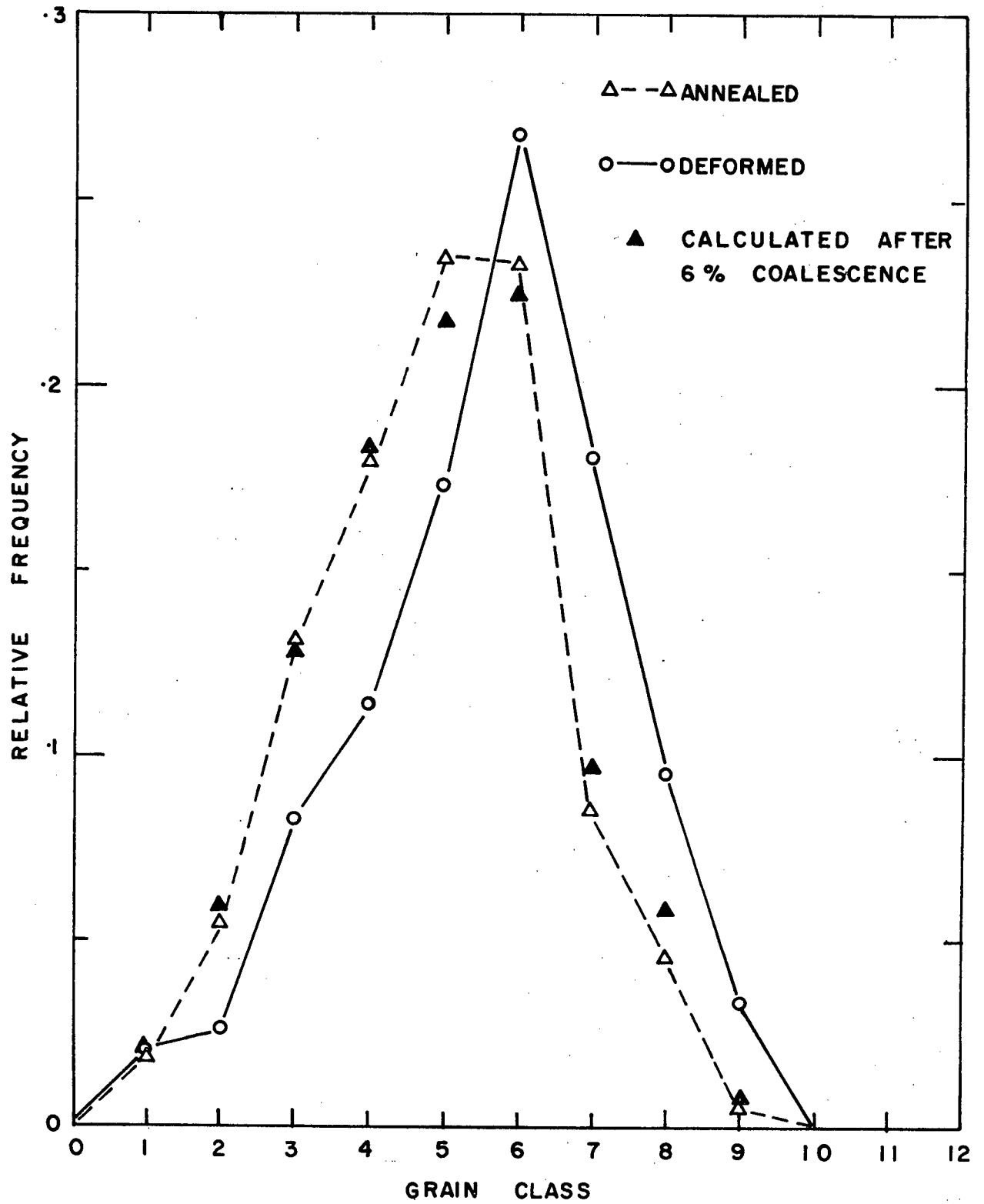


Fig.48. Comparison of Calculated and Experimental Grain Size Distributions.

BIBLIOGRAPHY

1. Hayden, H.W., Gibson, R.C., Merrick, H.F. and Brophy, J.H.,  
ASM Trans. 60, 3, (1967).
2. Woodford, D.A., ASM Trans. 62, 291, (1969).
3. Backofen, W.A., Turner, I.R. and Avery, D.H., ASM Trans. 57,  
980, (1964).
4. Alden, T.H. and Cline, H.E., Trans. AIME 239, 710, (1967).
5. Alden, T.H., Trans. AIME 236, 1633, (1966).
6. Floreen S., Scripta Met. 1, 19, (1967).
7. Gifkins, R.C., Jour. Inst. Metals., 95, 393, (1967).
8. Backofen, W.A. and Zehr, S.W., ASM Trans. 61, 300, (1968).
9. Morrison, W.B., Trans. AIME 242, 2221, (1968).
10. Surges, K., M.Sc. Thesis, University of British Columbia (1969).
11. Backofen, W.A. and Avery, D.H., ASM Trans., 58, 551, (1965).
12. Avery, D.H. and Stuart, J.M., 14th Sagamore Army Materials Re-  
search Conference, Aug. (1967).
13. Martin, P.J. and Backofen, W.A., ASM Trans. 60, 352, (1967).
14. Alden, T.H. and Schadler, H.W., Trans. AIME 242, 825, (1968).
15. Kossowsky, R. and Bechtold, J.H., Westinghouse Research Paper  
67-1F7 Solid-P3, (1967).
16. Chaudari, P., Acta Met., 15, 1777, (1967).
17. Packer, C.M. and Sherby, O.D., ASM Trans. 60, 21, (1967).
18. Johnson, R.H., Packer, C.M., Anderson, L, and Sherby, O.J.,  
Phil. Mag., 18, 1309, (1968).
19. Nuttall, K. and Nicholson, R.B., Phil. Mag. 17, 1087, (1968).

20. Packer, C.M., Johnson, R.H, and Sherby, O.D., Trans. AIME 242, 2485, (1968).
21. Cook, R.C., M.Sc. Thesis, University of British Columbia (1968).
22. Turner, D., M.Sc. Thesis, University of British Columbia (1971).
23. Naziri, H., Pearce, R. and Williams, D.A.C., Scripta Met., 3, 117, (1969).
24. Naziri, H. and Pearce, R., Scripta Met. 3, 807, (1969).
25. Hayden, H.W. and Brophy, J.H., ASM Trans. 61, 542, (1968).
26. Brophy, J.H., Lindinger, R.J. and Gibson, R.C., ASM Trans. 62, 230, (1969).
27. Alden, T.H., Acta Met., 15, 469, (1967).
28. Stowell, M.J., Robertson, J.L. and Watts, B.M., Metal Science Jour., 3, 41, (1969).
29. Lee, D., Met. Trans., 1, 309, (1970).
30. Lee, D., Acta Met., 17, 1057, (1969).
31. Backofen, W.A. and Lee, D., Trans. AIME, 239, 1034, (1967).
32. Backofen, W.A. Murty, G.S. and Zehr, S.W. Trans. AIME 242, 329, (1968).
33. Morrison, W.B., ASM Trans., 61, 423, (1968).
34. Holmes, E.L. and Winegard, W.C., Jour. Inst. Metals, 88, 468, (1959-60).
35. Gordon, P., Trans. AIME, 227, 699, (1963).
36. Cullity, B.D., Elements of X-Ray Diffraction, Addison-Wesley Eng., (1959).
37. Tegart, W.J. McG. Electrolytic and Chemical Polishing of Metals, Pergamon Press (1959).
38. Russell, R.R. and Alden, T.H., General Electric Research Center Report 68-C-190 (1968).

39. Hilliard, J.E., Metal Progress, p.99, May (1964).
40. Johnson, W.A., Metal Progress, p.87, Jan. (1946).
41. Dehoff, R.T. and Rhines, F.N., Quantitative Microscopy, McGraw Hill, (1968).
42. Garofalo, F., Fundamentals of Creep and Creep Rupture in Metals, Macmillian, (1965).
43. Rachinger, W.A., Jour. Inst. Metals, 81, 33, (1952).
44. Feltham, P., Acta Met., 5, 97, (1957).
45. Holmes, E.L. and Winegard, W.C., 224, 945, (1962).
46. Nielsen, J.P., Recovery, Recrystallization and Grain Growth, ASM, Cleveland (1965).
47. Fullman, R.L., Metal Interfaces, ASM, Cleveland (1951).
48. Lücke, K. and Detert, K., Acta Met., 5, 628, (1957).
49. Gordon, P. and Vandermeer, R.A., Trans. AIME 224, 917, (1962).
50. Li, J.C., Jour. Appl. Phys., 33, 2958, (1962).
51. Honeycombe, R.W.K., The Plastic Deformation of Metals, Edward Arnold Ltd. (1968).
52. Backofen, W.A. and Holt, D.L., ASM Trans. 59, 755, (1966).
53. Gifkins, R.C., Jour. Inst. Metals, 87, 255, (1958-59).
54. Hirst, H., Proc. Aust. Inst. Min. and Met., 121, 29, (1941).
55. Richardson, G.J., Sellars, C.M. and Tegart, W.J. McG., Acta Met. 14, 1225, (1966).
56. Byrne, J.G., ASM Trans., 56, 68, (1963).
57. Rhines, F.H., Bond, W.E. and Kissel, M.A., ASM Trans., 48, 919, (1956).
58. Adsit, N.R. and Brittain, J.O., Trans. AIME, 218, 765, (1960).
59. Strutt, P.R., Lewis, A.M. and Gifkins, R.C., Jour. Inst. Metals, 93, 71, (1964-65).

60. Gifkins, R.C., Fracture, Technology Press of M.I.T. and John Wiley, (1959).
61. Weinberg, F., Trans, AIME, 212, 808, (1958).
62. Puttick, K.E, and Tuck, B., Acta Met., 13, 1043, (1965).
63. Bell, R.L. and Langdon, T.G., Jour. Mat. Sci., 2, 313, (1967).
64. Gittins, A. and Gifkins, R.C., Metal Sci. Jour., 1, 15, (1967).
65. Couling, S.L. and Roberts, C.S., Trans. AIME 209, 1253 (1957).
66. Chang, H.C. and Grant, N.J., Trans. AIME 197, 305, (1953).
67. Gifkins, R.C., Trans. AIME 215, 1015, (1959).
68. Ishida, Y., Mullendore, A.W. and Grant N.J., Trans. AIME 233, 204, (1965).
69. Lee, C.H. and Maddin, R., Trans. AIME, 215, 397, (1959).
70. Fisher, G.L. and Maddin, R., Trans. AIME, 236, 853, (1966).
71. Forestieri, A.F. and Girifalco, L.A. Jour. Phys. Chem. Solids, 10, 99, (1959).
72. Buffington, F.S. and Cohen, M., Trans. AIME, 194, 859, (1952).
73. Ujiije, N., Averbach, B.L., Cohen, M. and Griffiths, V., Acta Met., 6, 68, (1958).
74. Jones, W.J.D. and Dover, W.D., Nature, 209, 704, (1966).
75. Brown, D.A. and Blackburn, A.F., Acta Met. 11, 1017, (1963).
76. Baluffi, R.W. and Ruoff, A.L., Jour. Appl. Phys. 34, 1634, 1848, 2862, (1963).
77. Romashkin, Y.P., Sov. Phys. Sol.State, 2, 2722, (1961).
78. Darby, J.B., Tomizuka, C.T. and Baluff, R.W., Jour. Appl. Phys., 32, 840, (1961).
79. Pearson, S., Board, A.J. and Wheeler, C., Phil. Mag. 6, 979, (1961).

80. Pines, B.Y. and Chaikovskii, E.F., Physics, Metal and Metall. 11, 155, (1961).
81. Chollet, P., Grosse, I. and Philibert, J., Compt. Rend. Acad. Sci, 252, 728, (1961).
82. Guy, A.G., and Philibert, J., Trans. AIME 221, 1174, (1961).
83. Bhat, T.A. and Vitovec, F.H., Jour. Inst. Metals, 98, 95, (1970).
84. Blackburn, D.A. and Brown, A.F., Jour. Inst. Metals, 91, 106, (1962-63).
85. Girifalco, L.A. and Grimes, H.H., NACA Tech. Note 4408, (1958).
86. Shewmon, P.G., Diffusion in Solids, McGraw-Hill (1963).
87. Desorbo, W., Bull. Amer. Phys. Soc. Series II, Vol.4, No.1.p.149, (1959).
88. Meakin, J.D. and Kloholm, E., Trans. AIME. 218, 463, (1960).
89. Barry, B.E. and Brown, A.F. Acta. Met. 12, 209, (1964).